Institut für Solare Energieversorgungstechnik
Verein an der Universität Kassel e.V.

Institut für Elektrische Energietechnik
Rationelle Energiewandlung

Erneuerbare Energien und Energieeffizienz

Renewable Energies and Energy Efficiency

Band 8 / Vol. 8

Herausgegeben von / Edited by
Prof. Dr.-Ing. Jürgen Schmid, Universität Kassel

Giovanni Mattarolo

Development and Modelling of a Thermophotovoltaic System

kassel university press

This work has been accepted by the faculty of electrical engineering / computer science of the University of Kassel as a thesis for acquiring the academic degree of Doktor der Ingenieurwissenschaften (Dr.-Ing.).

Supervisor: Prof. Dr.-Ing. J. Schmid
Co-Supervisor: Prof. Dr.-Ing. P. Zacharias

Defense day 29th November 2007

Bibliographic information published by Deutsche Nationalbibliothek
The Deutsche Nationalbibliothek lists this publication in the Deutsche Nationalbibliografie; detailed bibliographic data is available in the Internet at http://dnb.d-nb.de

Zugl.: Kassel, Univ., Diss. 2007
ISBN: 978-3-89958-375-5
URN: urn:nbn:de:0002-3754

© 2007, kassel university press GmbH, Kassel
www.upress.uni-kassel.de

Cover layout: Grafik Design Jörg Batschi, Kassel
Printed by: Unidruckerei, University of Kassel
Printed in Germany

A mamma e papà

Abstract

Thermophotovoltaic (TPV) generation of electricity is a technology based on the direct conversion of a radiation coming from a heat source into electric power by means of photovoltaic cells.

TPV is a highly multidisciplinary technology, which involves and relates different research fields. Heat transfer via conduction, convection and radiation, chemical reaction and diffusion, generation, selection, transmission and absorption of radiation and photovoltaic effect are the different processes involved in the device to realize the energy conversion.

Due to such a complexity, this technology has not yet reached a mature state: few TPV devices have been so far developed and brought successfully into operation and the highest system efficiency ever measured does not exceed 6.5%. However TPV generators could be soon competitive to other established electric generator technologies in the power range from some W to some kW. TPV, indeed, is a compact, reliable, quiet and safe technology with the potential for low cost and versatile fuel usage.

The present PhD thesis describes the development and modelling of a small TPV gas-fuelled prototype based on GaSb cells. Purpose of the work is to realize the first ever TPV system which can be used as tester, working under different operating conditions with different combinations of cells and emitter materials. This would allow to get a better knowledge of the TPV technology and to develop optimization criteria for TPV systems.

Besides the development of the prototype, another target of the work is to implement a theoretical simulation model of the TPV device and validate it, in order to realize a simulation tool which can be used for further analysis and optimization of the system. Several studies are already available in the literature, which deal with modelling of fuelled-TPV converters; however they are more focused on the spectral control and cell simulation and none of them takes into account the detailed modelling of the recuperative burner unit, which is indeed a key component where the heat is generated, converted into radiation by the emitter and partially recovered by the recuperative heat exchanger. The present work aims at developing a theoretical model of the whole TPV device: all the components and processes are considered, including also the combustion process and the heat transfer in the recuperator, as well as the reciprocal interactions between them.

The thesis can be divided basically in two parts: the first one gives an overview of the TPV technology, while the second one describes the experimental and theoretical work carried out to realize the TPV prototype and the simulation model.

The first chapter describes briefly the TPV generation principles and compares this energy conversion technology to the traditional PV technology. A short historical background of TPV is also given. The second chapter treats more in detail of the different components involved in a TPV device: definition of the efficiency, theoretical background, main characteristics and state of the art are given for each process and for a complete TPV system.

In the third chapter an overview of the possible applications where TPV could be soon an attractive technology is presented and a comparison is made with the other energy conversion technologies currently available, pointing out efficiency and cost thresholds to overcome in order that TPV becomes competitive. An example case is also given in which the effect of a small TPV system integrated on a standalone PV system is evaluated via simulation.

The approach followed to realize the device and develop the simulation model is explained and justified in the fourth chapter, while the fifth chapter deals with the design and the mathematical model of the system. The recuperative burner unit, the optical system, where the radiation is generated, selected and transmitted and the photovoltaic cells are described in detail; peculiarity of the device is its modular design, which allows to modify easily the operating conditions and the configuration of the system: five different emitter materials are used during experimental tests, with both gray and selective spectral properties, and are coupled to a quartz glass absorptive filter.

Parallely the mathematical models of the different processes are formulated for each component. Partial differential equation systems are used to define the heat transfer, chemical reaction and flowing of fluids processes inside the device, and are solved for each component with a commercial Finite Element Method based software. A two-band model is used to describe and simulate the spectral control of the optical system.

The sixth chapter shows the experimental and theoretical results obtained from tests and simulations, varying the operating conditions and the different emitter materials. The performance of the whole system and of the single components is analyzed and the validity of the different simulation models is evaluated. Some remarks are also made for further improvements of the system.

Part of this work has been carried out in the framework of the Research Training Network "Thermo-Photo-Voltaic cells based on GaSb" (contract number HPRN-CT-2001-00199).

Contents

Nomenclature

Symbol	Meaning	SI units
$[R]$, $[P]$	reactant and product concentration	$\mathrm{mol\,m^{-3}}$
a, b, c	stoichiometric coefficient	-
A	surface	$\mathrm{m^2}$
$\dot{C}$	heat capacity flow	$\mathrm{W\,K^{-1}}$
c_p	specific heat capacity	$\mathrm{J\,kg^{-1}\,K^{-1}}$
d	diameter, pore size	m
D	diffusion coefficient	$\mathrm{m^2\,s^{-1}}$
D_{ij}	multicomponent diffusion coefficient	$\mathrm{m^2\,s^{-1}}$
D^T	thermal diffusion coefficient	$\mathrm{kg\,m^{-1}\,s^{-1}}$
E	emissive power	$\mathrm{W\,m^{-2}}$
E_a	activation energy	$\mathrm{J\,mol^{-1}}$
E_b	black body emissive power	$\mathrm{W\,m^{-2}}$
$E_{b\lambda}$	monochromatic black body emissive power	$\mathrm{W\,m^{-2}\,m^{-1}}$
E_g	cell bandgap	J
E_{ph}	photon energy	J
F	heat exchanger empirical temperature factor	-
F_{ij}	view factor	-
FF	fill factor	-
G	irradiation	$\mathrm{W\,m^{-2}}$
I	electric current	A
I_0	saturation current	A
I_b	black body radiation intensity	$\mathrm{W\,m^{-2}\,sr^{-1}}$
$I_{b\lambda}$	monochromatic black body radiation intensity	$\mathrm{W\,m^{-2}\,m^{-1}\,sr^{-1}}$
I_D	diode current	A
I_{sc}	short circuit current	A
I_ϕ	directional radiation intensity	$\mathrm{W\,m^{-2}\,sr^{-1}}$
$I_{\lambda\phi}$	monochromatic directional radiation intensity	$\mathrm{W\,m^{-2}\,m^{-1}\,sr^{-1}}$
J	radiosity	$\mathrm{W\,m^{-2}}$
J	current density	$\mathrm{A\,m^{-2}}$
J_{sc}	short circuit current density	$\mathrm{A\,m^{-2}}$
j	diffusive mass flux	$\mathrm{kg\,m^{-2}s^{-1}}$
K	overall heat transfer coefficient	$\mathrm{W\,m^{-2}\,K^{-1}}$
K	permeability	$\mathrm{m^2}$
K_λ	spectral extinction coefficient	-
K_R	rosseland mean extinction coefficient	-

l	characteristic length	m
$\dot{m}$	mass flow	$\mathrm{kg\,s^{-1}}$
M	molecular mass	$\mathrm{g\,mol^{-1}}$
N_e	monochromatic electron flux	$\mathrm{electron\,m^{-2}\,s^{-1}\,m^{-1}}$
P	power	W
p	pressure	Pa
q	heat flux	$\mathrm{W\,m^{-2}}$
$q(\lambda)$	monochromatic radiative heat flux	$\mathrm{W\,m^{-2}\,m^{-1}}$
Q	thermal power	W
R	ohmic resistance	Ω
R	thermal resistance	$\mathrm{m^2\,K\,W^{-1}}$
s	fuel to oxygen stoichiometric ratio	-
T	temperature	K
t	thickness	m
t	time	s
T_C	cell temperature coefficient	$\%\,\mathrm{K^{-1}}$
u	velocity	$\mathrm{m\,s^{-1}}$
V	voltage	V
V_{oc}	open circuit voltage	V
w	mass fraction	-
x	coordinate	m
x	molar fraction	-
x	tortuosity	-
y	coordinate	m
z	coordinate	m

Greek letters

α	absorptivity	-
α	convection heat transfer coefficient	$\mathrm{W\,m^{-2}\,K^{-1}}$
$\Delta_C H$	heat of combustion	$\mathrm{J\,mol^{-1}}$
$\Delta_f H^0$	enthalpy of formation	$\mathrm{J\,mol^{-1}}$
Δp	pressure drops	Pa
ΔT	temperature difference	K
ΔT_{LMTD}	Log Mean Temperature Difference	K
δ_{ij}	Kronecker symbol	-
ϵ	emissivity	-
ϵ	thermal effectiveness	-
ϵ_ϕ	directional emissivity	-
ϵ_λ	monochromatic emissivity	-
$\epsilon_{\lambda\phi}$	monochromatic directional emissivity	-
η	efficiency	-
θ	polar direction	rad
λ	air number	-
λ	thermal conductivity	$\mathrm{W\,m^{-1}\,K^{-1}}$
λ	wavelength	m
μ	dynamic viscosity	Pa s

ξ	pressure loss coefficient	-
ρ	density	$\mathrm{kg\,m^{-3}}$
ρ	reflectivity	-
τ	transmissivity	-
ϕ	fuel equivalence ratio	-
ϕ	porosity	-
ω	reaction rate	$\mathrm{kg\,s^{-1}}$

Subscripts

b	black body
c	cell, cold
e	effective, emitter
f	fluid
g	gas, glass
h	hot
in	inlet
max	maximum
MPP	maximum power point
out	outlet
ph	photon, photovoltaic
s	sensor, solid
w	wall, wire

Constants

c	=	$3{\cdot}10^{9}\,\mathrm{m\,s^{-1}}$	light speed
g	=	$9.81\,\mathrm{m\,s^{-2}}$	acceleration due to gravity
h	=	$6.626{\cdot}10^{-34}\,\mathrm{J\,s}$	Planck's constant
k	=	$1.380{\cdot}10^{-23}\,\mathrm{J\,K}$	Boltzmann's constant
q	=	$1.6{\cdot}10^{-19}\,\mathrm{C}$	electron charge
R	=	$8.314\,\mathrm{J\,K^{-1}\,mol^{-1}}$	gas constant
σ	=	$5.670{\cdot}10^{-8}\,\mathrm{W\,m^{-2}\,K^{-4}}$	Stefan-Boltzmann constant

Dimensionless numbers

Le	=	$\lambda/(\rho c_p D)$	Lewis number
Nu	=	$\alpha l/\lambda$	Nusselt number
Pr	=	$c_p\mu/\lambda$	Prandtl number
Re	=	$\rho\,u\,l/\mu$	Reynolds number

1

Introduction

1.1 TPV concept

The thermophotovoltaic (TPV) generation of electricity is based on the direct conversion of a thermal radiation coming from an emitter at high temperature into electric power by using photovoltaic (PV) cells. As shown in Figure 1.1 a heat source (generally a combustion process) is used to heat up an emitter material that converts the thermal power into radiation. The radiation reaches the PV cells and it is converted into electric power. Generally the temperature of the emitter varies in a range between 1100 K up to 1800 K so that the radiation power is high enough to allow this conversion technology to be competitive and feasible.

1.2 Comparison with PV technology

Although the principle of the radiation conversion is the same as for solar PV devices, TPV systems show several and important differences. In a PV system the radiation source is the sun, which can be assumed to act as a black body with a temperature of around 6000 K and which is far away from the earth (about $150\,10^6$ km). In a TPV device the temperature of the emitter is much lower, but the photovoltaic cells are placed much closer to it, in the range of a few centimeters.

To analyze these differences in more detail it is useful to recall some basic concepts of the thermal radiation theory. The power radiated by a black body per unit area per unit bandwidth ($\mathrm{Wm^{-2}\,m^{-1}}$) is given by the Planck's law of radiation:

$$E_b(T,\lambda) = E_{b\lambda}(T) = \frac{2\pi hc^2}{\lambda^5}\left[\frac{1}{e^{\frac{hc}{\lambda kT}}-1}\right] \tag{1.1}$$

Where λ is the wavelength (m), T is the black body temperature (K), h is the Planck's constant ($6.626\,10^{-34}$ Js), c is the speed of the light and k is the Boltzmann's constant ($1.380\,10^{-23}$ JK).

The total power density emitted by a black body corresponds to the total thermal radiation emitted over the entire wavelength spectrum and, according to the Stefan-Boltzmann law, is related to the fourth power of the absolute temperature:

$$E_b(T) = \int_0^\infty E_{b\lambda}(T)\mathrm{d}\lambda = \sigma T^4 \tag{1.2}$$

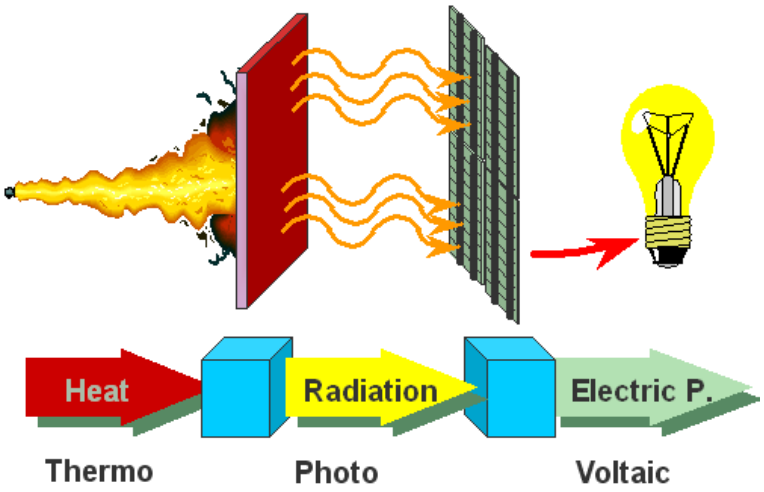

Figure 1.1: Principle of TPV conversion.

Where σ is the Stefan-Boltzmann constant ($5.670\,10^{-8}\,\mathrm{W\,m^{-2}K^{-4}}$).

Eq. 1.1 implies that a lower temperature (i.e. the temperature of the TPV emitter, here assumed for simplicity to act as a black body) corresponds to an emission spectrum shifted towards longer wavelengths (i. e. lower energy band gap). Indeed the wavelength λ_{max} at which the monochromatic black body emissive power $E_{b\lambda}$ has a maximum is inversely proportional to the emitter temperature (Wien displacement law). For TPV technology that means that using traditional Si cells, with a band gap of 1.1 eV, which corresponds to a wavelength limit of about 1.07 μm, a large part of the radiation absorbed by the PV cells would be lost in parasitic heating. This is shown in Figure 1.2, in which $E_{b\lambda}$ is plotted for different temperatures, together with the λ_{limit} of Si and GaSb cells, which have a band gap of 0.73 eV corresponding to a λ_{limit} of 1.7 μm. In order to overcome this problem, two different approaches can be followed:

- Cells with a low band gap are coupled to a broad band radiator at low temperature (900-1200 K): this would allow to exploit a bigger fraction of the emitted radiation but at the same time would imply higher thermalisation heat losses in the cells caused by the shortwave photons.

- Cells with high band gap are coupled to a selective emitter at high temperature (1200-1800 K) to realize a spectral selection of the emitted radiation. With an ideal optical system, made of a selective emitter and/or an optical filter, only photons close to the band gap energy would reach the cells while the long- and short-wave photons would be reflected back. This would allow to increase drastically the efficiency of the TPV device.

The second approach represents one of the fundamental peculiarities of the TPV conversion technology. The *spectral control* of the system is one of the key aspects for the success of this technology. TPV system configurations are normally in between these two opposite approaches. Both of them are described in more detail in the next chapter.

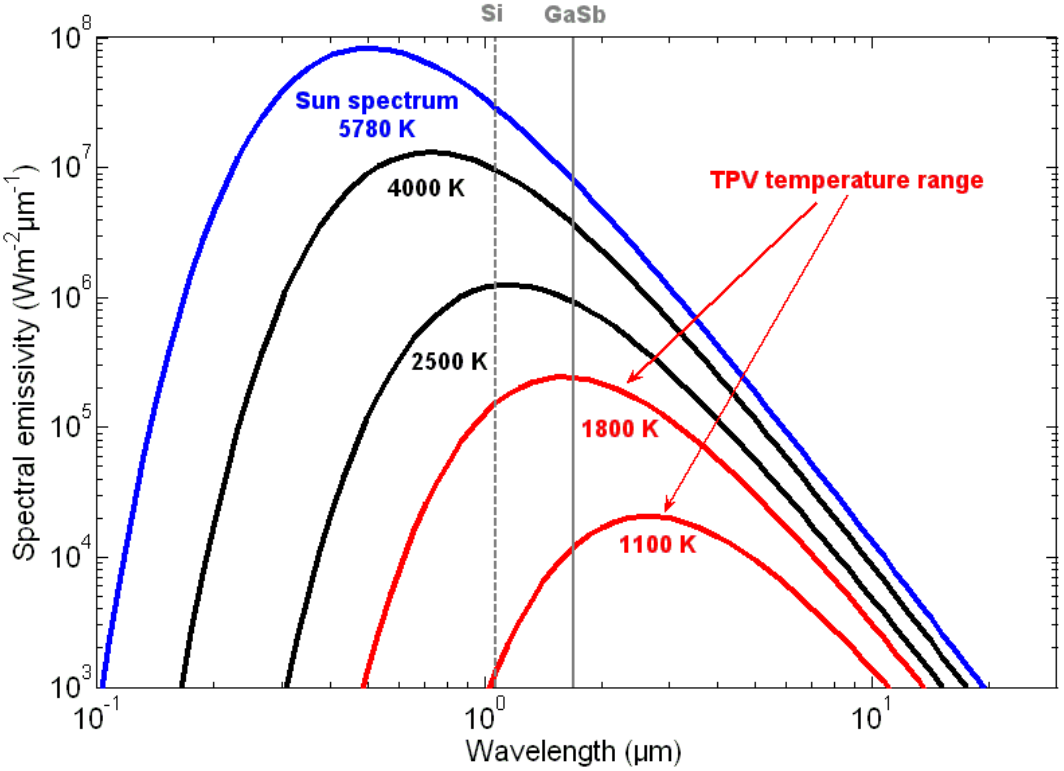

Figure 1.2: Black body spectral emissivity plotted in logarithmic axes, as function of the wavelength and of the temperature. The dashed and continuous vertical lines represent respectively the Si and GaSb cell bandgap.

Another key aspect that characterizes and makes the TPV technology different from normal PV is the high power density of the radiation. Because of the big distance between earth and sun and although the high temperature of the latter, the solar radiation incident on the outer earth atmosphere boundary has a power density of $0.135\,\mathrm{Wcm^{-2}}$, which becomes about $0.1\,\mathrm{Wcm^{-2}}$ on the earth surface because of radiation absorption by water vapour, CO_2 and other gases.

In TPV devices this value can be hundreds times higher, since emitter and cells are separated only few centimeters. Even if the power radiated by a surface varies with the fourth power of the absolute temperature (Eq. 1.2), the inverse square law of the power received, which depends on the distance between emitter and converter, is in this case dominant. Depending on the emitter temperature, radiation power density values up to $30\,\mathrm{Wcm^{-2}}$ can be reached. Therefore the power density output from a TPV converter is expected to be higher than that of a normal PV converter.

1.3 Historical background

The origin of the TPV technology goes back to the late 1950s and early 1960s. Most of the literature references [WWB61] [FBS64] [Bro95] [Cou99] [Nel02] [Nel03] cite Dr. Pierre Aigrain as the inventor of the TPV technology. Aigrain was visiting professor at MIT in late 1960 and early 1961. During a series of lectures he proposed a direct

energy conversion process consisting of a radiant emitter heated up by a flame and of a semiconductor photoconverter. However an internal report of MIT's Lincoln Laboratory proves that already in 1956 a first elementary TPV system has been realized: the U.S. Air Force, one of the funding agencies, was interested in developing techniques able to generate a small amount of electricity with fossil fuels. Dr Henry H. Kolm [Kol56] used a commercial camping lantern with a Welsbach mantle and a silicon solar cell to create a simple TPV device. He suggested also some improvements for the system and estimated a potential conversion efficiency of 5-10% for this new technology. No further research was carried out, however, at the Lincoln Laboratory. Recently Guazzoni [GM04] reported that Kolm met Dr. Aigrain in 1960 at a conference in Lyon and told him about his experimental experience. Dr. Aigrain was then aware of the Kolm research when he carried out his first studies on TPV.

The lectures of Dr. Aigrain were the input for a series of conference papers [WS67] and journal articles [Wed63] published by the MIT faculty and former MIT students. Most of the research work was concentrated on the development of Ge cells [G$^+$68] [Sch71].

The US Army at Fort Monmouth also played an important role in the development of the TPV technology in the 1960s. One of its objectives was to realize a portable power source with low noise and TPV was one of the best candidates for this purpose. Besides a monitoring work at university and industrial level to keep pace with the development of TPV, the research activity at Fort Monmouth contributed to the advancing of the technology in system design [KG72] and material studies [Gua72]. For the first time the high temperature emittance properties of the rare earth oxides has been reported and these materials were considered as potential emitters to be used in TPV systems.

In the same early period the interest of the industry for this new technology grew up too: General Motors (GM) in particular was very active in TPV research and development [Hau63]. In the framework of a TPV development programme the concept of a cell back surface reflector for spectral control was conceived and implemented for the first time [Wer63].

In the middle of the 1970s the TPV research suffered a significant slowdown and came almost to a halt. First the US Army decided to use thermoelectric as low-noise power source conversion technology, then GM stopped TPV development because of the energy crises and the need of improving the fuel consumption efficiency and the emission reductions.

However the energy crises of 1970s generated some interests in TPV for solar energy conversion. First studies concerning the possibility to shift the solar spectrum to longer wavelengths to match better the available PV cells were carried out [Hor77] [Swa80]. In the same period incentives for solar energy conversion supported the first research on solar TPV in Europe [WR79] [DM79]. In general in the 1980s the TPV research was not very active. This was mainly caused by the lack of funding: the photoconverters available for TPV applications (basically based on Si) were not of high quality and high values of efficiency could not be expected.

The situation changed when low-bandgap III-V devices became available. The utilization of cells based on these materials (GaSb, GaAs, InGaSb, ...) allowed both to exploit a larger part of the radiation spectrum and to use radiators at a temperature lower than that required for Si cells, making the TPV technology more feasible and

reliable. Furthermore, the parallel fast growth of electronic and opto-electronic technologies was fundamental for the development of crystal growth techniques and device fabrication based on the III-V compounds. In this sense the work of Fraas [F$^+$89] at Boeing, who developed and fabricated Zn-diffused GaSb cells, was a milestone for a new phase in the TPV research, based on the utilization of low-bandgap cells. Since the early 1990s several TPV research programmes started in US and the NREL (National Renewable Energy Laboratory) played an important role by sponsoring a series of TPV conferences. Also in Europe there was a renewed interest in the technology, with several institutes involved in the development of TPV systems (Fraunhofer ISE in Freiburg, Paul Scherrer Institut in Viligen and ISET in Kassel). As a further confirmation of the TPV activity in Europe, the last three international conferences on TPV were organized in Rome (2002), Freiburg (2004) and Madrid (2006).

In the last years TPV development seems to slowdown both in US and in Europe, mainly because of lack of funding and increased interest in other renewable energy sources and energy conversion technologies. There are still important international projects running (e.g. the FULLSPECTRUM project [L$^+$05] [L$^+$04]), but the very next future does not seem very promising as it was few years ago.

The technology did not reach yet a maturity and a quality sufficient to find concrete applications for the industrial market. The state of the funding and of the research on TPV looks like a perfect vicious circle: the potential to break down the critical limit of 10% of efficiency and therefore to gain the interest of the industry is there, but on the other hand the industry is not interested in investing in a technology that so far cannot guarantee to be competitive on the market.

2

TPV systems: components and state of the art

2.1 TPV system: overview and efficiency

TPV generation of electricity is a highly interdisciplinary technology. The conversion process of thermal radiation coming from the heat source into electricity includes several thermo-physical phenomena related to the different parts of the TPV system.

Basically a TPV device is composed by the following main components:

- Heating system: it releases the heat power needed to heat up the emitter. In a TPV device all the different heating techniques can be used to supply the thermal power (e.g. recuperative burner, solar concentrator, nuclear reaction)
- Optical system: it is composed by emitter, filter and a reflecting frame used to minimize the radiation losses between emitter and cells. The function of the optical system is to convert the heat power of the heating system into radiation and transfer it to the cells, realizing at the same time a spectral selection of the radiation.
- Thermophotovoltaic cells: they convert the radiation into electric power. Their design is slightly different from the normal PV cell one because the radiation density is very high. For the same reason it is fundamental to keep down their temperature by means of a cooling system to avoid their damaging.

In Figure 2.1 an example scheme of a fuelled-TPV system is shown. In this case the heating system consists of a recuperative heat exchanger and a combustion chamber.

Since a TPV device is composed by different components, its total efficiency can be seen as the product of all the efficiencies related respectively to each single energy transfer that takes place in the system. Referring to a fuelled TPV system, the following efficiencies can be defined:

$$\eta_{burner} = \frac{Q_{rad-burner}}{P_{chem}} \tag{2.1}$$

It is the efficiency of the recuperative burner unit, seen as the fraction of the chemical power P_{chem} supplied into the device and converted into radiation power $Q_{rad-burner}$.

$$\eta_{optical} = \frac{Q_{rad-cells}}{Q_{rad-burner}} \tag{2.2}$$

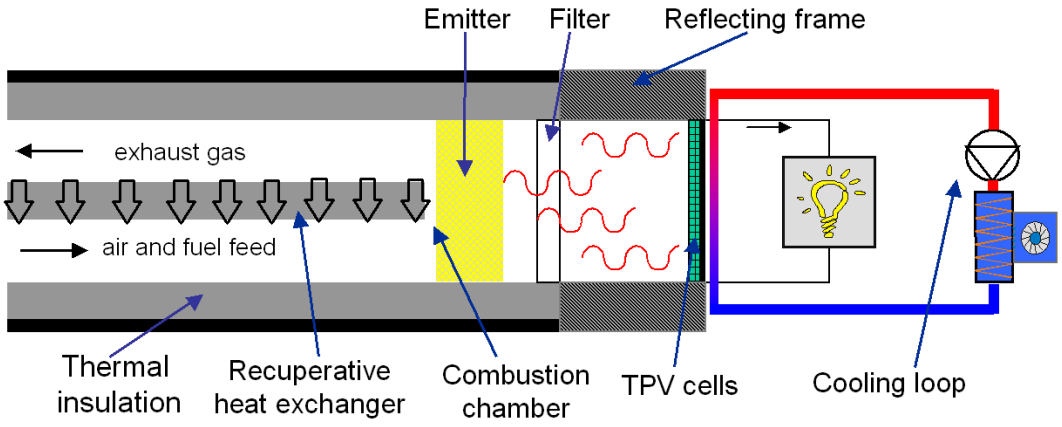

Figure 2.1: Simple scheme of a fuelled TPV system.

It is the optical-geometric efficiency: it can be seen as the ratio between the radiating power incident on the photocells $Q_{rad-cells}$ and the radiating power coming from the burner $Q_{rad-burner}$. It takes into account the losses caused by the absorption of radiation between the emitter and the cells.

$$\eta_{spectral} = \frac{Q_{rad-matching}}{Q_{rad-cells}} \tag{2.3}$$

The spectral efficiency describes how well the irradiation matches the absorption spectrum of the photocells. It corresponds to the part of the radiation incident on the cells that can be converted into electric power (i.e. the part of the radiation spectrum with wavelengths shorter than λ_{limit}).

$$\eta_{PV} = \frac{P_{el}}{Q_{rad-matching}} \tag{2.4}$$

The efficiency of the photocells corresponds to that part of the radiation convertible by the cells, which is finally converted into electric power.

The total efficiency of the system therefore depends on all the processes above described and corresponds to:

$$\eta_{TPV} = \eta_{burner}\,\eta_{optical}\,\eta_{spectral}\,\eta_{PV} = \frac{P_{el}}{P_{chem}} \tag{2.5}$$

In the following section the thermo-physical processes taking place in a TPV system and the efficiencies defined above are described in more detail. The state of the art of the different technologies involved is also given.

2.2 Heat sources available for TPV

An important peculiarity of the TPV technology is the possibility to use any heat source to heat up the emitter. The only requisite is that the temperature should be high enough for the TPV conversion. This makes TPV a flexible and versatile technology.

Several studies and designs for TPV systems have been proposed, based on different conventional and non-conventional heating systems. They can be resumed in the following list:

- Nuclear-fuelled TPV, based on a radioisotope general-purpose heat source (GPHS), conceived for deep space missions [SOK97] [Wil06].
- Bio-fuelled TPV, based e.g. on the combustion of wood-powder [BM94].
- Solar TPV, in which the solar radiation is concentrated by an optical system and can reach concentration ratio up to 4600 X [V$^+$06].
- Conventionally fuelled-TPV systems, in which the heat source is realized by combustion of either gaseous fuel (i.e. methane, propane, natural gas) or liquid fuel (i.e. diesel, hydrocarbon fuels). The majority of the TPV systems designed and implemented so far belongs to this last category.

The present work deals with conventionally fuelled TPV systems, focusing in particular on gas fuelled TPV.

2.3 Recuperative burner unit

In a fuelled-TPV system the burner provides the thermal power that must be converted into radiation. Generally a heat exchanger is coupled to the burner in order to recover the enthalpy of the exhaust gases at high temperature and to preheat the air and the fuel coming into the device. This allows to increase drastically the efficiency of the system and at the same time to reach a higher temperature in the combustion chamber (i.e. higher emitter temperature). In case of combined heat and power units (CHP units) the heat exchanger is used for heating purposes besides improving the electric efficiency of the TPV device.

2.3.1 Heat exchanger

Theoretical background

In a recuperative heat exchanger a cold fluid and a hot fluid flow in channels separated by a solid wall and exchange thermal power by convection and conduction. There are many different heat exchanger designs, which are derived basically from three fundamental heat exchanger typologies: counter-current, parallel flow and cross-flow (Figure 2.2). To evaluate the performance of an heat exchanger it is normal practice to refer to its thermal efficiency or effectiveness ϵ.

Referring to Figure 2.3 and assuming a specific heat capacity c_p (Jkg^{-1}K^{-1}) not dependent on the temperature, the heat exchanged by the two fluids is equal to:

$$Q = \dot{m}^h c_p^h \left(T_{in}^h - T_{out}^h\right) = \dot{m}^c c_p^c \left(T_{out}^c - T_{in}^c\right) \tag{2.6}$$

The superscripts h and c refer respectively to the hot and the cold fluid. The product $\dot{m}c_p$ can be seen as a heat capacity flux $\dot{C}$ (W K^{-1}).

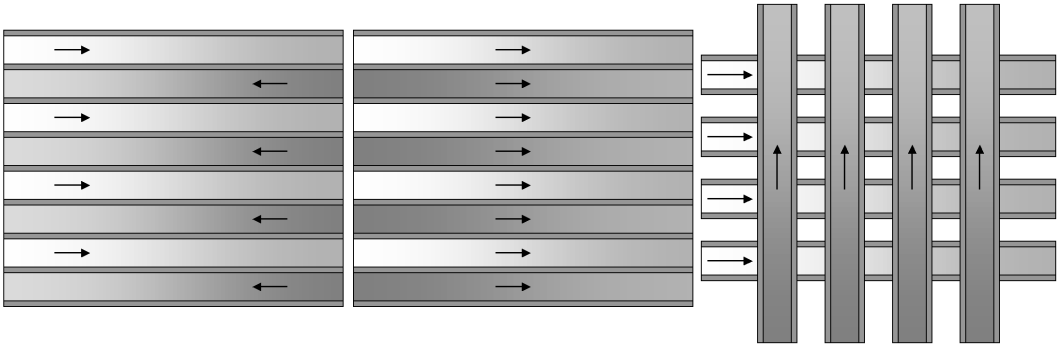

Figure 2.2: The three basic heat exchanger typologies: counter-current, parallel flow and cross-flow.

An ideal heat exchanger can be thought as a counter-current heat exchanger with an infinite heat transfer surface. Figure 2.3 shows the typical temperature profiles in counter-current and parallel flow types, compared with the temperature profile of an ideal heat exchanger. Under such hypothesis, the heat exchanged Q by two fluids in an ideal heat exchanger corresponds to the maximum thermal power that the two fluids can exchange:

$$Q = Q_{max} = \dot{C}_{min} \left(T^h_{in} - T^c_{out} \right) \tag{2.7}$$

with $\dot{C}_{min}$ referring to the fluid with the lower heat capacity flux.

The effectiveness ϵ of an heat exchanger, therefore, is defined as the ratio between the heat power Q exchanged in the real component and the power Q_{max} that the same hot and cold fluids, at the same inlet conditions $(T^c_{in}, T^h_{in}, \dot{m}^c, \dot{m}^h)$ can exchange in an ideal heat exchanger.

$$\epsilon = \frac{Q}{Q_{max}} \tag{2.8}$$

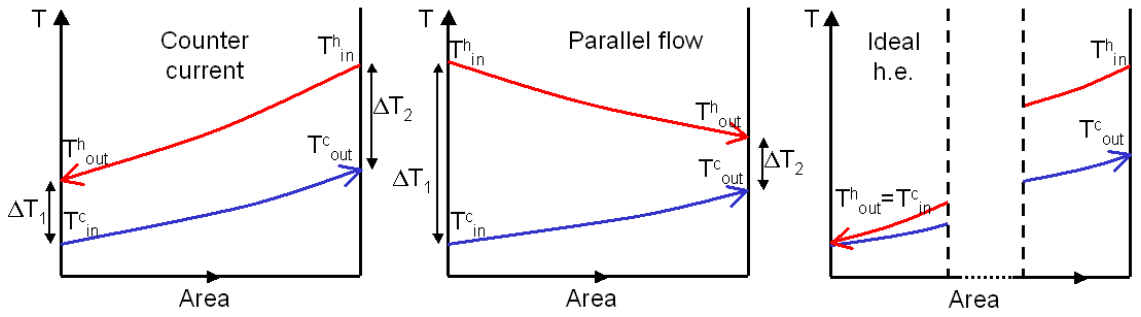

Figure 2.3: Typical temperature profiles in counter-current and parallel flow heat exchangers, compared with those of an ideal heat exchanger.

In order to evaluate which parameters are the most important in the design of an heat exchanger, it is useful to recall the expression normally used to estimate the heat flux exchanged in a heat exchanger:

$$Q = AKF\Delta T^{counterflow}_{LMTD} \tag{2.9}$$

Where A is the heat transfer surface, K is the overall heat transfer coefficient ($\mathrm{Wm^{-2}K^{-1}}$), F is an empirical temperature factor depending on the heat exchanger arrangement and ΔT_{LMTD} is the so called Log Mean Temperature Difference and referring to Figure 2.3 is defined as:

$$\Delta T_{LMTD} = \frac{\Delta T_1 - \Delta T_2}{\ln \frac{\Delta T_1}{\Delta T_2}} \tag{2.10}$$

The superscript *counterflow* refers to the counter-current case.

The overall heat transfer coefficient K ($\mathrm{W\,m^{-2}\,K^{-1}}$) corresponds to the total thermal transmittance between the two fluids and it is equal to the inverse of the total thermal resistance R_{tot} ($\mathrm{m^2\,K\,W^{-1}}$).

The heat transfer process between the two fluids can be seen as a series of three different processes: convection between hot fluid and channel wall, conduction through the channel wall and convection between cold fluid and channel wall. Therefore the total thermal resistance can be represented as the series of the three thermal resistances associated to each of these processes. In the case of fluids separated by a plane horizontal wall, it follows:

$$R_{tot} = R^c_{conv} + R_{cond} + R^h_{conv} = \frac{1}{\alpha_c} + \frac{t_w}{\lambda_w} + \frac{1}{\alpha_h} \tag{2.11}$$

Where t_w is the wall thickness, λ_w is the wall thermal conductivity ($\mathrm{Wm^{-1}K^{-1}}$) and α_c and α_h are the convection heat transfer coefficient ($\mathrm{W\,m^{-2}K^{-1}}$) between cold/hot fluid and wall. Therefore K corresponds to:

$$K = \frac{1}{\frac{1}{\alpha_c} + \frac{t}{\lambda_w} + \frac{1}{\alpha_h}} \tag{2.12}$$

The convection heat transfer coefficient α depends on the fluid cross section geometry, on the fluid dynamics conditions and on the fluid thermophysical properties. Normally α is calculated by using empirical expressions which are functions of the dimensionless Reynolds, Prandtl and Nusselt numbers:

$$Re = \frac{\rho u l}{\mu} \qquad Pr = \frac{c_p \mu}{\lambda} \qquad Nu = \frac{\alpha l}{\lambda} \tag{2.13}$$

In Eq.2.13 l is a characteristic length of the duct cross section, u is a characteristic fluid velocity and μ is the dynamic viscosity of the fluid. Generally, for fluids flowing in ducts, the convection heat transfer coefficient is expressed in the form:

$$Nu \propto Re^m Pr^n \tag{2.14}$$

with m and n positive constants smaller than the unity. Empirical expressions used to calculate the convection heat transfer coefficient for different configurations and flow patterns are available in any heat transfer book or heat exchanger manual [B$^+$85] [KB01].

Heat exchangers for TPV applications

Eq.2.9-2.13 point out the critical aspects related to heat exchanger design to take into account in the realization of the component. Some fundamental requirements must be fulfilled in order to optimize the heat transfer process, which are:

- Large heat transfer surface.
- High thermal conductivity of the heat exchanger walls/channels.
- Small dimension of ducts/channels (i.e. higher fluid speed): this improves the convection heat transfer coefficient, since $Re \propto l^{-1}$. However this implies also increased pressure drops and risk of noise and channel degradation. A compromise must be found in the final heat exchanger design.

Beside the requirements above cited, due to the extreme operating conditions, the heat exchangers for TPV applications must satisfy other specific needs, in order to ensure good performance and durability:

- Resistance to high temperatures and high temperature gradients (i.e. thermal shock). In this sense it is fundamental the choice of the materials: often the high temperatures reached in the combustion chamber do not allow to use even high temperature alloys. Ceramic materials (e.g. silicon carbide) are in these cases the only possible solution.
- Compact design and very good thermal insulation to minimize the heat losses.
- The inner walls of the heat exchanger must be impermeable to the fuel to avoid leakages. In case of not perfect sealing the negative pressure gradient between the inlet and the outlet of the exchanger would support the flow of fuel into the exhaust channels lowering the system efficiency and creating the risk of auto ignition. Therefore particular attention must be paid when materials are used, which have a porous structure or tend to deteriorate at high temperature in the long term.

Several heat exchanger recuperator designs for TPV applications have been proposed and realized. Most of them are based on the simple and very efficient counter current tube-in-tube configuration. In the inner channel the combustion air is supplied whereas the exhaust gas flows in the outer annular channel.

[SMH00] and [HMS02] used high temperature alloys (i.e. Inconel) to realize this component. The latter reports a recuperator efficiency of 61%, with a burner temperature of 1200 °C. An interesting modification of the tube-in-tube concept has been proposed by [FS+01]: it consists of a two-columns stack of rings and finned discs. The inner column, closer to the combustion chamber, is made of Inconel and stainless steel, the outer one of aluminum. The thermal efficiency reported for this recuperator is 75%, with an emitter temperature of 1275 °C. As further improvement [F+02c], the heat exchanger has been realized with a similar design, but using silicon carbide (SiC). [WC99] proposed a recuperator composed of two different sections: the first one, for the higher temperature area, is a simple convoluted wall ceramic heat exchanger made of SiC, able to reach up to 1425 °C but with a low efficiency. The second section consists of a cross-flow heat exchanger obtained by superposition of metallic layers: its efficiency is up to 80% but the design is complex and difficult to realize.

Another typology of heat exchangers that deserves a separate comment is the *regenerative heat exchanger* one. In a regenerative heat exchanger hot fluid and cold fluid occupy alternatively the same space (*bed*), which contains a matrix of material that

works as a heat sink or heat source for the fluid. This principle can be realized in two different ways. One possibility is that the bed is fixed and the flow directions are alternatively switched; in this case electro-valves are needed to regulate the flow direction. Otherwise the bed rotates and transfers continuously the heat absorbed from the hot fluid to the cold fluid and viceversa (rotary heat exchanger). Figure 2.4 shows the operation principle of both the typologies. Depending on the temperature of the hot fluid, metallic matrix or advanced porous ceramic materials (SiC typically) are used for the beds.

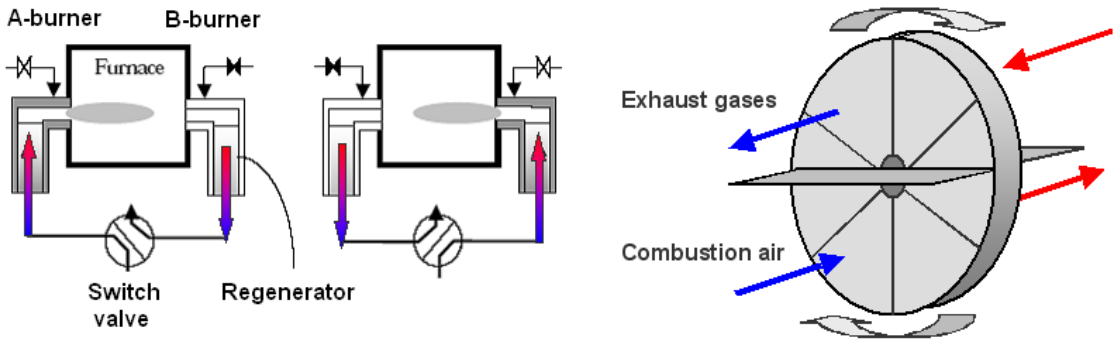

Figure 2.4: Regenerative heat exchangers: operation scheme for the two different typologies.

Regenerative heat exchangers are more complex than the recuperative ones: they have several components, some of them moving, and they need often a control system. On the other hand they present a much more compact and lighter design, a large exchange surface-to-volume ratio and they reach a very high thermal efficiency (up to 95%): important aspects that could make these component very attractive for the TPV technology.

Experimental working TPV devices with this type of heat exchanger are not reported so far in the literature. [CdRL03], [CdRL06] published a study where a regenerative rotating heat exchanger integrated in a TPV system is designed, simulated and tested showing a thermal efficiency of over 80%. [F$^+$02b] designed a TPV device based on the integration of a TPV cell array in a ceramic industrial furnace equipped with a commercial regenerative burner (200 kW of thermal power). A pilot furnace experiment with the regenerative burner and a water cooled silicon carbide emitter tube has been carried out showing promising results.

2.3.2 Burner unit

Combustion technology overview

The present section intends to give a quick theoretical overview on chemical reactions and combustion phenomena. The most important concepts are here cited and briefly described. More detailed explanations can be found in any thermodynamics and chemistry literature (e.g. [W$^+$01]).

Combustion is an exothermic chemical reaction between a fuel and an oxidizer (oxygen-containing substance), involving release of energy as heat. Generally the re-

action takes place in a small fraction of the available volume: the reaction zone or flame. A reaction example is the combustion of methane (CH_4) and oxygen:

$$CH_4 + 2O_2 \rightarrow 2H_2O + CO_2 \tag{2.15}$$

A combustion is defined as stoichiometric when the quantity of oxidizer is exactly the amount that is necessary to burn a quantity of fuel completely. In case of air-fuel mixtures it is common to refer to the air number λ, defined as:

$$\lambda = \frac{\left(\frac{x_{air}}{x_{fuel}}\right)}{\left(\frac{x_{air}}{x_{fuel}}\right)_{stoich}} = \frac{\left(\frac{w_{air}}{w_{fuel}}\right)}{\left(\frac{w_{air}}{w_{fuel}}\right)_{stoich}} \tag{2.16}$$

or to the reciprocal value, the fuel equivalence ratio ϕ ($\phi = 1/\lambda$). x and w are respectively molar and mass fractions. Pure fuel corresponds to λ=0 and ϕ=∞ while pure air corresponds to λ=∞ and ϕ=0. Each mole of dry air is composed by 0.78 mol of N_2, 0.21 mol of O_2 and 0.01 mol of noble gases, therefore $x_{air} = 4.762\, x_{O_2}$. This must be taken into account for a correct calculation of the stoichiometric fuel molar fraction.

The reaction in Eq.2.15 is an example of a global reaction. The overall combustion process indeed consists of a sequence of several *elementary reactions* in which very unstable and reactive species appear. The elementary reactions are the only ones that occur at molecular level exactly in the way described by the reaction equation. This series of reaction is called *detailed chemical mechanism* or *reaction mechanism* of a combustion process and it is fundamental to describe its kinetics.
Considering the following general reaction:

$$aR_1 + bR_2 + cR_3 \rightarrow dP_1 + eP_2 \tag{2.17}$$

The rates of reactants consumption and products formation are expressed by:

$$\frac{d[R_1]}{dt} = -a\omega, \qquad \frac{d[R_2]}{dt} = -b\omega, \qquad \frac{d[R_3]}{dt} = -c\omega,$$
$$\frac{d[P_1]}{dt} = d\omega, \qquad \frac{d[P_2]}{dt} = e\omega \tag{2.18}$$

with ω being the *reaction rate* and expressed in the form:

$$\omega = k[R_1]^{\alpha}[R_2]^{\beta}[R_3]^{\gamma} \tag{2.19}$$

where k is the so called reaction rate constant, $[R_i]$ is the concentration of the i^{th} reactant ($mol\,m^{-3}$) and the exponents α, β and γ depend on the reaction mechanism of the combustion process and define the order of the reaction. Only in case of an elementary reaction these exponents coincide with the stoichiometric coefficients *a, b* and *c* of Eq.2.17.

The reaction rate constant is given by the Arrhenius equation:

$$k = Ae^{\left(-\frac{E_a}{RT}\right)} \tag{2.20}$$

The quantities A and E_a are respectively the so called pre-exponential factor and the activation energy ($J\,mol^{-1}$): generally they are calculated from experimental tests or from

statistical mechanics. The activation energy corresponds to the energy that must be overcome in order to make a chemical reaction occur. R is the gas constant ($8.314\,\mathrm{J\,K^{-1}\,mol^{-1}}$) and T is the absolute temperature. Very important consequences of Eq.2.19-2.20 are that the reaction rate is not affected by the amount of products and it increases very fast with the temperature.

The heat produced by a combustion process is equal to the amount of fuel burnt multiplied by the heat of combustion ($\Delta_c H$), which corresponds to the heat released per mole of fuel, when the combustion is complete and both the reactants and the products are at 298.15 K and 1 atm. The heat of combustion can be obtained from experimental tests or it can be calculated as the difference between the enthalpy of formation ($\Delta_\mathrm{f} H^0$) of products and reactants:

$$\Delta_C H = \sum \nu_i \, \Delta_\mathrm{f} H_i^0 \tag{2.21}$$

where ν_i is the stoichiometric coefficient of the i^{th} species involved in the reaction.

Basically the combustion phenomena can be divided into two categories: premixed and not-premixed combustion. In a premixed combustion fuel and oxidizer are first mixed and then burnt. Referring to the definition of air number (Eq.2.16) a premixed flame can be divided into three groups: rich combustion, where $\lambda < 1$ and the fuel does not burn completely, stoichiometric combustion ($\lambda = 1$) and lean combustion, where $\lambda > 1$. The advantages of the premixed combustion are the simple control of the process and the uniform flame temperature profile obtained. Furthermore, by premixing at lean conditions, high temperatures are avoided with the consequence of low production of pollutant nitric oxides (NOx), and small amounts of soot are formed. On the other hand, in the premixed combustion the risk of explosion due to the collection of large volumes of premixed reactants and the risk of auto-ignition and backfire in case of preheating of the mixture make this process less safe than the not-premixed combustion.

In the not-premixed combustion fuel and oxidizer mix and burn simultaneously, with a more complex chemistry. The air number covers indeed the whole range of values, from 0 (fuel) to ∞ (air): as consequence not-homogeneous temperature profiles and temperature peaks are generated. Nevertheless the not-premixed combustion is generally preferred to the premixed one because the risks of explosion and auto ignition are not present.

A problem that must be faced in combustion technology is the high emission of NOx. Nitric oxides (NO and NO_2) are toxic and pollutant agents produced during combustion processes: their emissions increase drastically at very high temperatures. Traditional methods used to reduce the NOx emissions consist of realizing staged combustion and decreasing the peak temperature by using excess air or by recirculating part of the exhaust gases [Fla01]. Recently a patented technique [WW92] based on a flameless combustion (FLOX®) has been developed: it is based on mixing air and fuel with exhaust gases into a strong recirculating flow. In these conditions no temperature peaks occur and there is a drastic reduction of NOx.

Burner configurations for TPV applications

In a TPV system, burner configuration and emitter shape are strictly related. The fundamental aspects to consider for good system performances and high burner efficiencies

are:

- Optimization of the heat transfer between flame/exhaust gas and emitter;
- High emitter temperature (i.e. high power radiation density);
- Homogeneous temperature field all over the emitter surface;

The most common burner design used for TPV reported in literature is the radiant tube burner configuration: the combustion takes place in the inner part of the tube and the exhaust gases, while flowing back into the recuperator, heat the emitter, which is the impermeable outer wall of the tube (Figure 2.5). To improve further the heat transfer

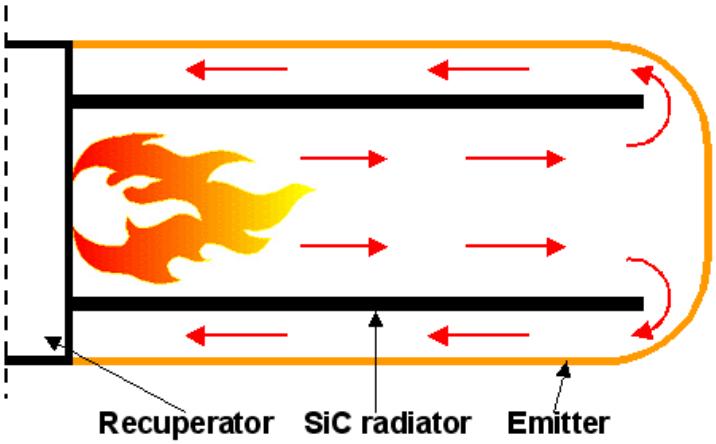

Figure 2.5: Concept of the radiant tube burner.

to the emitter a gray-body radiator tube made of SiC is inserted in the inner part of the burner, in direct contact with the flame. In this way the emitter is heated up both via convection by the exhaust gases flowing between the SiC tube and the external emitter wall, and via radiation by the SiC radiator itself. Several similar TPV burner arrangements have been proposed based on this principle, with both gas [FS+01] [AKG+04] and liquid fuels [D+99] [MSWC99] [HMS02]. A design based on a commercially available radiant tube with a FLOX® burner has also been developed and tested [F+02c].

In all the fuelled TPV systems with such a configuration the combustion process is a not-premixed one. This is done, as described in the section above, to avoid risk of explosion and backfire and to be able to preheat the combustion air.

Few authors report the burner efficiency η_{burner} measured in experimental tests: Horne [HMS02] reached a burner efficiency of 56.5% with a diesel fuelled-TPV system. Fraas reports a radiation to chemical power conversion ratio of 75% for a system able to operate with 8 kW of thermal power [FS+01] and of 70% for a recuperative burner unit based on a FLOX® burner able to supply 200 kW of thermal power [F+02b].

Besides the radiant tube burner configuration, where the emitter is impermeable to the fluids, there are other TPV systems in which the emitter is porous and permeable so that the flue gas flows through it or the combustion itself takes place in it (surface flame

type burner), heating the emitter to incandescence. This is the case of systems having the emitter made of a honeycomb [QH03], foam [BDP+04] or mantle ceramic structure [DBvRP03].

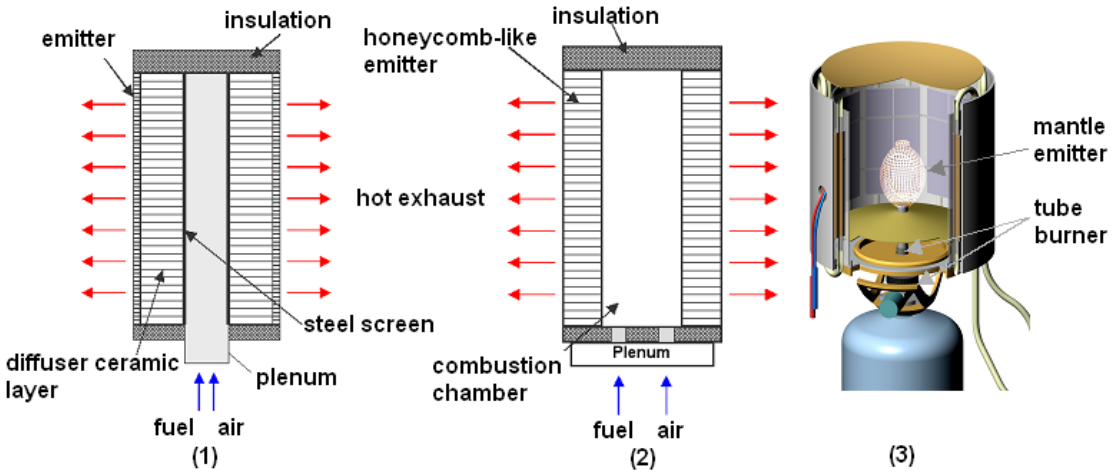

Figure 2.6: TPV burner configurations with premixed flame: (1) and (2) are burners coupled to honeycomb emitter [QH03], (3) shows a tube burner with a mantle emitter [DBvRP03].

Such TPV devices reported in literature are based on a premixed combustion burner design: Bunsen burner, metallic diffuser/rod system or plenum where air and fuel mix before the combustion are the possible configurations (Figure 2.6). In the latter case a stainless steel screen is used to prevent the propagation of the flame in the mixing chamber. In such burner units the heat recovering of the flue gas is absent or only partially carried out, implying a small burner efficiency: [QH03] reports η_{burner} up to 40% and [DBvRP03] of about 30%.

2.4 Optical system

2.4.1 Spectral properties and radiative heat transfer

The function of the optical system is to generate, select and transmit the thermal radiation to the cells. In a TPV system, the spectral control is fundamental in order to recover the part of the radiation spectrum that cannot be converted into electric power by the cells and that otherwise would be absorbed as thermal heat, reducing the system efficiency. The selection of the radiation is based on the fact that almost all the real surfaces do not behave as a black body, but they absorb only a part of the incident radiation.

Dimensionless quantities are used to describe the radiation properties of real surfaces: absorptivity α, transmissivity τ and reflectivity ρ represent respectively the fraction of the irradiation absorbed, transmitted and reflected by the surface and their sum is one, while the emissivity ϵ is defined as the radiation emitted divided by the radiation emitted by a black body at the same temperature:

$$\epsilon = \frac{E(T)}{E_b(T)} \tag{2.22}$$

These radiation properties are function of temperature T, wavelength λ and polar and azimuthal directions θ and ϕ.
Absorptivity and emissivity are related by the Kirchhoff's law, which states that for any surface they have the same value:

$$\alpha(\lambda, \theta, \phi, T) = \epsilon(\lambda, \theta, \phi, T) \tag{2.23}$$

At a given temperature T the monochromatic directional emissivity corresponds to:

$$\epsilon_{\lambda\phi} = \frac{I_{\lambda\phi}}{I_{b\lambda}} \tag{2.24}$$

$I_{\lambda\phi}$ is the monochromatic directional radiation intensity ($\mathrm{W\,m^{-2}\,m^{-1}\,sr^{-1}}$), which is the power emitted per unit bandwidth, per unit area projected in θ and ϕ directions, into a solid angle $\mathrm{d}\omega$ with spherical coordinates θ and ϕ. In the case of a black body, the intensity $I_{b\lambda}$ does not depend on the direction and it is related to the monochromatic black body emission by the relation:

$$E_{b\lambda} = \pi\, I_{b\lambda} \tag{2.25}$$

From the definition of emissivity and Eq.2.24, the monochromatic hemispherical emissivity is defined as:

$$\epsilon_\lambda = \frac{\int_{\phi=0}^{2\pi} \int_{\theta=0}^{\pi/2} I_{\lambda\phi}(T) \cos\theta \sin\theta \,\mathrm{d}\theta \mathrm{d}\phi}{\pi I_{b\lambda}} \tag{2.26}$$

while the directional emissivity is given by:

$$\epsilon_\phi = \frac{I_\phi}{I_b} \tag{2.27}$$

where I_ϕ and I_b are respectively the directional radiation intensity and the black body radiation intensity, which are calculated by integrating $I_{\lambda\phi}$ and $I_{b\lambda}$ over the whole radiation spectrum. Eq.2.22 can be rewritten as:

$$\epsilon = \frac{E}{E_b} = \frac{\int_0^\infty \epsilon_\lambda E_{b\lambda} \mathrm{d}\lambda}{\int_0^\infty E_{b\lambda} \mathrm{d}\lambda} \tag{2.28}$$

The numerator of Eq.2.28 corresponds to the total thermal emission of a radiation coming from a real surface at a given temperature T.

In case of an enclosure with several not black body surfaces, like in a TPV system, the radiative heat exchanged by each surface depends on the radiative properties and on the geometric disposition of all the surfaces. Assuming for simplicity that all the n surfaces are grey (i.e. they have constant spectral properties, reflect diffusively and are opaque), the net heat power exchanged by the i^{th} surface is:

$$Q_i = A_i(J_i - G_i) \tag{2.29}$$

where A is the surface area, G is the irradiation ($\mathrm{W\,m^{-2}}$), which is the radiation power incident on the surface and J is the radiosity ($\mathrm{W\,m^{-2}}$), which corresponds to the sum of the radiation emitted and reflected by the surface:

$$J_i = \epsilon_i E_{bi} + \rho_i G_i \tag{2.30}$$

Combining Eq.2.29 and Eq.2.30 yelds to:

$$Q_i = \frac{A_i \epsilon i}{1 - \epsilon i}(E_{bi} - J_i) \tag{2.31}$$

The incident radiation on the i^{th} surface $A_i G_i$ consists of the sum of the radiations from all the surfaces impinging on A_i:

$$A_i G_i = J_1 A_1 F_{1-i} + J_2 A_2 F_{2-i} + ... + J_n A_n F_{n-i} \tag{2.32}$$

where F_{i-j} is the so called $viewfactor$ and corresponds to the fraction of diffused radiation that leaves the surface A_i and reaches the surface A_j. Basing on the above equation and on the reciprocity property of the view factor ($A_i F_{i-j} = A_j F_{j-i}$) Eq.2.29 can be rewritten as:

$$Q_i = A_i \left(J_i - \sum_{j=1}^{n} J_j F_{i-j} \right) \tag{2.33}$$

While the radiation exchange between two surfaces A_i and A_j is given by:

$$Q_{i \rightleftarrows j} = (J_i - J_j) A_i F_{i-j} = (J_i - J_j) A_j F_{j-i} \tag{2.34}$$

Writing Eq.2.31-2.33 for each of the n surfaces, a $2n$ equation system for $2n$ unknowns is obtained and its solution gives the radiosity J and either the radiative heat power exchanged Q or the temperature T for each surface, depending on the surface boundary conditions specified. More detailed information on spectral properties and radiative heat transfer can be found in [SH92].

2.4.2 Spectral control in TPV systems

Spectral control in TPV system is based on the idea of exploiting the radiative properties of particular materials that present high values of ϵ_λ or τ_λ in the wavelength range corresponding to the cell bandgap and low values of both of them in the remaining part of the spectrum. An elementary scheme representing the optical system concept is shown in Figure 2.7. By recirculating the photons with energy lower than the cell bandgap the spectral efficiency $\eta_{spectral}$ (Eq.2.3) is increased with the consequences that a lower power is needed to reach the working temperature of the emitter and a lower heat load acts on the temperature-sensitive PV cells.

An ideal spectral control can be thought as an optical system that emits only in correspondence of λ_{limit} and reflects back to the heat source all the other wavelengths. That would mean a higher system efficiency since the heat losses caused by the thermalization of higher energy photons equal to zero, but at the same time such a design would imply a small radiation density reaching the cells and therefore a small output power density. The case with a high emission in the UV area, on the other hand, would increase the power density but at the same time the heat losses too. Therefore a compromise must be found in the design of the TPV optical system.

Basically all the optical systems proposed for TPV are composed by the following components:

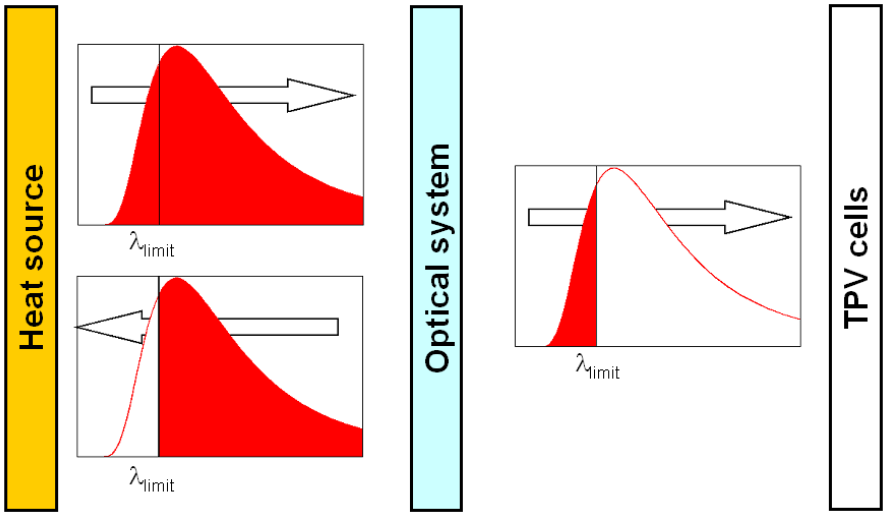

Figure 2.7: Optical system concept.

- Emitter: it can be either a selective emitter or a broad band emitter. The selective one theoretically presents a narrow bandgap with high emissivity values only in correspondence of the TPV cell bandgap and low ϵ_λ in the remaining part of the spectrum. A broad band emitter instead has high emissivity over the whole radiation spectrum.
- Filter: generally it is a low bandgap filter and it transmits only the photons with energy higher than the cell bandgap, reflecting back the rest of the radiation. It can be placed between emitter and cells or it can be directly deposited on the front surface of the cells.
- Anti-Reflecting layer: it reduces the number of convertible photons reflected by the cells. It is deposited on the front surface of the cell ($\lambda/4$ layer).
- Back surface cell reflector: layer generally made of gold to send back to the emitter photons which otherwise would pass through the cells.

As pointed out in the burner unit section, a fundamental requirement for the components of the system is the resistance to extreme thermal conditions: the emitter and the filter, if this is placed between emitter and cells, must be able to operate at very high temperatures without getting damaged or deteriorating. Therefore high melting point, low thermal expansion coefficient to assure thermal shock stability and high thermal conductivity to allow a uniform emission are the most important properties to look at in the choice of the component design. Such a problem does not concern the filter in case it is deposited directly on the cells: the cells are cooled down and the temperature on their front surface is not high enough to damage the filter.

2.4.3 Emitter materials

A quite comprehensive overview of emitter technology for TPV can be found in [Cou99] and in [Gom02]. The emitter materials used are either ceramic or metallic.

One of the most used materials as broad band emitter is the silicon carbide (SiC), which has a high emissivity, around 0.9, over the whole spectrum. This ceramic material withstands high temperatures (melting point of 2700 °C) and has a high thermal conductivity: properties that make it a good candidate for TPV applications, coupled to a IR filter [HMS02].

Another category of ceramic materials used for the spectral control is the series of rare earth elements (lanthanide series). Rare earth oxides have a very high melting point (over 2400 °C) and very good spectral properties since they radiate in a relatively narrow band of wavelengths. The peak band is determined by their composition and electronic structure (Figure 2.8). On the other hand they present low thermal shock

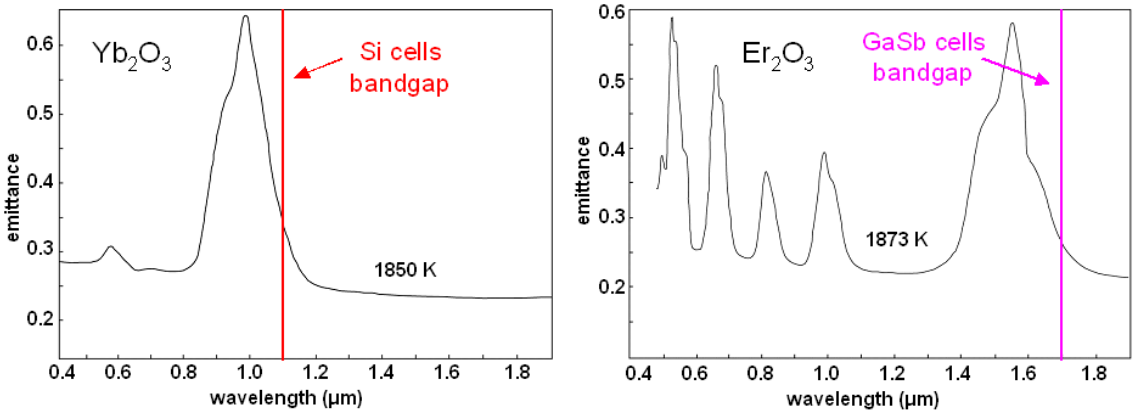

Figure 2.8: Monochromatic emissivity of ytterbium oxide and erbium oxide plotted respectively with the λ_{limit} of Si and GaSb cells [Gua72].

stability and low thermal conductivity. Ytterbium (Yb), erbium (Eb), thulium (Tm) and holmium (Ho) oxides are the most commonly used for those applications, depending on the bandgap of the cells. Different techniques have been developed to produce emitters based on these materials. Rare earth oxides-based emitters have been realized in a mantle structure [B+02], showing good radiative properties but poor mechanical resistance, or as a coating sprayed over a porous ceramic substrate (SiC) [BDP+04]. Another method proposed is to realize thin films of rare earth oxides and porous garnet structure (e.g. $Er_3Al_5O_{12}$) over refractory ceramic materials as SiC, graphite, alumina or over high temperature metals like tungsten and $MoSi_2$ [GC02], [DL+03]. The use of an intermediate low thermal emissivity layer could improve further the emitter selectivity [TD06].

A different class of lanthanide oxides-based materials are the Melt Growth Composites (MGCs) eutectic ceramics. MGCs have a microstructure, in which continuous network of Al_2O_3 and oxide garnet compound crystals interpenetrate without grain boundaries, presenting therefore excellent high temperature characteristics (operating conditions up to 1700 °C). These composites, developed recently, seem to fulfill very well the optical and mechanical requirements for TPV applications [NOWY05].

Metals have also been considered as emitters for TPV: they present generally a low emissivity in the mid (3-15 μm) and far infrared regions (15-1000 μm) and very good resistance at high temperatures. In particular tungsten has been proposed in combination with GaSb cells, since its emissivity peak coincides almost with the cell bandgap and

it has excellent thermal behavior up to 2000 K. On the other hand, like almost all the

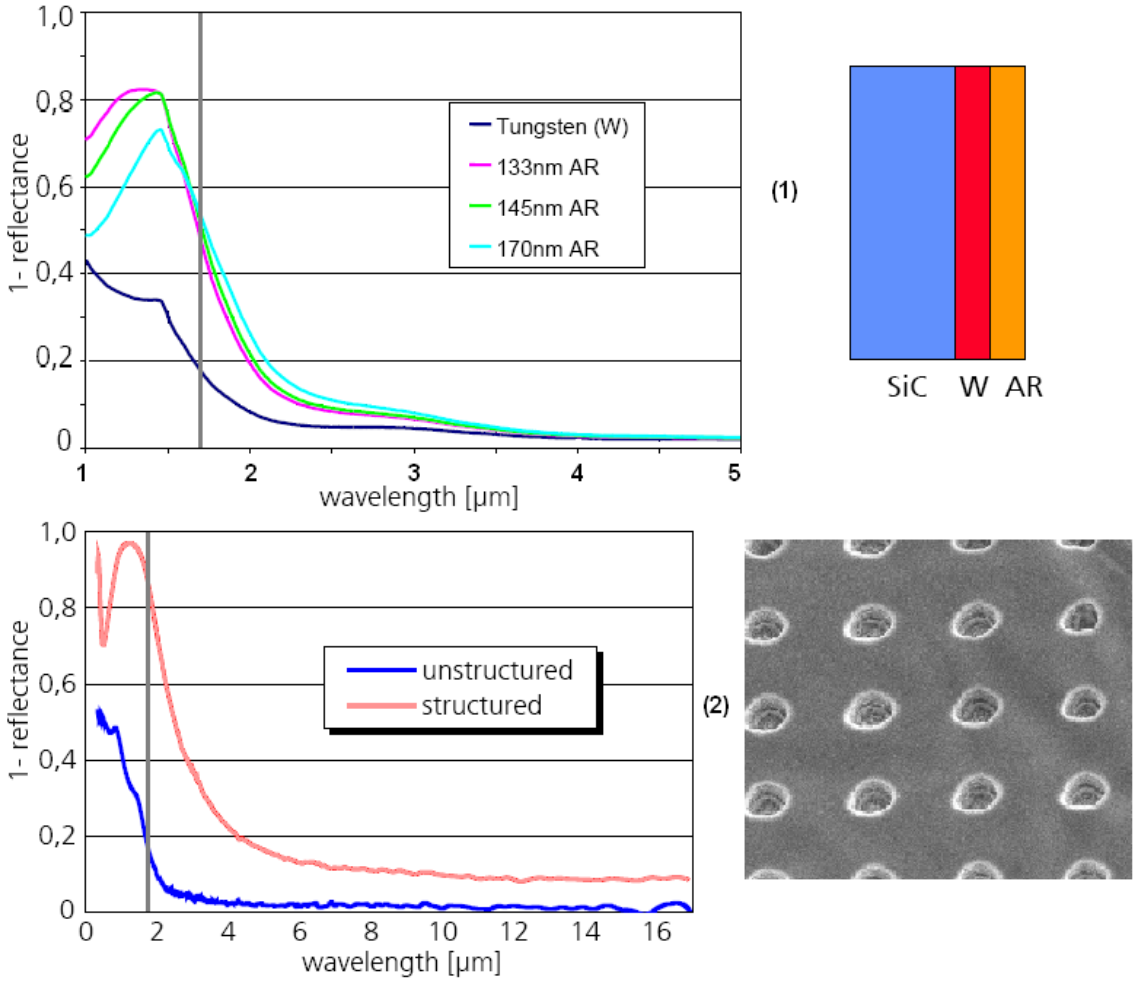

Figure 2.9: Tungsten radiative properties: the quantity (1-ρ) is plotted (1) comparing normal tungsten with tungsten coated with an AR coating of different thicknesses [FSAM00], and (2) comparing unstructured tungsten with surface relief gratings etched in tungsten [HBGW99].

metals, if used in air it oxidizes loosing its selective radiative properties. Therefore in TPV applications it can be used only in vacuum or in an inert gas atmosphere. Different techniques have been proposed to realize and improve tungsten-based emitters. An efficient and relatively simple method is to apply a dielectric AR coating on the metal [FSAM00](Figure 2.9). Other approaches aim to modify the tungsten radiative properties, i.e. realizing sharp emissivity peaks, by controlling and engineering the physical structure of the material (Figure 2.9). This is the case of tungsten 1D and 2D surface-relief gratings [HBGW99], [SKY02] or of tungsten 3D photonic crystals [FLEK$^+$02]. These last two approaches allow to realize a better and more selective spectral control, but present still the problem of structure durability caused by diffusion phenomena at high temperatures.
Besides tungsten also high refractory alloys have been considered for TPV applications: [RKS$^+$99] and [QH06] use alloys based on Fe, Cr and Al (Kanthal) to realize gas-fired metal radiant burners.

2.4.4 Filters and AR coatings

In TPV applications filters are generally used to reflect back to the emitter the part of the radiation with wavelengths longer than the cell bandgap. Basically filters for TPV can be divided in four different categories:

- Quartz glass: placed between emitter and cells, it acts as an absorptive filter, having high emittance values for $\lambda > 4\mu$m and high transmittance values in the lower wavelength range. Therefore only a part of the low energy photons reaches the cells eventually. Generally a quartz glass is used in a TPV system to protect the cells from the heat source and realize a first selection of the radiation reducing the thermal load on the cells. The quartz glass alone does not realize an efficient selection of the radiation and normally it is coupled to a more selective filter. Nevertheless there are examples of TPV applications where a single- or double-layer quartz glass window is the only filter present in the device [AKG+04], [DBvRP03].

- Interference (or dielectric) filters: they are low-pass filters realized as a multi-layer stack of thin-film dielectrics [D+99], [F+02c]. They operate based on the principle of interference: alternate layers of dielectrics (generally two materials, one with high and one with low refractive index) select the radiation reinforcing the transmission of certain wavelengths and interfering with other ones. They can be deposited over the cells to be kept at low temperature and not to deteriorate, or over a quartz glass placed between emitter and cells.

- Plasma filters based on Transparent Conducting Oxides (TCOs): they consist of a highly doped semiconductor layer deposited over the cells or over a dielectric substrate (e.g. glass) and have optical properties with a reflectance region like metals and low absorption regions like insulators [BMD+02]. Put in series with low-pass filters, they form a tandem filter that can reach very high spectral efficiency (up to 83% for a 0.52 eV bandgap cell [R+04]).

- Frequency Selective Surface (FSS) filters: they are realized as an array of metallic nanoscale antenna deposited on a dielectric substrate. They have spectral properties that make them good candidates for TPV applications [HMS02]: they act as a bandpass filter with a transmittance peak occurring at a frequency that can be tuned changing the antenna design. On the other hand, compared to the tandem filters, they present a higher absorptivity. Spectral efficiencies up to 64.3% (in combination with GaSb cells) are reported for FSS filters [HMHS04].

Together with or alternatively to the filter an AR coating is deposited over the cells to increase the radiation absorption in the sub-λ_{limit} region. The most common approach is to realize a coating with a single- or double- dielectric (interference) layer. Another technique proposed is based on the deposition of a coating made of TCOs [RVA+04].

2.4.5 Reflecting frame

Besides the spectral control of the system, to improve the system efficiency it is also crucial to minimize the part of radiation lost in the ambient or absorbed by internal

surfaces that do not realize an efficient spectral selection and convert part of the radiation into thermal losses.

From the optical point of view, an ideal TPV system would consist of a series of cell arrays disposed spherically around a small emitter, surrounding it completely so that all the thermal radiation impinges either the emitter or the cells. In real TPV systems this configuration is not realizable: besides emitter, filter and cells, other surfaces are involved in the thermal radiation heat transfer. To optimize the optical efficiency (Eq.2.2) these surfaces must have a very high reflectivity over the whole radiation spectrum and act as reflecting frames. Glass with thin gold (IR) mirror [DBvRP03], titanium shields [AKG+04] or simple reflecting mirrors [FS+01], [D+99] are some of the solutions applied to TPV devices reported in literature.

2.5 Thermophotovoltaic cells

2.5.1 Photovoltaic effect

The operation of photovoltaic cells is based on photogeneration of electrons and separation of charge carriers.

When a photon hits a semiconductor material with energy higher than the semiconductor band gap it can generate a electron-hole pair: the photon energy is absorbed by an electron with the highest energy level and bounded to neighboring atoms (electron in the valence band) exciting it to an energy level where the electron is free to move and generate current (conduction band). The hole generated by the missing electron can be occupied by another electron in the valence band: in this way a hole can move through the crystal lattice of the semiconductor material and mobile electron-hole pairs are generated. The average distance travelled by the charge carriers before recombination is called *diffusion length*. The band gap of a semiconductor material (i.e. the cell band gap E_g) corresponds to the energy gap between the valence band and the conduction band energy levels (Figure 2.10).

The photo-generated charge carriers are separated due to the p-n junction structure of the cells. A p-n junction consists of a semiconductor layer of the n-type (high concentration of outer electrons weakly-bounded to the atoms) and a semiconductor layer of the p-type (high number of holes) put together in close contact. Photovoltaic cells are large area p-n junctions. The higher concentration of electrons in the n-type layer generates diffusion of electrons in the p-type layer and recombination with the holes present in it. This diffusion current is balanced by an electric field caused by the unbalanced charge distribution. As a consequence, in steady state conditions, the area close to the junction where the diffusion process takes place and the electrostatic field is present does not have any moving charge carrier anymore and it is called depletion region (or space charge zone). The diffusion electric field acts as a separation medium in case that an electron-hole pair is produced after absorption of a photon with energy large enough: if the pair is generated on the p-side the electric field accelerates the electron into the n-side and viceversa if the absorption takes place in the n-side the generated hole is brought into the p-side. A prerequisite necessary for the charge separation is that the diffusion length must be large enough so that the charge can arrive into the depletion region.

When subjected to a voltage potential, the p-n junction behaves like a diode: applying a negative voltage to the n-region (forward bias) the diffusion voltage is reduced and the electric field strength in the depletion region decreases, with a resulting net diffusion current through the p-n junction. On the other hand, applying a positive voltage to the n-region (reverse bias), the depletion region increases preventing the diffusion current flow. The current-voltage characteristic (*IV curve*) of a diode is described by the Shockley diode equation (or diode law):

$$I_D = I_0 \left[\exp\left(\frac{qV}{kT}\right) - 1 \right] \tag{2.35}$$

where q is the magnitude of charge of an electron ($1.6\,10^{-19}$ C), V is the voltage across the diode, k is the Boltzmann's constant and T is the absolute temperature. I_0 is the so called saturation current of the diode.

If the n- and p-side metal contacts of the cell are galvanically connected, and high energy photons impinge on the cell, electrons flow through the connection from the n-type side to the p-side, where they recombine with the holes (Figure 2.10). The equivalent

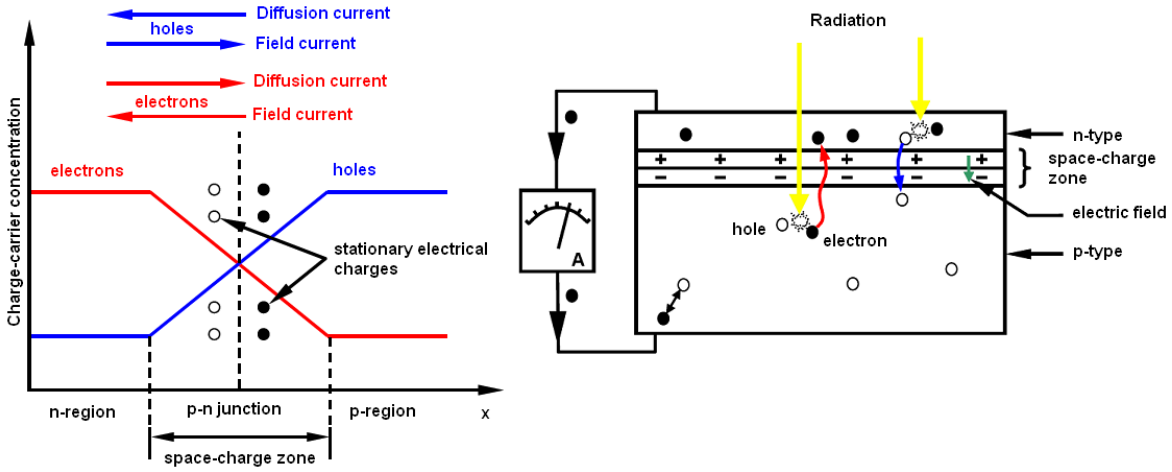

Figure 2.10: Distribution of charge carriers at a p-n junction and operating principle of a solar cell [KG99].

circuit for an ideal photovoltaic cell, therefore, consists of a photocurrent source I_{ph} and of a diode (p-n junction) and a resistor R_{load} connected in parallel (Figure 2.11). The current flowing through the load in the ideal case results:

$$I_{cell} = I_{ph} - I_D = I_{ph} - I_0 \left(\exp\left(\frac{qV}{kT}\right) - 1 \right) \tag{2.36}$$

Figure 2.12 shows the typical IV curve of a photovoltaic cell plotted together with the corresponding power curve. In case of shorting the contacts, the cell current equals the *short circuit current* I_{sc} and the power is zero. By increasing the load the power increases as well, reaching a maximum at the so-called *Maximum Power Point* (MPP) in correspondence of the current I_{MPP} and the voltage V_{MPP}. Increasing further the load the current decreases rapidly and in case of an infinite load (i.e. open circuit) reaches

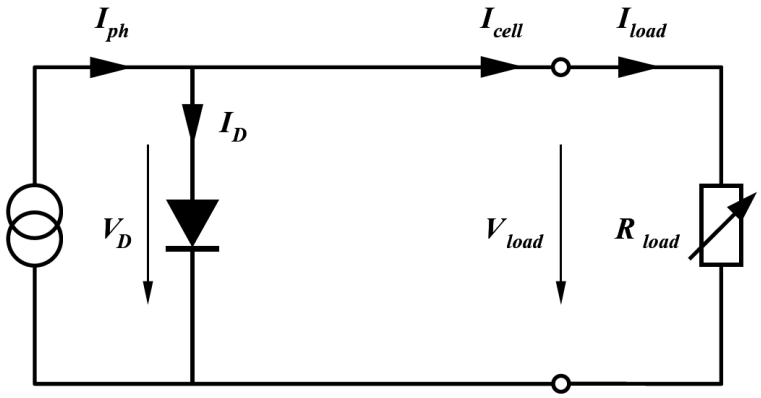

Figure 2.11: Equivalent circuit of an ideal solar cell.

zero, at the so called *open circuit voltage* V_{oc}. For higher values of the cell band gap E_g, under a constant black body radiation, I_{sc} decreases (there are less photons with energy higher than E_g) while V_{oc} increases. A parameter used to evaluate the quality of the cell

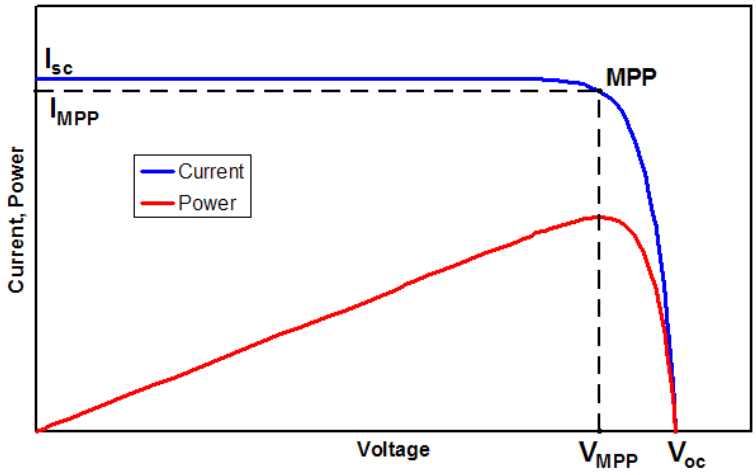

Figure 2.12: Qualitative IV and power curve of a photovoltaic cell.

is the *Fill Factor* (FF) which is expressed by:

$$FF = \frac{V_{MPP} I_{MPP}}{V_{oc} I_{sc}} \tag{2.37}$$

There are two main phenomena that limit the efficiency of the cell and must be taken into account to evaluate correctly its performance:

1. Photon absorption probability: this is expressed by the Quantum Efficiency (QE), which is the ratio of the electron-holes pairs generated to the number of photons with a given energy impinging on the solar cell. The QE therefore relates the response of a solar cell to the radiation spectrum and it is expressed as a function of the wavelength. The quantum efficiency is called External (EQE) when it refers

to all the incident radiation, including the part reflected or transmitted through the cell, while the Internal Quantum Efficiency (IQE) is calculated taking into account only the part of the radiation absorbed by the cell. For wavelengths longer than λ_{limit} the QE is zero.

2. Thermalisation: in case of photons with energy larger than the band gap, not all the energy of the photon is useful to generate an electron-hole pair, but only that part necessary to overcome the cell band gap E_g. The excess energy is dissipated as heat into the crystal lattice.

Figure 2.13 shows the equivalent circuit of a real photovoltaic cell connected to a load. Besides the diode and the load, two further resistances are present in the circuit: a series resistance (R_s) representing the bulk material resistance and the resistance of the front and back cell surface contacts, and a parallel resistance (R_p) representing leakage currents due to impurities present in the p-n junction causing a partial shorting of the junction. With reference to Figure 2.13 and Eq.2.35, it follows:

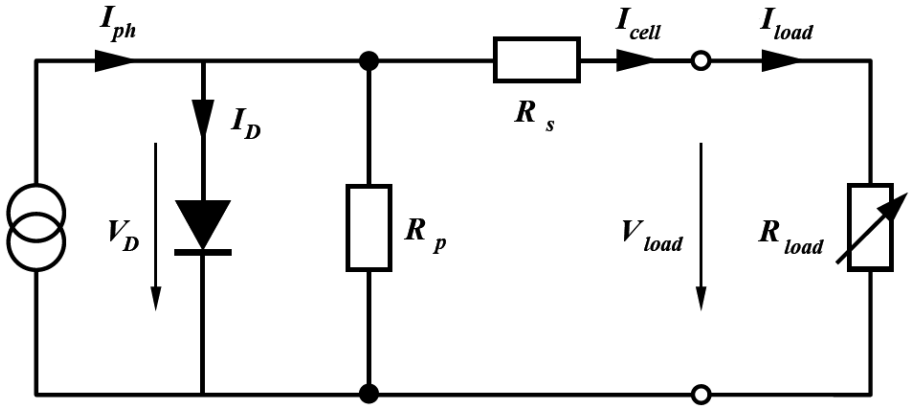

Figure 2.13: Equivalent circuit of a real solar cell [KG99].

$$I_{cell} = I_{ph} - I_0 \left(\exp\left(\frac{q}{kT}(V_{load} + I_{cell} R_s) \right) - 1 \right) - \frac{V_{load} + I_{cell} R_s}{R_p} \tag{2.38}$$

High R_s and low R_p affect the IV curve reducing the fill factor and therefore the cell performance.

Another important parameter that influences the behavior of the cell is the temperature. By increasing it I_{sc} increases slightly while V_{oc} decreases strongly. This temperature-depending behavior is generally taken into account by using cell temperature coefficients, which are experimentally measured and define the percentage variation of the cell parameters per temperature degree. For example for Si solar cells the short circuit current temperature coefficient $T_{c-I_{sc}}$ is about 0.07 %/K, the open circuit voltage temperature coefficient $T_{c-V_{oc}}$ is -0.4 %/K and the MPP temperature coefficient $T_{c-P_{MPP}}$ is -0.4 %/K. For GaSb cells, under a radiation density corresponding to one sun, these values are respectively around 0.03 %/K, -0.59 %/K and -0.76 %/K; at higher radiation densities the absolute values of $T_{c-V_{oc}}$ and $T_{c-P_{MPP}}$ decrease slightly, improving the cell performance [SAB+05]. More details and explanations concerning this topic can be found in any specific book (e.g. [Gre92]).

2.5.2 Characteristics and efficiency measurement of TPV cells

According to Eq.2.35 I_{sc} and V_{oc} increase respectively linearly and logarithmically with the irradiation; the fill factor increases as well with the open circuit voltage. Therefore at higher radiation densities the performance and the efficiency of the cell improve. Nevertheless the higher current density implies also higher series resistances. For this reason cells for TPV applications, like all the concentrator cells, present a design slightly different from normal PV cells: in order to minimize the resistance losses and increase their efficiency they are realized with a low-resistivity substrate and the top contact grid has finer fingers in a larger number.

Unlike the solar PV technology, in TPV there are not yet reference conditions to measure the efficiency of a TPV cell because the spectrum of the incident radiation is not constant, like the solar radiation, but depends on the characteristics of the optical system. A simple method to calculate the efficiency of a TPV cell is described in [SDOB04] and it consists of the following four steps:

1. Measurement of the cell EQE.

2. Calculation of the short circuit current density J_{sc} (unit of Am^{-2}) of the cell subjected to a well defined TPV emitter spectrum. J_{sc} can be expressed as the ratio between the radiation energy and the photon energy (i.e. number of photons) at a wavelength λ multiplied by the EQE and integrated over the usable part of the spectrum:
$$J_{sc} = \frac{1}{hc} \int_0^{\lambda_{limit}} E_\lambda \lambda \, EQE \, \mathrm{d}\lambda \tag{2.39}$$
with h being the Planck's constant and c the light speed.

3. Measurement of IV curves under different illumination levels to derive V_{oc} and FF versus J_{sc}.

4. Determination of the cell efficiency for any spectrum by using $V_{oc}(J_{sc})$ and $FF(J_{sc})$. The IV curves do not depend on the radiation spectrum as long as the short circuit currents generated are the same.

Therefore the TPV cell efficiency (Eq.2.4) is expressed as:
$$\eta_{PV} = \frac{P_{el}}{Q_{rad-matching}} = \frac{FF \, J_{sc} \, V_{oc}}{q_{rad-matching}} \tag{2.40}$$

2.5.3 Cell types and state of the art

As described in 1.2, all the TPV configurations can be referred to two basic cases: low band gap cells with a low temperature broad band emitter and high band gap cells with a high temperature selective emitter. Thus it makes sense to classify cells used for TPV applications in high-, medium- and low-band gap cells. Presently most of the work on TPV devices is focused on III-V semiconductors. The following sections give a general overview on these three categories of cells, pointing out their advantages and disadvantages, and present the most recent results reported in literature. A detailed description of the different techniques used to realize and characterize materials and

cells goes beyond the purpose of this work. A detailed overview on these topics can be found in [And02], [Bit03], [Wan04] and [WAA+04].

High band gap cells

Silicon cells ($E_g = 1.1\,\text{eV}$) have been proposed for TPV applications in the past years. Their technology is very well known and they are so far the cheapest cells available on the market. TPV systems based on commercial Si cells have been successfully built and showed promising results [BMD+02]. Nevertheless, because of their high band gap, these cells have a limited efficiency and require a very high emitter temperature in order to reach acceptable power density outputs (over 1800 K). For these reasons and the contemporary development of middle- and low-band gap cells with higher efficiencies, Si cells are not considered interesting anymore for TPV applications.

Middle band gap cells

Cells with a band gap of about 0.7 eV are currently the most investigated for TPV systems. This band gap corresponds to the spectrum peak wavelength λ_{max} in the case of a black body at 1600 K. Their combination with rare earth or metal emitters allows to reach a convertible radiation power about twice bigger than the Yb_2O_3 emitter-Si cells configuration.

GaSb cells ($E_g \simeq 0.7\,\text{eV}$) are so far the cells with the most mature technology and present the highest values of efficiency. Recent experimental results [SDOB04], [V+06] showed cells with EQE in the range of 80-88%, V_{oc} up to 0.49 V and FF over 0.7 for a current density of $5\,\text{Acm}^{-2}$. Coupled to a tungsten emitter at 1900 K they reached an efficiency of 27% with spectral cut-off at 1820 nm. However a method for the series production of the cells has not yet been developed.

Ge cells(E_g=0.66 eV) have also gained interest for TPV applications: even if they have a lower efficiency than GaSb cells, they are much cheaper and have a higher reflectivity in the infrared region. Efficiencies of 16% have been shown for Ge cells in combination with tungsten spectra at 2000 K (FF=0.7) [FDO+06].

Other TPV cells still under development are based on ternary and quaternary semiconductors, thus on a more complex and expensive technology. The spectral response of such cells can be controlled by varying the alloy composition. For middle band gap cells two different heterostructures are under development: the ternary alloy InGaSb on InP substrate with a band gap ranging from 0.5 up to 0.73 eV (limited by lattice mismatch to the higher values) and the quaternary alloy InGaAsSb on GaSb substrate, with a band gap range between 0.5 and 0.7 eV. In particular lattice matched $In_{0.53}Ga_{0.47}As$/InP cells (E_g=0.73 eV) present good characteristics and performances for TPV applications.

Low band gap cells

The possibility to use low band gap cells ($E_g < 0.5\,\text{eV}$) for TPV has been investigated only recently and seems attractive for low temperature applications (less than 1200 K). The realization of such cells is still in a first development phase and it is based on quaternary semiconductor alloys: GaInAsSb on InAs substrate and InAsPSb on GaSb or InAs substrate [GAG+06] are the two heterostructures proposed for this type of cells.

2.5.4 Cell cooling system

In operating conditions the part of the radiation which is nor reflected neither converted into electric power is absorbed as heat load by the cells. For a safe and efficient operation of the TPV system this heat flux must be dissipated: cells at high temperature, indeed, are less performing (negative MPP temperature coefficient) and are exposed to risk of damage and degradation for temperatures higher than 60-70 °C. Therefore it is fundamental to apply the cells over a heat sink (generally aluminum or copper) cooled by air or water. A critical aspect in the TPV cell thermal management is to realize a good thermal contact between heat sink and cells and to assure the series connection of the cells: the substrate of the heat sink must have high thermal conductivity and must be at the same time an electrical insulator to avoid the shorting of the cell back contacts. Furthermore its thermal expansion coefficient should be close to that of the cells to avoid mechanical stress. Aluminum nitride (AlN) and beryllium oxide (BeO) with λ respectively over $140\,\mathrm{Wm^{-1}K^{-1}}$ and over $250\,\mathrm{Wm^{-1}K^{-1}}$ are ceramic insulator materials that fulfill these requirements and are used for TPV cell substrates.

2.6 TPV systems: state of the art

In these last years several TPV designs have been proposed and simulated theoretically but eventually only few of them have been practically realized and tested successfully with all their components installed. The development of TPV systems includes not only the design of the single components, but also their assembling into a complete and operating device and very often it is this final step that presents practical problems not taken into account in the preliminary theoretical work.

Table 2.1 gives an overview of the TPV systems developed and tested successfully in these last years, with their characteristics, operating conditions and performances. All the models except the Midnight Sun® are based on a cylindric system configuration and have water-cooled cells. In most of the cases the cells used are based on GaSb. The cells price represents still a limit for the realization of high power output TPV systems: the 1.5 kW and 5 kW prototypes proposed by Fraas could not be tested experimentally because of the large amount of cells required. Many of these systems are conceived as CHP devices, for heating purposes. The highest system efficiency obtained experimentally is 5.9%, for the diesel fired system developed by Horne. The next target of the TPV research community in the short-term is to break the 10% efficiency threshold.

2.7 TPV technology: advantages and limits

After presenting and describing the different processes and components involved typically in a thermophotovoltaic system it makes sense to recall briefly the main characteristics of TPV pointing out why TPV can be an attractive and interesting energy conversion technology. The potential advantages of this technology are the followings:

- Robust and reliable technology: in a TPV system there are not moving parts, therefore low maintenance is required.

TPV system	Design characteristics	Operating conditions	Performance
50 W prototype [Bit03]	Butane fuel, no recuperator, Si cells, Yb_2O_3 mantle emitter, Glass with gold coating mirrors, Tap water cooling (14 °C).	$P_{thermal}$: 2 kW $T_{emitter}$: 1735 K T_{cells}: 23 °C	P_{output}: 47.9 W $P_{density}$: 0.1 Wcm^{-2} η_{burner}: 30% η_{TPV}: 2.4%
200 W prototype [Bit03]	Similar to the 50 W system, No recuperator: CHP purposes, Yb_2O_3 foam emitter.	$P_{thermal}$: 16 kW	P_{output}: 86 W η_{TPV}: 0.54%
Midnight Sun [FBH+99]	Propane fuel, no recuperator, CHP, GaSb cells, SiC emitter, dielectric filter.	$P_{thermal}$: 7.3 kW $T_{emitter}$: 1470 K T_{cells}: 75 °C	P_{output}: 100 W $P_{density}$: 0.4 Wcm^{-2} η_{TPV}: 2%
1.5 kW residential TPV CHP [FS+01] [F+02c]	Propane fuel, low NOx radiant tube burner, tube-in-tube recuperator, GaSb cells, ARW foil on SiC tube, dielectric filter on a outer quartz glass tube, Inert atmosphere between SiC and glass tube.	$P_{thermal}$: 12 kW $T_{emitter}$: 1520 K T_{cells}: 50 °C	P_{output}: 1.5 kW * $P_{density}$: 1 Wcm^{-2} * $\epsilon_{recuperator}$:0.75 $\eta_{spectral}$: 75% η_{TPV}: 10.8% *
5 kW generator tubes [F+02b]	Tube placed in a furnace Emitter surrounds cells array, GaSb cells, Al_2O_3 tube coated with ARW foil, dielectric filter.	$P_{thermal}$: 200 kW $T_{emitter}$: 1430 K	Whole system not tested $P_{density}$: 0.76 Wcm^{-2} η_{burner}: 75%
Portable diesel TPV system [HMS02]	Diesel fuel, recuperator, GaSb cells, SiC emitter, infrared FSS band-pass filter, Double wall evacuated quartz tube between emitter and cells, Reflecting gold coating.	$P_{thermal}$: 3130 W $T_{emitter}$: 1470 K	P_{output}: 185 W $P_{density}$: 0.85 Wcm^{-2} $\epsilon_{recuperator}$: 0.61 η_{burner}: 63% $\eta_{optical}$: 88% η_{TPV}: 5.9%
Low band gap cells system [QH02]	Natural gas fuel, partial heat recovering, InGaAsSb cells (0.53 eV), SiC emitter, optical short-pass filter.	$P_{thermal}$: 6.9 kW $T_{emitter}$: 1190 K	$P_{density}$: 0.54 Wcm^{-2} P_{output}: 160 W η_{burner}: 26% $\eta_{spectral}$: 42% η_{TPV}: 2.3% *
Fraunhofer ISE prototype [AKG+04]	Methane fuel, partial heat recovering, GaSb cells, SiSiC tube coated with tungsten, Reflecting titanium shield, inert argon atmosphere.	$P_{thermal}$: 1.8 kW $T_{emitter}$: 1470 K T_{cells}: 50 °C	$P_{density}$: 0.2 Wcm^{-2} η_{burner}: 60% η_{TPV}: 1.7% +

*: not yet experimentally demonstrated

+: extrapolated from the best cell array tested to the 16 modules case

Table 2.1: TPV systems: state of the art.

- High power density output: power densities higher than $1\,\mathrm{Wcm^{-2}}$ can be obtained, hundred times higher than normal PV.
- Versatile usage of fuel: any heat source can theoretically be used to heat up the emitter.
- High cell efficiency thanks to the spectral control and the photon recycling.
- Suitable for CHP applications: the thermal power can be recovered through an heat exchanger for heating purposes.

Despite these positive aspects, TPV did not reach yet a mature state. The efficiencies reported so far are still lower than 10%. Further development is needed to make the technology interesting for the industrial market.

The biggest limit of TPV is represented by the high temperatures required in operating conditions and therefore by degradation and thermal stress phenomena: there is still too few experience and knowledge on materials withstanding high temperatures (over 1600 K) and high temperature gradients, which can be used in TPV systems.

Furthermore there is not yet a safe and relatively cheap method for the series production of GaSb cells, the most used so far in TPV technology: this limits the development and testing of large TPV systems. Even more complex is the realization of ternary and quaternary semiconductor-based cells, but the semiconductor technology has been putting more effort on this field recently.

Besides these practical problems it must be pointed out that TPV is a complex technology and the total system efficiency depends not only on each single process efficiency (Eq.2.5), but also on the whole system design and arrangement: each single component must be optimized not independently, but taking into account its interactions with the other parts of the system. The multidisciplinary character of TPV requires experience and knowledge on different technology fields (burner, radiator, photovoltaic and heat recuperation technologies). Seldom a research institute can deal with all these topics: therefore partnerships play a fundamental role to increase experience and knowledge on TPV and support its development.

Nevertheless, for some specific applications, TPV could be very soon an attractive and feasible energy conversion technology and play an important role in some niche market areas, as described in the next section.

3

Market applications and economic analysis

3.1 TPV applications

At the moment TPV is still in a development and prototyping phase: low efficiencies and high system costs are the main issues to overcome to realize competitive commercial applications. One of the main limits is given by the high price of the middle- and low-band gap cells, since they cannot yet be realized with a low cost series production technique. Presently the few data available show a GaSb cell price of $10000\,\$\,\mathrm{kW}^{-1}$. The target is to reach a price of $2000\,\$\,\mathrm{kW}^{-1}$ in the short term and of $300\,\$\,\mathrm{kW}^{-1}$ in the long one [FAH03].

Even if TPV did not reach yet a mature state, its main characteristics (fuel versatility, high density power output, safety and reliability, no moving parts, no noise) make it an attractive technology in different energy production fields. Basically TPV devices are feasible for systems where a small amount of power is required, in a range from some W to some kW, and where high temperature processes are involved.

In particular applications, although the TPV-generated energy price is still very high, TPV could be very soon competitive with other conversion technologies currently available. These applications are resumed in the following list and are analyzed in more detail in the next sections:

- Solar thermophotovoltaic
- Small power supply for off-grid applications
- Auxiliary Power Unit
- Portable generators
- Off-grid heating appliances
- Cogeneration (CHP units)
- Waste heat recovering

Solar thermophotovoltaic

Solar thermophotovoltaic systems (STPV) represent one of the most promising TPV applications. In STPV, solar concentrators (e.g. Fresnel lens or meniscus lens) are used to focus the solar light on the emitter material with concentration ratios up to 4600 X. On one side the selective emitter decreases the radiation quality reducing its temperature, but on the other hand it operates a spectral control, together with filter and cell AR coating: the useless part of the radiation, which in normal PV concentrator is lost, is re-sent to the emitter as an additional power and recycled so that higher system efficiencies can be reached. The high concentration ratios imply a very high emitter temperature (over 2000 K) and therefore a power density higher than in normally heated TPV systems.

Compared to normal PV, STPV requires a much smaller cell active area and offers the possibility to reduce the system costs, since the cells are the most expensive component. On the other hand solar concentrators have generally the disadvantage of using only a fraction of all the solar radiation, not being able to concentrate the diffuse and scattered part of the light.

Recent studies [V$^+$06] showed that system efficiencies of 24% and 29% are possible with respectively GaSb based cells and tandem TPV cells.

Small power supply for off-grid applications

Off-grid systems requiring a small and continuous amount of power (50-100 W) are the ideal candidates for the use of TPV systems and their commercialization in the near future.

In this type of off-grid applications two system configurations are possible: a single generator or a hybrid system, based for example on PV arrays. In the latter case the use of a small TPV system as back-up generator can be advantageous, reducing significantly the costs of the whole system.

Stand alone photovoltaic systems used for telecommunication, data transmission and telemetry represent therefore an accessible, attractive and relatively big niche market for TPV: only in Germany some thousands of such systems are installed every year [RS01]. That would mean a potential worldwide market for TPV devices of several thousands of units per year.

In the last chapter section an example case is described, in which the application of a small TPV system as back-up generator for a stand-alone PV system is simulated: an economical analysis is carried out to evaluate the impact of the TPV device on the whole system and to compare TPV to the other possible concurrent technologies.

Auxiliary Power Units

Auxiliary power units (APU) are generally Internal Combustion Engine (ICE) generators used in vehicles to supply power on board independently from the main engine; they are present mainly in recreation vehicles, trucks and sailing boats. They are installed for heating/air conditioning purposes, battery charging and for working also in stand-by mode and require an amount of power in the range of 200 W-2 kW. TPV systems could gain the interest of this market (ten thousands of units per year equivalent to over ten

million euro): their big advantage compared to the ICEs is the low-noise operation, most of all when the vehicle is in stand-by. Nevertheless, to become competitive in this market, TPV systems must reach higher efficiencies (η_{TPV} >10%) and lower costs.

Portable generators

The critical requirements that a portable generator must fulfill are fuel availability, high power-weight ratio and high efficiency: for power output lower than 1 kW TPV can become very competitive in the next future compared to ICEs and fuel cells. The efficiency of internal combustion engines at such a low power output drops down under 10%; furthermore ICEs are noisy. Fuel cells have a much higher efficiency, but their use as portable generators is limited by the large weight and the possibility to use only hydrogen and methanol as fuel. In [YSY03] a comparison between competing portable power generators has been carried out showing that TPV systems with an efficiency of 8% can already offer a better performance than the other technologies and become therefore very attractive for a world wide market with over 300000 units per year [Bar].

Off-grid heating appliances

So far the only TPV system that reached a pre-production phase and has been sold in 20 exemplars is the Midnight Sun® [FBH$^+$99], a TPV device designed for off-grid operation and heating purposes (see Sec.2.6). The power produced by the cells is used to operate the heating system (control, fun, valves) without needing a grid connection and further electricity costs. Here the system efficiency does not play an important role: only a minimum amount of electric power is required.

TPV systems generating a thermal power of 5-20 kW and producing 30-100 W of electric power (i.e. with efficiencies lower than 1%), could find immediate applications in not grid-connected buildings and also as internal heating installations.

The market of heating appliances is relatively large: half million of heating units for floor installations are realized every year [Bar] and even at an earlier development stage TPV could reach a significant quote in that market.

Combined heat and power units (CHP)

The market of CHP units for residential purposes (single- and multi-family housing) is growing rapidly: decentralized cogeneration of power and heat is advantageous economically and more friendly environmentally. A recent study [F$^+$02a] showed that for mini- and micro-CHP (electric output power lower than 3 kW) there is a potential market estimated in 11 million installations only in Europe.

The high operating temperatures of TPV systems make this conversion technology ideal for this application. Economical analysis have been carried out and proved that TPV CHP devices for residential and industrial purposes can become a cost efficient technology in the very near future. TPV systems able to generate a power of 1-1.5 kW and a thermal power varying between 12 and 20 kW could reach a price of about 0.1-0.15 € kWh^{-1} and result more convenient than traditional combustion engines or fuel cells [PBD$^+$03], [FAH03].

Heat waste recovering

TPV has been considered as one of the possible technologies to recover the waste heat from high-temperature industrial processes (iron and steel, ceramic and glass, aluminum alloy and brick sectors). The application of TPV cell arrays inside industrial furnaces can help to save a considerable amount of energy and to convert waste streams in a useful source. Furthermore, compared to the other technologies available to recover industrial waste heat by producing electric power (high pressure boiler coupled to a steam turbine, flue gas feeding a turbine, stirling engine, thermoelectric elements), TPV is simpler and can withstand and operate at higher temperatures.

A first project to recover the waste heat of glass furnaces by means of water cooled cylindrical TPV devices has started in 2001 [Jx001]. Cylindrical TPV systems, with an inner water cooled TPV cell array, are planned to be inserted inside a furnace and heated from outside. The potential thermophotovoltaic electric power that can be generated in the USA glass industry has been estimated in 67 MW. These numbers have been recently confirmed by a UK study [BFP04], which showed that there is a potential for a TPV power production of tens of MW in the UK industry, taking into account all the high-temperature industrial processes (T>1300 K).

3.2 Competing technologies

The following sections present briefly the competing energy conversion technologies and compare them to TPV, pointing out their status and their characteristics. A resume of all these technologies is given in Table 3.1.

Thermoelectric generators

Thermoelectric (TE) generators are the most direct competitors of TPV systems since they are based as well on the direct conversion of heat into electric power. This technology seems very attractive for the recovering of heat waste at low temperatures but it is not yet used on a large scale.

Like TPV, TE systems do not present moving parts, they are reliable and do not need maintenance. Depending on the temperature difference between cold and hot side, they are able to provide a power output density up to 1 Wcm^{-2}. The big advantage of thermoelectric systems, compared to TPV, is that they can operate in a much wider temperature range. Generally thermoelectric materials can work up to 1200 K, but due to electric contacts and mechanical stability problems, they are normally designed for a maximum temperature of 600-700 K.

The biggest limit of TE generators is their low efficiency: systems available on the market report a maximum efficiency of about 4.5% [The07]. The power output for a single module generally is in a range between few watts up to 500 W. The price for a TE module varies between 5 and 10 €/W generally, while the cost of a whole TE generator between 50 and 100 €/W [Glo07].

Technology	Advantages	Limits
Thermoelectrics	Low maintenance, reliability Low temperatures	Limited efficiencies High costs
Fuel cells	High efficiencies Wide temperature range Pollution free High power density	Hydrogen and methanol fuelled Reliability problems at high temperatures High costs
Internal Combustion Engines	Good efficiencies Long-term experience High reliability Ideal for small- and micro-CHP Several typologies available	Noisy Limited performance at low power ranges Maintenance required
External Combustion Engines (Stirling and Rankine)	High efficiencies Ideal for micro-CHP Low noise	High costs Still in a field test phase
TPV	Safe and reliable Versatile fuel usage Low maintenance Low noise	High operating temperatures Complex technology Low efficiency: still in a development phase

Table 3.1: Comparison of TPV with other competing energy conversion technologies.

Fuel cells

Fuel cells are presently one of the most advancing energy conversion technologies. Their power range varies from some W up to several MW, depending on the fuel cell type.

The main advantages of fuel cells are their high system efficiencies (up to 50% in stationary systems), high power density, free-pollution emissions and low-noise operation. Furthermore high temperature fuel cells can be used as CHP units. On the other hand there are two main factors that limit the diffusion of fuel cells and their production on a large scale: they are fuelled mainly with hydrogen or methanol, whose production, transportation and distribution is difficult, and their cost is still to high to compete with other mature and more reliable technologies.

For low power range applications there are two fuel cell typologies under development: Direct Methanol Fuel Cells (DMFC) and Reformed Methanol Fuel Cells (RMFC). The first systems recently available on the market have an efficiency up to 20% [Efo07], [Ult07] and a price which varies between 50 and 80 €/W.

Another attractive application for fuel cells, in which they can be a direct competitor of TPV, is the cogeneration of power and heat. Several systems based on Solid Oxide Fuel Cells, Molten Carbonate Fuel Cells or PEM are already commercially available,

with electric power outputs varying from 1 kW for a single family housing up to 250-500 kW for decentralized energy supply and industrial applications, and prices in the range of 4500-12000 €/kW_{el} [Bar05].

The use of fuel cells as auxiliary power unit has been also investigated: the prototyping of a APU based on a SOFC able to provide up to 2 kW of electric power with an efficiency of 25% is under development [Bos05].

Internal Combustion Engines and new motor concepts

Combustion generators are the most diffused energy conversion technology. Several typologies of ICE are available on the market, covering all the different power ranges. They are characterized by a long-term experience, good efficiencies (up to 25-30%), high reliability and low costs. On the other hand they are noisy, require maintenance and especially, their efficiency decreases drastically at low power outputs (under 10% for power outputs lower than 1.5 kW).

Markets where ICE and TPV can be competitors are basically those of APU and CHP units. In both of these application areas the traditional ICEs are still the market leaders: a portable genset of 900 VA has a price of about 1 € W^{-1} and an efficiency of 6-7% [YSY03], while combined heat and power units for single- and multi-family housing supplying up to 5 kW of electric power have a price between 2500 and 6000 € kW^{-1} [Mic07].

Beside ICEs, new motor concepts are currently under development for the realization of micro-CHP units [Wil04]. External combustion engines are indeed cleaner, quieter and more efficient than traditional generators. CHP systems based on Rankine [Ota07] and Stirling [Whi07] engines have been brought recently into the market. Those units are designed to supply up to 3 kW of electric power with an overall electric-thermal efficiency of over 90%. Nevertheless their price is still too high to be competitive in the market (over 5000 € kW^{-1}).

3.3 Example case: TPV device as back-up generator for standalone PV systems

To evaluate the convenience and the feasibility of a TPV system used as small power supply for off-grid applications a simulation has been carried out, in which a small TPV back-up generator is integrated into a standalone photovoltaic system.

Different scenarios have been taken into account and compared. Freiburg has been chosen as location of the system and the solar irradiation all along the year has been calculated from local insolation data. The load required has been set to a value of 50 W, typical for off-grid repeaters and telecommunication stations.

The system is composed by PV panels, batteries, the TPV system and the gas fuel bottle. As solar panel, the model BP Solar 4170 has been chosen. It has a peak power of 170 W, at the price of 4500 € kW^{-1} installed. Batteries are composed of 12 cells of 2 V voltage each, placed in series (24 V). The TPV device added to the PV system is supposed to be able to supply a power of 100 W. Methane and propane are used as fuel and the gas bottle has the standard capacity of 100 kg.

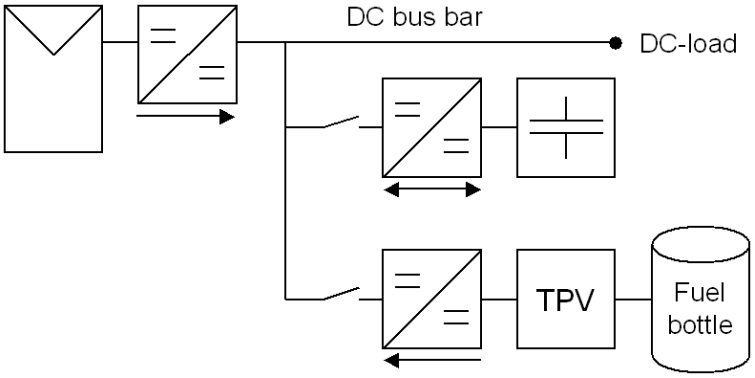

Figure 3.1: Scheme of the standalone photovoltaic system integrated with the TPV device used in the simulation.

The simulation has been carried out using the software Simplorer and the Alternative Power Library developed by ISET, which includes realistic mathematical models of electrical and mechanical components. A simple model of a TPV system has been also implemented: an efficiency of 10% has been assumed, in order to calculate the amount of fuel necessary to produce an output power of 100 W. A scheme of the whole system is represented in Figure 3.1.

Depending on the insolation and on the battery state of charge (SOC) conditions, three different operating states of the standalone system have been defined:

1. $P_{PV} > P_{load}$: the TPV device is not in operation, the power for the load is supplied by the PV modules and the battery is charged with a power equal to $P_{PV} - P_{load}$, if the SOC is lower than 95%.

2. $P_{PV} < P_{load}$ and SOC>50%: the TPV device is not in operation and the battery discharges supplying the power $P_{load} - P_{PV}$.

3. $P_{PV} < P_{load}$ and SOC<50%: the TPV system switches on: it supplies a power to the load equal to $P_{load} - P_{PV}$ and recharges the battery up to a SOC of 80%.

Dynamic simulations have been carried out assuming a time period of one year: the battery capacity and the number of PV modules have been varied independently, to calculate in each case how many hours the TPV system must operate to avoid loss of load.

TPV working hours	Battery capacity (Ah)						
	100	200	300	400	500	600	900
No TPV (0 h)		44	21	16	13	12	11
300 h	44	11	9	8	8	8	7
500 h	18	9	7	7	7	7	6
1000 h	9	5	5	5	4	4	4

Table 3.2: Simulation results: number of solar panels required for the PV system depending on battery capacity and TPV yearly working hours.

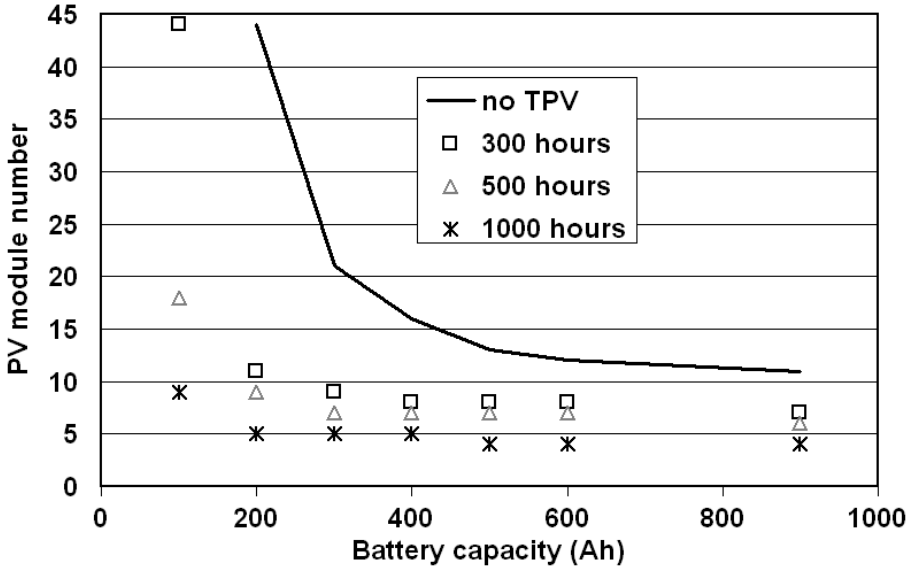

Figure 3.2: Simulation results: number of solar panels required depending on battery capacity and TPV yearly working hours.

Figure 3.2 and Table 3.2 show the effect of the TPV device on the whole system: even assuming a maximum of only 300 working hours per year, the number of PV modules needed decreases drastically.

Component	Price	Lifetime
PV modules	4500 € kW^{-1}	25 years
Battery	200 € kWh^{-1}	5 years
TPV system	2500 €	5000/10000 hours

Table 3.3: Prices and lifetimes of the standalone system components assumed in the simulation.

The annual costs for each different case have been calculated to evaluate whether the use of the TPV device is convenient. Table 3.3 shows the price of the system components and their lifetime. In a first analysis, a price for the TPV device of 2500 € has been assumed, corresponding to 25 € W^{-1}, and two different lifetimes have been considered: 5000 and 10000 hours of operation.

The resulting annual costs are plotted in Figure 3.3 as function of the battery capacity and of the TPV system lifetime. Five combinations out of the six considered give lower annual costs than in the case of the standalone system without TPV. The cost reduction is in a range between 16.5% and 25.6% (see Table 3.4).

A further calculation has been made to evaluate which is the maximum price of the TPV device to make its integration in the system still advantageous. A lifetime of 5000 hours and an operating time of 500 hours per year have been assumed with the price of the TPV device varying in a range between 2500 and 4500 €. Figure 3.4 shows the results: even at a price of 4000 €, the utilization of the TPV system is still advantageous. In this last case the fuel bottle lifetime is equal to 3.5 year.

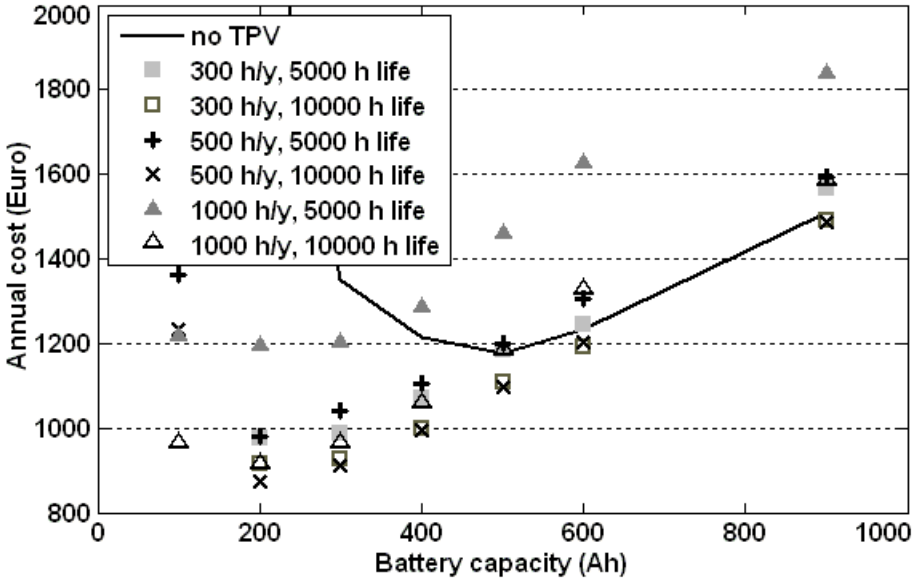

Figure 3.3: Simulation results: annual cost of the whole system calculated varying the capacity of the battery, the TPV yearly working hours (300, 500 and 1000 hours) and the lifetime of the TPV device (5000 and 10000 hours).

TPV working hours	TPV lifetime (hours)	Energy demand fraction	Cost reduction
300	5000	6.8%	17%
300	10000	6.8%	22.2%
500	5000	11.4%	16.5%
500	10000	11.4%	25.6%
1000	5000	22.8%	-1.7%
1000	10000	22.8%	22.0%

Table 3.4: Simulation results: TPV contribution in the energy demand and cost reduction compared to the best case of standalone system without TPV.

The results of the simulation proved that the use of a TPV device as back-up generator for small standalone systems offers the possibility to reduce the overall costs assuring the system operation for a long time without requiring maintenance. Compared to the present technologies commercially available (Table 3.5) TPV seems to have the potential to become soon competitive in this niche market.

From the economical point of view the efficiency of the TPV system is not a critical issue in this standalone application: the only consequence of a lower efficiency is a higher fuel consumption, which does not affect significantly the overall costs. On the other hand a TPV system efficiency high enough is fundamental for a practical reason: generally small standalone systems are installed in places difficult to be reached and are designed to last years without maintenance. A low efficiency system would require a more frequent substitution or refilling of the fuel bottle: in the simulation case, with 500 working hours per year and an efficiency of 5% instead of 10 % the bottle lifetime would be reduced to 1.7 years, doubling therefore the maintenance needed.

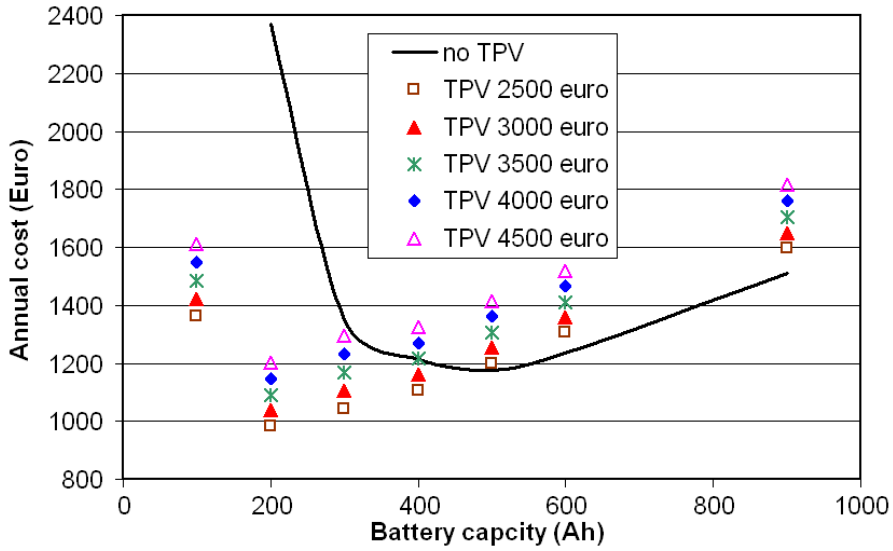

Figure 3.4: Simulation results: annual cost for the off-grid system depending on the price of the TPV device assuming 500 working hours per year and a lifetime of 5000 hours.

	Thermoelectric generators*	Direct Methanol Fuel Cell (DMFC)+	TPV (target values)
Efficiency	3%	20%	10%
Output	21 W	65 W	100 W
Price	2100 €	3500 €	4000 €
Lifetime	20 years	3000 hours	5000 hours

*: [Glo07], [Sus07]

+: [Efo07], [Udo07]

Table 3.5: Comparison of small power generators available on the market with the performance and price targets of a small TPV device.

4

Background and approach of the present work

4.1 Past projects

The present thesis is a continuation and represents the current state of the art of the TPV research carried out at the ISET institute in the last decade, in collaboration also with Karlsruhe and Kassel universities.

In 1995, indeed, a first theoretical analysis for the potential of TPV conversion of electricity has been carried out in a master thesis [Mai95]. The possibility to use Si cells coupled to an ytterbium oxide mantle as emitter has been investigated. Nevertheless the poor mechanical properties of the emitter did not allow to obtain significant experimental results.

A first operating TPV system for CHP applications has been developed in 1997 in the framework of a PhD project [Laq97]. It consisted of a normal gas heating system which has been integrated with Si cells (active area of about 400 cm^2) and with an emitter made of a ceramic porous material covered by a thin layer of ytterbium oxide. The burner was able to supply a thermal power up to 16 kW, generating a maximum electric output of 50 W, which corresponds to a system efficiency of 0.31%.

In 2001 another TPV device has been realized by Volz [Vol01], based on GaSb cells and Kanthal wires used as emitter. Peculiarity of this system is the highly efficient recuperative heat exchanger, based on a microchannel counter-current design. The system has been tested with one GaSb cell (1 cm^2), producing an output of 0.64 W, in front of a chemical power supplied of 1.5 kW.

The present work has been partially carried out in the framework of the Research Training Network "Thermo-Photo-Voltaic cells based on GaSb" [Duf05], a project funded by the European Community (contract number: HPRN-CT- 2001-00199), which involved seven European research institutes and universities and one private company. Target of the project, which lasted three years (2002-2005), was to develop a gas-fired TPV device based on GaSb cells with a total efficiency of at least 2%. The majority of the partners have been involved in the fabrication and the characterization of the cells. Targets of ISET, instead, have been to develop the recuperative burner unit and to assemble all the components, in part realized by the other institutes, building the

final TPV prototype. Besides the experimental work, another task was to develop a theoretical simulation model of the system. Table 4.1 gives an overview of the partners involved and of the different tasks of the project.

RTN "Thermophotovoltaic cells based on GaSb"		
CEA	Commissariat à l'Energie Atomique, Grenoble, France	
FhG-ISE	Fraunhofer ISE, Freiburg, Germany	
ISET	Institut fuer Solare Energieversorgungstechnik, Kassel, Germany	
UAM	Universidad Autonoma de Madrid, Madrid, Spain	
UCM	Universidad Complutense de Madrid, Madrid, Spain	
ITN	Instituto Tecnologico e Nuclear, Lisbon, Portugal	
AUTH	Aristotele University of Thessaloniki, Thessaloniki, Greece	
WT	Wafer Technology LTD, Milton Keynes, UK	
Task 1	TPV cells	
	Substrate	CEA, WT, EPM, UAM
	Cell	CEA, ISE, UAM
	Characterization	UAM, UCM, ITN, AUTH
Task 2	Burner unit	
	Burner and recuperator	ISET
	Emitter	CEA, ISET
	Simulation	CEA, ISET, ISE
Task 3	TPV system	
	Device and complements	ISET
	Simulation	ISET, CEA

Table 4.1: Partners and tasks of the RTN "Thermophotovoltaic cells based on GaSb".

4.2 Present work: experimental and theoretical approach

The work of Volz has been the starting point for the present PhD thesis: the design of the recuperative burner unit has been kept, and a few modifications have been carried out on it in order to improve the reliability of the component and its performance.

The approach undertaken for the development and the realization of the whole system and of the single components is based on two driving ideas:

- Use of components and materials directly available on the market: such a TPV device would imply reduced costs and it would be already oriented to a possible series production.

- Realization of a TPV device that can be used as a tester using different system configurations by varying fuels, emitter materials, filters and cells. Such a TPV tester would allow to analyze the performance of an operating TPV system under

different conditions, allowing a better understanding of the technology and an optimization of the device.

Besides the experimental building and testing of the device, the other target of the work is to develop a theoretical simulation model of the TPV system.

Presently models and approaches to simulate a TPV system are available in literature [AHL03] [ZHS+01] [BFPP05], but none of them takes into account the recuperative burner unit. Nevertheless heat exchanger and burner play a significant role in the whole system design. The temperature field in the burner area, where the emitter is placed, is the critical factor in order to evaluate the optical properties and the performances of filter, emitter and cells. The radiation power density depends strongly on the emitter temperature ($P_{radiation} \propto T^4$). Furthermore, the radiation spectrum changes with the temperature influencing the behavior of the optical system and the efficiency of the cells. Thus, the total efficiency and the power output of the system, cannot be correctly evaluated leaving out of consideration design and configuration of the burner.

One of the most challenging aspects in TPV design, due to its multidisciplinary aspect, is to optimize not only the single components, but also the whole device, taking into account all the interactions between the different processes involved.

Purpose of this work, therefore, is to realize a simulation model of the whole device, taking into account also the heat recuperation and the combustion process. The approach used to realize this model, is to model all the components separately, in a first step, and then couple them together in order to simulate and investigate the reciprocal interactions.

To develop this theoretical model a commercial Finite Element Method (FEM) based software is used (Comsol Multiphysics®). The geometry of the components, the partial differential equations (PDE) describing the thermo-physical processes involved and the boundary conditions are set, implemented and numerically solved with this software.

5

Development of a TPV system: design and modelling of the components

This chapter describes the design and the model formulation of the system. In order to illustrate more clearly the work approach followed, the theoretical formulation model and the design of each component, which are strictly correlated, are discussed together in same sections.

5.1 Recuperative heat exchanger

5.1.1 Heat exchanger design

The heat exchanger used in the TPV system has the same design proposed by Volz [Vol01]. It is a recuperator realized using a commercial porous ceramic material with a matrix of square microchannels realized in it.

The material used is porous cordierite, a ceramic compound that presents thermophysical properties which make it suitable for high temperature applications: it can operate over 1300 °C, it withstands high temperature gradients and due to its low thermal expansion coefficient ($0.4{\cdot}10^{-6}\,\mathrm{mK}^{-1}$) it is highly resistent to thermal shock.

The heat exchanger is 230 mm long with a square section (100 mm on a side). The microchannels have a dimension of 1.6 mm with a wall thickness of about 0.3 mm and form a matrix of 52x52 ducts (Figure 5.1). Combustion air (cold fluid) and exhaust gas (hot fluid) flow in opposite direction in each second row of the matrix. Figure 5.2 shows how the recuperator works in operating conditions. The air is supplied through a small chamber at the bottom of the recuperator, where the exhaust gas channels are sealed, so that the air flows only into the combustion air channels. In the upper part of the heat exchanger, close to the burner, the combustion air channels of a same row, in the middle of the exchanger section, are sealed on the top and put in communication by eliminating the dividing walls, so that all the air enters the combustion chamber on the two sides of the recuperator section. The exhaust gas produced in the burner enters the recuperator in the central part of its section and, for each channel row, it is distributed over all the exhaust gas channels by sawing and eliminating for a short length the channel walls. In

the same way the combustion products are collected at the bottom of the recuperator, just above the inlet air chamber, and carried outside the device by a flexible pipe.

The ceramic material used is porous and therefore permeable to the fuel. The pressure difference between inlet and outlet could cause fuel leakage into the exhaust gas channels, with consequent decrease of the system performance and risk of auto-ignition. For this reason the ceramic body has been immersed in a SiO_2 suspension, in order to coat it with a thermal resistent impermeable ceramic layer.

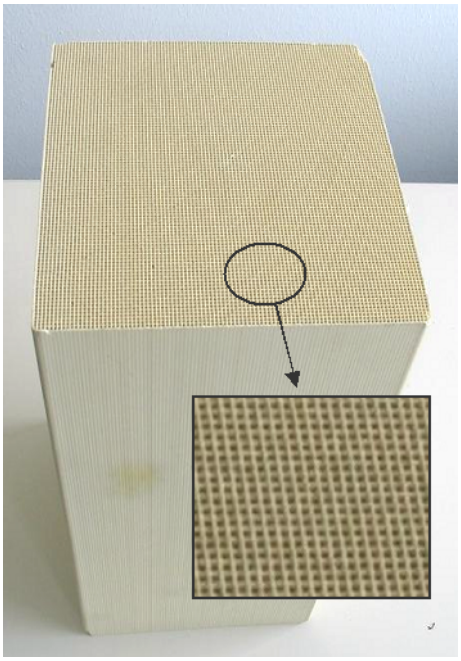

Figure 5.1: The ceramic porous material with the microchannel matrix used to realize the recuperative heat exchanger.

The ceramic recuperator is thermally insulated with a high temperature insulation material (Wacker WDS superFLEX®) and the unit is sealed on the perimeter with stainless steel plates.

5.1.2 Heat exchanger model

The processes involved in the recuperator are the flowing of compressible fluids and the heat transfer through conduction and convection. The partial differential equations (PDE) representing such phenomena are the continuity and Navier-Stokes equations, and the energy equation, which are expressed respectively as follows:

$$\frac{\partial \rho}{\partial t} + \nabla(\rho \vec{u}) = 0 \tag{5.1}$$

$$\frac{\partial(\rho \vec{u})}{\partial t} + \rho \vec{u} \nabla \vec{u} = \nabla[\bar{\Pi}] + \rho \vec{g} \tag{5.2}$$

$$\frac{\partial(\rho c_p T)}{\partial t} + \nabla(\rho c_p T \vec{u}) = \nabla(\lambda \nabla T) \tag{5.3}$$

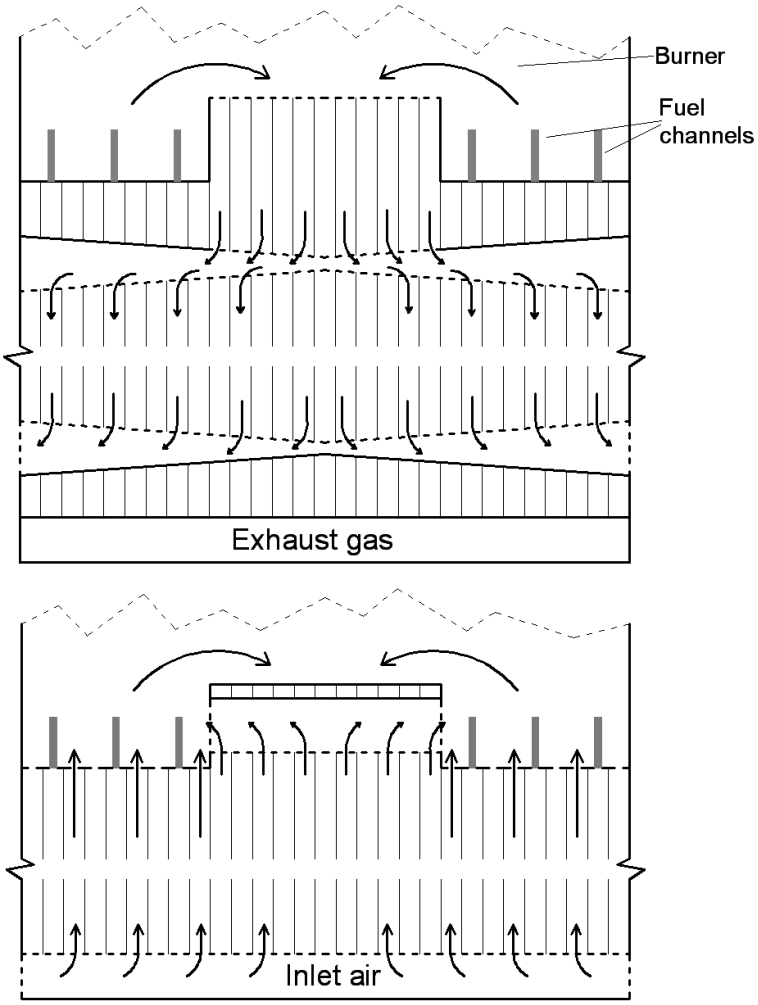

Figure 5.2: Operation principle of the recuperative heat exchanger: flowing of exhaust gas and combustion air in two contiguous microchannel rows of the matrix [Vol01].

In Eq. 5.2 $\vec{g}$ represents the gravity acceleration vector $(0, 0, -g)$ and Π is the surface stress tensor. The fluids treated are gases and can be assumed to be isotropic and Newtonian (i.e. linear relationship between stresses and shear strain), therefore the tensor can be expressed as:

$$\Pi_{ij} = -\left(p + \frac{2}{3}\mu\nabla\vec{u}\right)\delta_{ij} + \mu\left(\frac{\partial u_i}{\partial x_j} + \frac{\partial u_j}{\partial x_i}\right) \tag{5.4}$$

where δ_{ij} is the Kronecker operator, defined as: $\begin{array}{lll}\delta_{ij} = 1 & \text{if} & i = j \\ \delta_{ij} = 0 & \text{if} & i \neq j\end{array}$

Air and fuel are not premixed in the recuperator: the fuel, methane, flows through small pipes inserted into the air channels (see following section). Due to the recuperator design it is reasonable to assume that air and fuel enter the burner at the same temperature. Therefore, to simplify the model formulation and evaluate correctly at the same time the total heat capacity flux entering the system, it is assumed that in the inlet channels air and fuel are already premixed. This assumption is taken into account only for the heat exchanger simulation model. Basing on this hypothesis and on the fact

that chemical reactions do not take place in the recuperator, the fluids at the inlet and at the outlet of the channels are mixtures having a constant composition, which can be calculated from the equation of the methane-air reaction:

$$CH_4 + 2\,\lambda\,O_2 + 2(\lambda\,3.762)N_2 \rightarrow 2H_2O + CO_2 + 2(\lambda - 1)O_2 + 2(\lambda\,3.762)N_2 \qquad (5.5)$$

where λ is the air number ($\lambda \geq 1$). It is assumed that the fuel is completely burned in the combustion chamber.

For the evaluation of the thermo-physical properties of the mixtures, a value of 0.7 is assumed for the Prandtl number (Eq. 2.13), which is a realistic value for air and many gases [DLR].

The specific heat capacity c_p of a mixture with n species at a fixed temperature T and pressure p is calculated by doing a mass fraction averaging:

$$c_p = \sum^{n} w_i c_{p_i} \qquad (5.6)$$

where w_i is the mass fractions of the i^{th} component. The expression of the specific heat capacity for each of the species present in Eq.5.5 is obtained from literature [Cha98] as a function of the temperature at atmospheric pressure.

The viscosity μ of the mixture is calculated by following a method presented in [Wil50], in which the viscosity of a mixture is defined as:

$$\mu = \sum_{i=1}^{n} \frac{x_i \mu_i}{\sum_{j=1}^{n} x_j \phi_{ij}} \qquad (5.7)$$

where x_i is the molar fraction of the i^{th} component and ϕ_{ij} corresponds to:

$$\phi_{ij} = \frac{\left[1 + \left(\frac{\mu_i}{\mu_j}\right)^{1/2} \left(\frac{M_j}{M_i}\right)^{1/4}\right]^2}{\left[8\left(1 + \frac{M_i}{M_j}\right)\right]^{1/2}} \qquad (5.8)$$

M_i is the molecular mass of the i^{th} component. The viscosities of pure components $\mu_i(T)$ are calculated from expressions available in literature [BBKM87], [ABG+00]. The thermal conductivity λ of the mixture can be then calculated from the definition of Pr and from the values of c_p and μ.

The geometry of the heat exchanger is too complex to be reproduced and simulated in a theoretical model. In order to evaluate the temperature of the combustion air at the inlet of the burner and the temperature of the exhaust gas at the outlet of the recuperator a 2D symmetric model is implemented, as showed in Figure 5.3. The channel rows are represented as thin flat parallel ducts. An empirical expression is used to evaluate the heat losses into the ambient via natural convection [B+85]. The temperature of combustion air and exhaust gas entering the heat exchanger and the mass flow of air and methane are set as boundary conditions.

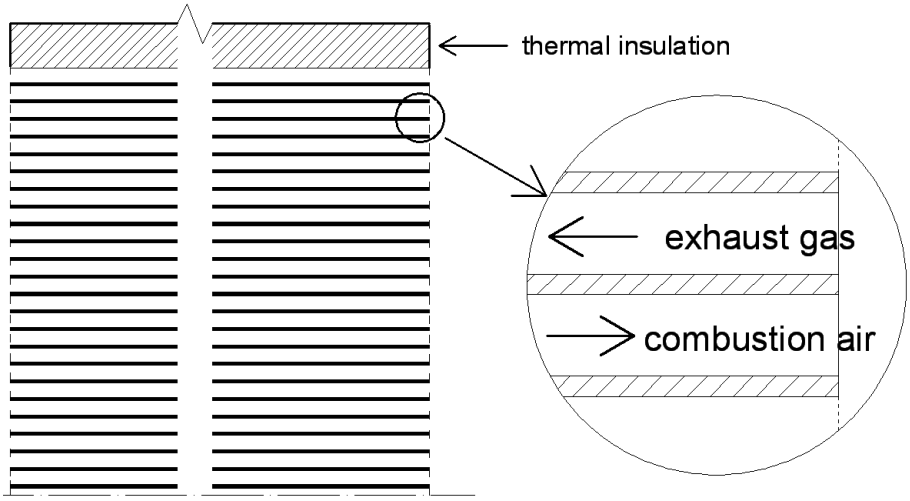

Figure 5.3: The geometric model used for the heat exchanger simulation.

5.2 Burner

5.2.1 Burner design

The combustion chamber is realized as a cavity in the upper part of the heat exchanger. This enables to have a compact design and to reduce the thermal losses due to the connection between the two components.

Because of the high temperature at which combustion air and fuel are pre-heated, the fluids are supplied separately in the burner to avoid risks of auto-ignition and backfire. The combustion realized, therefore, is a not-premixed one. The fuel is supplied through 78 small cylindric impermeable ceramic pipes with an inner diameter of 1 mm, which are inserted inside the combustion air channels, in the lateral parts of the heat exchanger (see Figure 5.2 and 5.4). Because of the small pipe diameter and the small velocities of fuel and air (lower than 1.5 ms^{-1}), the flame is laminar. The inlet sections of the fuel pipes are located in a separated and sealed chamber placed under the air inlet chamber. The disposition of the fuel pipes allows to generate a homogeneous temperature field in the combustion chamber and therefore a uniform emitter temperature. The ignition is realized with an electrical spark ignition system (Eichhoff E3748).

The burner is designed to supply a maximum thermal power of around 1300 W, with the possibility to vary both fuel and air mass flows. The unit is closed and sealed on the top by a quartz glass. In order to be able to open and inspection easily the combustion chamber, the glass is not placed directly over the burner but over a stainless steel frame, which is flange-connected to the top of the combustion chamber and sealed on the perimeter by a high temperature silicon adhesive tape (IPS Glass Cloth Tape 8321).

A practical problem pointed out by Volz in his work, is to guarantee the sealing between quartz glass and metal frame avoiding at the same time the breaking of the former due to high thermal stresses generated by the different thermal expansion coefficient of the two materials. The problem has been solved by gluing the quartz glass on the frame by using a high temperature silicon adhesive paste, which damps the thermal

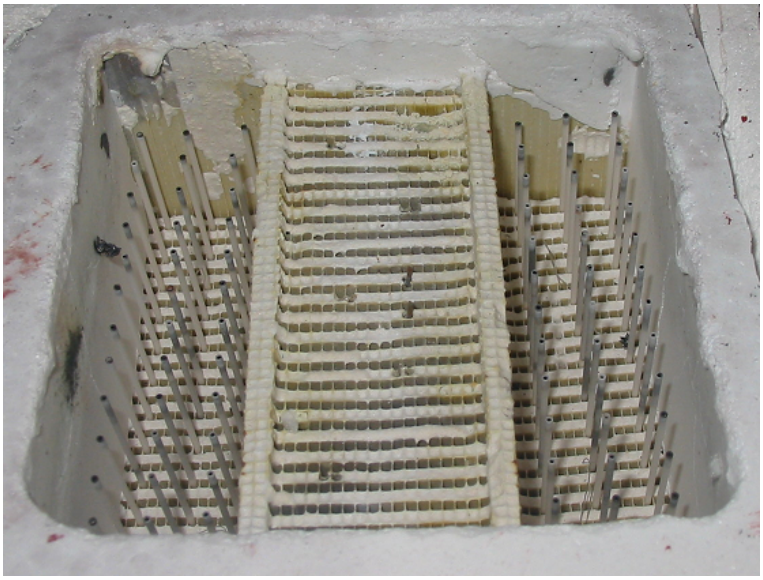

Figure 5.4: The combustion chamber with the fuel pipes inserted into the air channels.

stress between glass and metal (Figure 5.5). A thin layer of high temperature insulating material (Cerachem Blanket® from Thermal Cermics) is used between glass and combustion chamber, around the burner section, to minimize the lateral heat losses and avoid too high temperatures for the silicon sealing. During the experimental tests the

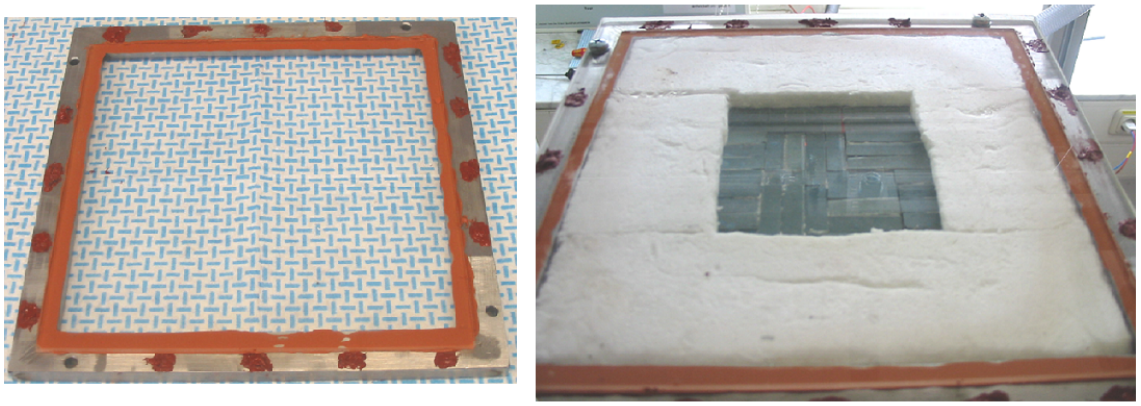

Figure 5.5: On the left the quartz glass is glued over the metal frame using a high temperature silicon paste; on the right the glass closes and seals the burner unit, covered by the emitter and surrounded by a layer of thermal insulating material.

emitter material is placed inside or on the top of the burner cavity, in contact with the flame and the exhaust gas (Figure 5.5).

In operating conditions the area of the burner where the heat transfer between flue gas and emitter material takes place (see Figure 5.6) is always filled with Kanthal wires. These wires can act directly as emitter (see next section) or can support the transfer of heat from the exhaust gas to the emitter material, if the latter is placed over the burner cavity. In this case, indeed, the wires increase the heat flux towards the emitter:

they support the gas mixing and absorb via convection the heat of the gas, re-radiating it to the emitter material. If the metal wires were not present in the burner the heat transfer between flame and emitter would be much worse, being limited to a laminar convection heat transfer between gas and emitter wall. Therefore at a same emitter temperature, i.e. same emitted power, the temperature of the exhaust gas entering the recuperator would be much higher, with the consequent risk of damage or degradation of the component.

5.2.2 Modelling approach and formulation

Model complexity

In a combustion process, besides fluid dynamics and heat transfer, chemical reactions and diffusion are the other phenomena to be taken into account and modelled.

As written in Sec.2.3.2, a real chemical reaction consists of hundreds of elementary reactions, which involve many unstable and reactive species. To realize a realistic theoretical model of a not-premixed combustion, all these reactions and species should be included into the model, taking into account also the reaction rate for each reaction (Eq.2.19) and the diffusive mass flux j (unit in $\mathrm{kg\,m^{-2}\,s^{-1}}$) for each i^{th} species, which is expressed by the equation:

$$j_i = -\rho \sum_j D_{ij} \nabla w_j - \frac{D_i^T}{T} \nabla T \tag{5.9}$$

in which D_{ij} is the multicomponent diffusion coefficient (in $\mathrm{m^2 s^{-1}}$), w is the mass fraction and D^T is the thermal diffusion coefficient (in $\mathrm{kg\,m^{-1} s^{-1}}$). The first term in the right hand of Eq.5.9 represents the first Fick's law and corresponds to the mass flux generated by concentration gradients, while the second term represents the mass flux generated by the temperature gradient (thermal diffusion). To implement a realistic theoretical model, all the diffusion coefficients D_{ij} and D_i^T should be estimated or calculated.

Such a realistic modelling approach, however, is very complicated and goes beyond the purposes of the present simulation. Target of the burner simulation, indeed, is to calculate the temperature field in the combustion chamber in order to be able to evaluate the temperature on the emitter surface, and not to estimate the amount and the concentration of each single species generated during the chemical reaction. Therefore simplifying assumptions are needed for the development of a less complicated but still valid theoretical model.

Furthermore the geometry of the combustion chamber is very complex: its representation in a 3D geometric model, even using symmetries, would imply an enormous computational effort for the solution of a FEM based model, requiring a too high number of mesh elements. Therefore a simplification in the geometrical model is also required to be able to simulate the combustion process in the burner.

Geometrical model implementation

Referring to Figure 5.6, the approach followed to simplify the geometrical model can be resumed in the following three steps:

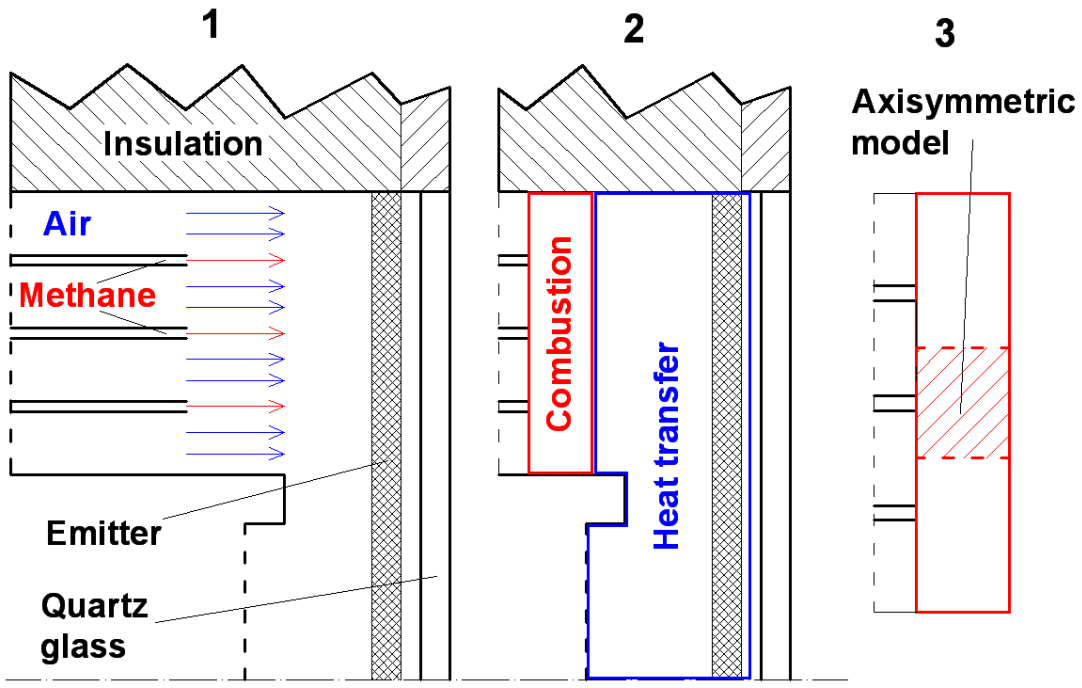

Figure 5.6: The modelling approach for the combustion process is resumed in three steps: 1- Burner real geometry; 2- Assumption of a delimited combustion area; 3- Use of an axis-symmetric model.

1. Air and fuel enter the burner already pre-heated, at a very high temperature (over 900 °C) with the consequence of a very high reaction rate (see Eq.2.20).

2. It can be assumed that the combustion takes place almost instantaneously, involving only a small part of the whole combustion chamber. Therefore the burner can be divided into two parts: the first one, smaller, in which air and fuel react and burn, and the second one in which there is no chemical reaction but only heat transfer.

3. The geometric model can be further simplified by realizing an axis-symmetric model for a single fuel pipe, instead of considering the whole burner cross section area. The temperature and velocity fields calculated can be extrapolated and extended to the whole burner section.

Theoretical combustion model: formulation and validation

The approach used to simplify the theoretical formulation of the model consists of representing the chemical reaction as a single-step reaction mechanism. That means to consider only the overall reaction (Eq.5.5) and to use a single empirical expression to define the reaction rate, instead of taking into account all the intermediate elementary reactions (see Eq.2.19):

$$\omega = k(\rho_{CH_4})^a(\rho_{O_2})^b \tag{5.10}$$

In the equation above ρ_i is the partial density of the ith component ($\rho_i = \rho\, w_i$), a and b are empirical factors and k is the reaction rate constant. With such an approach

the independent species to consider in the modelling and simulation are only the initial reactants and the final products of the reaction. Expressions defining the empirical factors and the reaction rate are available in literature [WD81], [HEE99] and refer to the case of a premixed combustion. In the TPV system the combustion is not-premixed, but it is almost instantaneous and takes place where air and fuel mass fractions are stoichiometric. Therefore it makes sense to use such a technique for the present case, assuming as reference the reaction rate expression used for the case of a stoichiometric premixed combustion [DLR].

The thermo-physical properties of the species and of the gas mixture are evaluated assuming, as in the previous section, a Prandtl number equal to 0.7, and a Lewis number equal to 1. The Lewis number (Le) is a dimensionless number defined as:

$$Le = \frac{\lambda}{\rho c_p D} \tag{5.11}$$

A value of 1 for Le is a realistic estimation for many gases and allows to calculate the diffusion coefficient D for the mixture without needing to calculate or estimate the multicomponent diffusion coefficients D_{ij}: the matrix D is thus assumed to be diagonal, with a constant value $D_{ii} = D$. As a further simplification the thermal diffusion is neglected: generally this term does not affect significantly the diffusion mass flux.

The PDE system describing the combustion process, includes the continuity and Navier-Stokes equations (Eq.5.1-5.2), the energy equation and the diffusion equation, based on the Fick's law and on the assumptions described above:

$$\frac{\partial \rho}{\partial t} + \nabla(\rho \vec{u}) = 0 \tag{5.12}$$

$$\frac{\partial(\rho \vec{u})}{\partial t} + \rho \vec{u} \nabla \vec{u} = \nabla[\bar{\Pi}] + \rho \vec{g} \tag{5.13}$$

$$\frac{\partial(\rho c_p T)}{\partial t} + \nabla(\rho c_p T \vec{u}) = \nabla(\lambda \nabla T) + \omega(\Delta_C H)_{\mathrm{CH_4}} \tag{5.14}$$

$$\frac{\partial(\rho \vec{w})}{\partial t} + \nabla(\rho \vec{w} \vec{u}) = \nabla(D \rho \nabla \vec{w}) - \vec{s}\omega \tag{5.15}$$

In Eq.5.14 the last term on the right hand is the heat flux generated by the combustion of the fuel which burns at a reaction rate ω. For the methane the heat of combustion is $5{\cdot}10^7\,\mathrm{J\,kg^{-1}}$.

Eq.5.15 is a system of three PDEs describing the diffusion and reaction process. The mass fractions of methane, oxygen and exhaust gas (CO_2+0.5H_2O) are taken as independent variables, i.e $\vec{w} = (w_{\mathrm{CH_4}}, w_{\mathrm{O_2}}, w_{exh})$. The vector $\vec{s}$ is equal to $(1, s, -(1+s))$, where s is the fuel/oxygen stoichiometric mass ratio. The mass fraction of the last species, N_2, is calculated imposing the sum of all the mass fractions equal to 1:

$$\sum_i w_i \equiv 1 \tag{5.16}$$

The simplified model formulation described above must be validated in order to be used in the combustion chamber simulation. The case of an axis symmetric not-premixed laminar air-methane flame reported in literature, presenting detailed chemical

simulation models and experimental results [MSC80] [SMK89] [XSLL93], is taken as reference case for the simplified model. This combustion process is simulated, based on the simplified model formulation, and the results obtained are compared with those present in literature. Figure 5.7 shows the geometry of the model taken as reference case [MSC80].

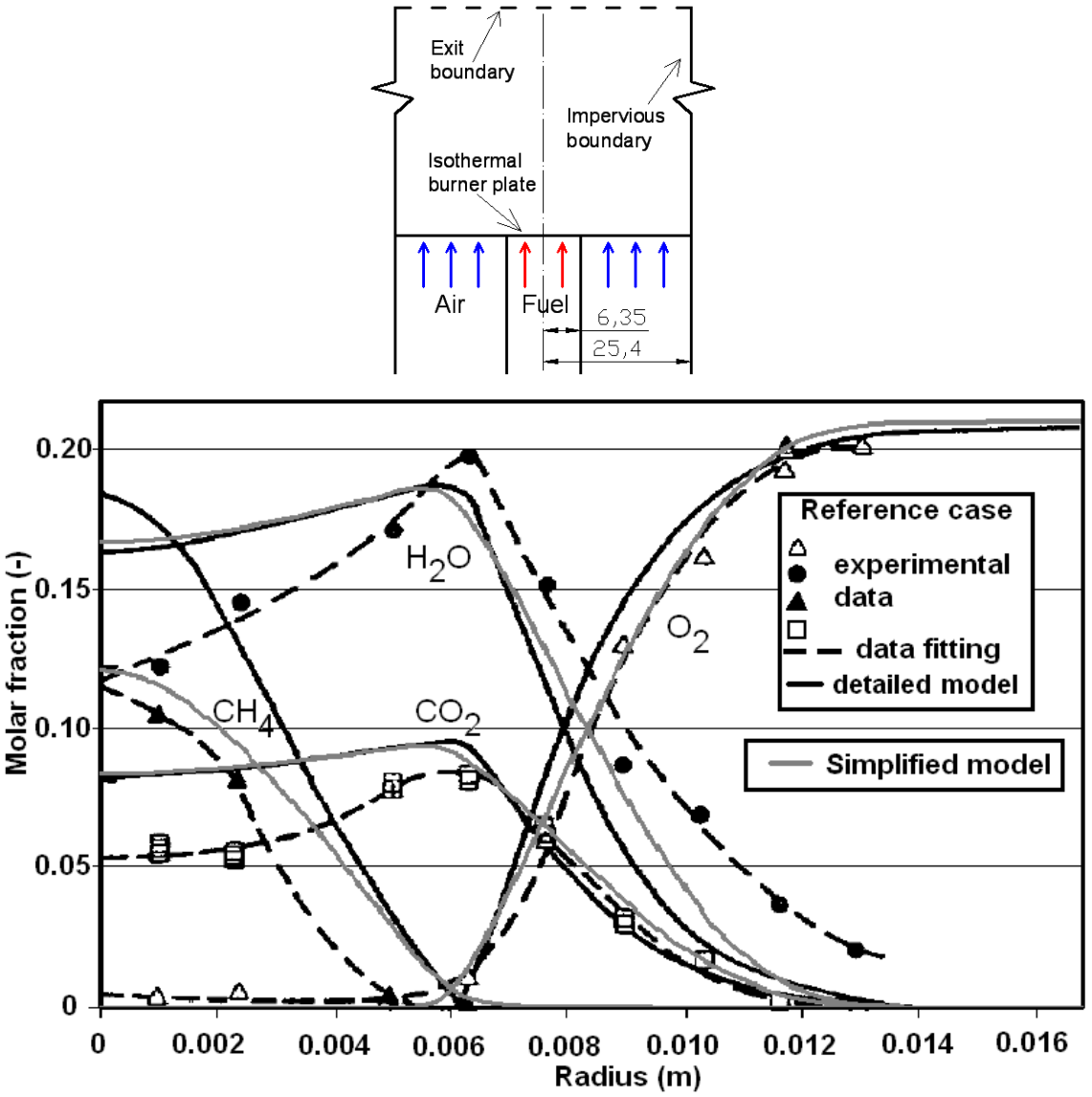

Figure 5.7: Combustion model geometry of the reference case (lengths expressed in mm) and comparison between results reported in literature [MSC80] and results obtained by using the simplified formulation. The graph shows the molar fraction radial profiles of the different species 2.4 cm above the burner plate.

The reaction rate ω (Eq.5.10) is calculated by using the empirical expression proposed in [HEE99]:

$$\omega = 8.45\,10^{11}\,(\rho w_{CH_4})^{1.8}(\rho w_{O_2})\,exp\left(-\frac{E_a}{RT}\right) \tag{5.17}$$

Where E_a is equal to $125.6\,\mathrm{kJ\,mol^{-1}}$. The comparison of experimental and detailed

chemical model results reported in literature with those obtained with the simplified model formulation showed a good agreement (see Figure 5.7): the simplified model can be considered valid and can be used for the simulation of the combustion process in the TPV system.

Flame-emitter heat exchange

Referring to the modelling approach presented in Figure 5.6 and in Sec.5.2.2, the heat exchange between flame and emitter material is assumed to take place after the combustion of the fuel: the process can be simulated without taking into account chemical diffusion and reaction, but considering only fluid dynamics and heat transfer through convection, conduction and radiation. The fuel, indeed, is assumed completely burned and the mixture of exhaust gas and unburned air has a constant composition.

As pointed out previously, metal wires are present in the combustion chamber to improve the heat transfer between gas and emitter material. The wires are randomly placed in the burner and behave similarly to an open-cells highly porous material or to a packed bed made of thin particles with a very high porosity.

The transfer of heat in this kind of structures is enhanced due to three reasons:

1. The heterogeneous gas-wires structure has a higher thermal conductivity than the gas alone, due to the high thermal conductivity of the metal wires.

2. The porous material supports the mixing of the flow: a turbulent flow regime is realized and the heat transfer via convection is enhanced.

3. The effect of the heat transfer via radiation becomes dominant due to the high surface area to volume ratio of the structure and to the high temperatures reached, and contributes to improve significantly the overall heat transfer process between exhaust gas and emitter.

The approach used to implement a heat transfer model in the burner is therefore to consider the heterogeneous structure consisting of exhaust gas and metal wires as a single homogeneous opaque fluid phase having the same thermo-physical properties of the gas, but a higher thermal conductivity λ_{tot} which depends on the three phenomena cited above. The model, thus, can be reduced to a simple convective heat transfer process between a solid wall (emitter surface) and a highly conductive fluid at high temperature. λ_{tot} is defined as the total equivalent thermal conductivity and can be expressed as the sum of three different thermal conductivities [BS78]:

$$\lambda_{tot} = \lambda_e + \lambda_d + \lambda_{rad} \tag{5.18}$$

where λ_e represents the effective thermal conductivity of the heterogeneous structure, λ_d represents the dispersion thermal conductivity due to the mixing of the flow through the wires and λ_{rad} is the contribution of the radiation to the total thermal conductivity.

A correct evaluation of the three conductivities in the equation above is a very challenging task in the case of heterogeneous and randomly placed structures. Many expressions present in literature are based on empirical correlations which often are valid only for particular and specific cases. A correct evaluation of λ_{tot} and a validation of the model via formulation of specific empirical expressions would require detailed and

precise measurements for each of the different heat transfer processes taking place inside the Kanthal wire matrix. However this goes beyond the purposes of the present theoretical and experimental work. The method described below used to calculate the different terms of λ_{tot} is based on some simple assumptions and aims at describing the whole heat transfer process between exhaust gas and emitter material.

The effective thermal conductivity λ_e is calculated as proposed in [CLTC05], by referring to the Effective Medium Theory for a randomly distributed heterogeneous structure:

$$(1-\phi)\frac{\lambda_s-\lambda_e}{\lambda_s+2\lambda_e}+\phi\frac{\lambda_f-\lambda_e}{\lambda_f+2\lambda_e}=0 \tag{5.19}$$

In the equation above ϕ is the porosity of the material, which corresponds to the ratio between the volume occupied by the fluid and the total volume of the porous material. The subscripts s and f refer respectively to the solid and the fluid part of the material. The calculation of the porosity in the case of the TPV system burner filled with the Kanthal wires is straightforward since the volume of the combustion chamber and the weight of the wires can be easily measured and the density of Kanthal is known.

The dispersion thermal conductivity λ_d is expressed as a function of the Reynolds number based on the material permeability Re_K and of the Prandtl number based on the effective conductivity Pr_e [CM00]:

$$\frac{\lambda_d}{\lambda_e}=C_D(Re_K Pr_e) \tag{5.20}$$

C_D is an empirical constant that can be assumed with a reasonable estimation equal to 0.1, while Re_K and Pr_e are given by;

$$Re_K=\frac{\rho_f u_f\sqrt{K}}{\mu_f} \qquad Pr_e=\frac{\mu_f c_{p_f}}{\lambda_e} \tag{5.21}$$

where K is the porous material permeability calculated from a semi-empirical model proposed in [DMCL94]:

$$K=\frac{\phi d_p^2}{108\chi(\chi-1)} \tag{5.22}$$

d_p represents the pore size, while χ is the tortuosity, a dimensionless parameter of the porous matrix. The Kanthal wires used in the combustion chamber have a spiral shape and different lengths, therefore a correct and precise definition of these two parameters is not possible. In order to evaluate d_p and χ the metal wire matrix in the burner is assumed to have a geometry consisting of mutually orthogonal wires generating cubic cells of size d_p (see Figure 5.8). By knowing the porosity of the Kanthal matrix in the burner and the wire diameter d_w and from simple geometric calculations, the size of the cell results:

$$d_p=\sqrt{\frac{3d_w^2\pi}{1-\phi}} \tag{5.23}$$

For the assumed metal grid geometry the tortuosity χ is given in [Du 92] and [DMCL94] and is expressed as:

$$\frac{1}{\chi}=\frac{3}{4\phi}+\frac{\sqrt{9-8\phi}}{2\phi}cos\left(\frac{4\pi}{3}+\frac{1}{3}acos\left(\frac{8\phi^2-36\phi+27}{(9-8\phi)^{3/2}}\right)\right) \tag{5.24}$$

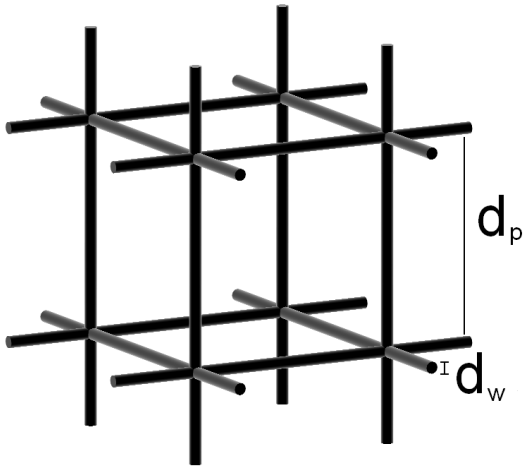

Figure 5.8: Geometric model of the Kanthal wires placed in the combustion chamber used for the calculation of the dispersion conductivity λ_d.

From Eq.5.20-5.24 it is finally possible to evaluate the dispersion conductivity λ_d.

The calculation of the radiative thermal conductivity λ_{rad} is based on the so called Rosseland approximation [SH92], which assumes that the local radiative heat flux q_{rad} depends on the gradient temperature and it is expressed by the equation:

$$q_{rad} = \frac{16\sigma T^3}{3K_R}\nabla T = \lambda_{rad}\nabla T \tag{5.25}$$

where K_R is the Rosseland mean extinction coefficient defined by:

$$\frac{1}{K_R} = \frac{\int_0^\infty \frac{1}{K_\lambda}\frac{\partial E_{b\lambda}(T,\lambda)}{\partial E_b(T)}\mathrm{d}\lambda}{\int_0^\infty \frac{\partial E_{b\lambda}(T,\lambda)}{\partial E_b(T)}\mathrm{d}\lambda} \tag{5.26}$$

with K_λ being the spectral extinction coefficient. To evaluate K_λ and therefore λ_{rad} in the Kanthal wire case a semi-empirical model proposed in [ZLH04] is taken as reference and used for the present work. The model defines the extinction coefficient as a function of the porosity ϕ and of the strut diameter d_w for highly porous open-cells metal foams with gray radiative properties:

$$K_\lambda = C\frac{(1-\phi)^n}{d_w} \tag{5.27}$$

where C and n are material constants. To adapt this model to the metal grid in the burner of the TPV device, it is assumed for simplicity that the Kanthal wires behave as gray bodies. The values of C and n are taken from [ZLH04], in which the properties of highly porous metal foam with different pore sizes are investigated.

Figure 5.9 shows how the 2D model is implemented. The temperature and the velocity of the exhaust gas are those resulting from the combustion simulation and are extrapolated to the whole flow cross section. The temperature of the emitter is calculated with an iterative process, together with the radiative flux generated and transmitted towards the cells (see next section). The fluid dynamic and heat transfer PDE equations,

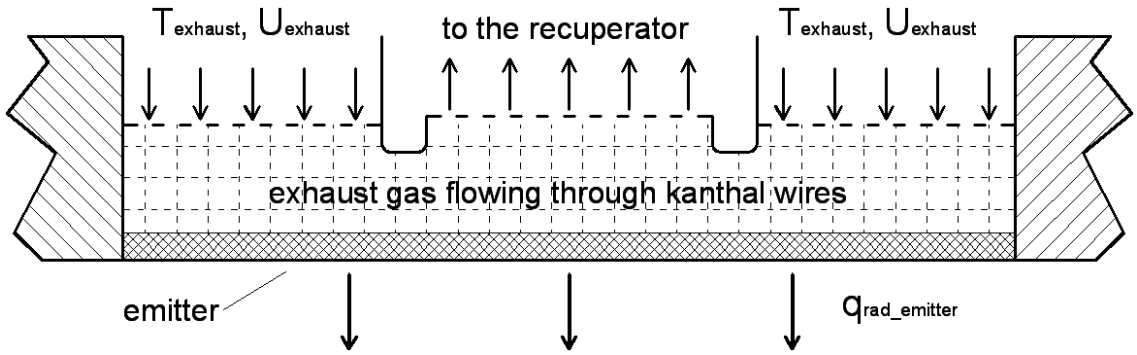

Figure 5.9: Modelling approach used for the flame-to-emitter heat transfer simulation.

similarly to Eq.5.1-5.3, are rewritten as follows:

$$\frac{\partial \rho}{\partial t} + \nabla(\rho \vec{u}) = 0 \tag{5.28}$$

$$\frac{\partial(\rho \vec{u})}{\partial t} + \rho \vec{u} \nabla \vec{u} = \nabla[\bar{\Pi}] + \rho \vec{g} \tag{5.29}$$

$$\frac{\partial(\rho c_p T)}{\partial t} + \nabla(\rho c_p T \vec{u}) = \nabla(\lambda_{tot} \nabla T) \tag{5.30}$$

In Eq.5.30 λ_{tot} is the total equivalent thermal conductivity given in Eq.5.18 and it is higher than the conductivity of the exhaust gas.

The radiative thermal flux $q_{rad\,emitter}$ released towards the cells is set as boundary condition on the emitter surface and it is calculated depending on the temperature field in the combustion chamber and on the optical system properties (see next section). The radiation absorption and emission of the combustion products CO_2 and H_2O in the burner are not taken into account: the small thickness of the gas layer in the combustion chamber and the low partial pressures make their influence on the overall heat transfer process negligible [BS06].

5.3 Optical system

5.3.1 Components and design

This section deals with the description and the simulation of the optical system, without taking into account the cells, which are described in a section apart.

Figure 5.10 is a scheme of the optical system design: the emitter material placed over the combustion chamber, the absorptive quartz glass filter and the reflecting frame are the components involved in the selection and the transmission of the radiation.

Emitter materials

As described in Chapter 4, one purpose of the experimental work is to realize a TPV tester, in order to compare the behavior of the system under different configurations. To follow this approach five emitter materials with different spectral properties have been used in the system (see Figure 5.11):

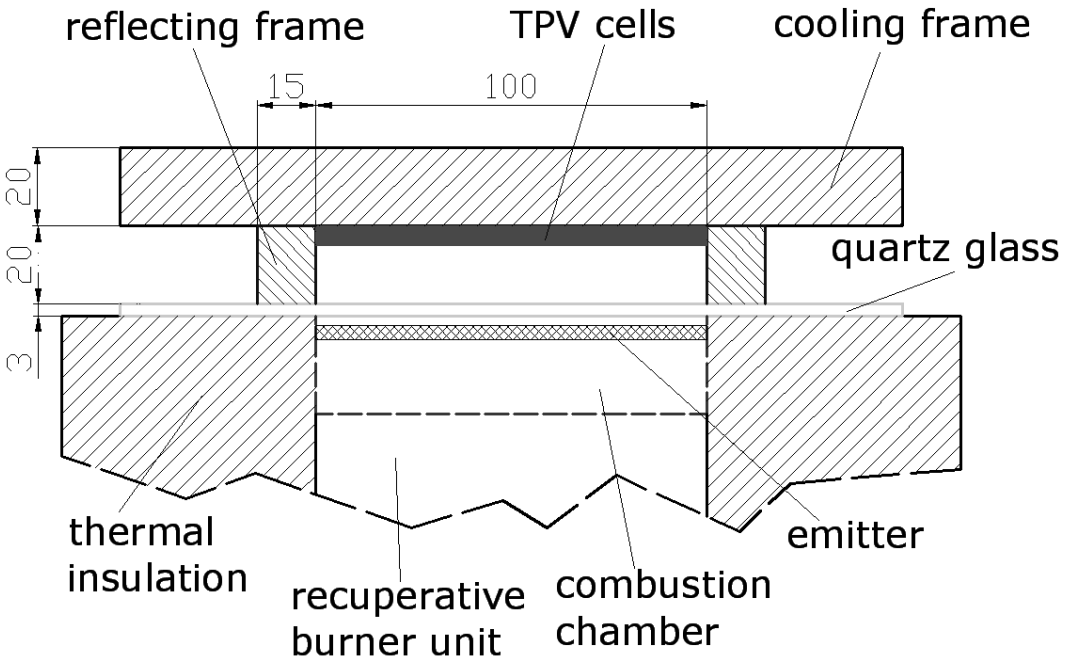

Figure 5.10: Scheme of the optical system design (lengths expressed in mm).

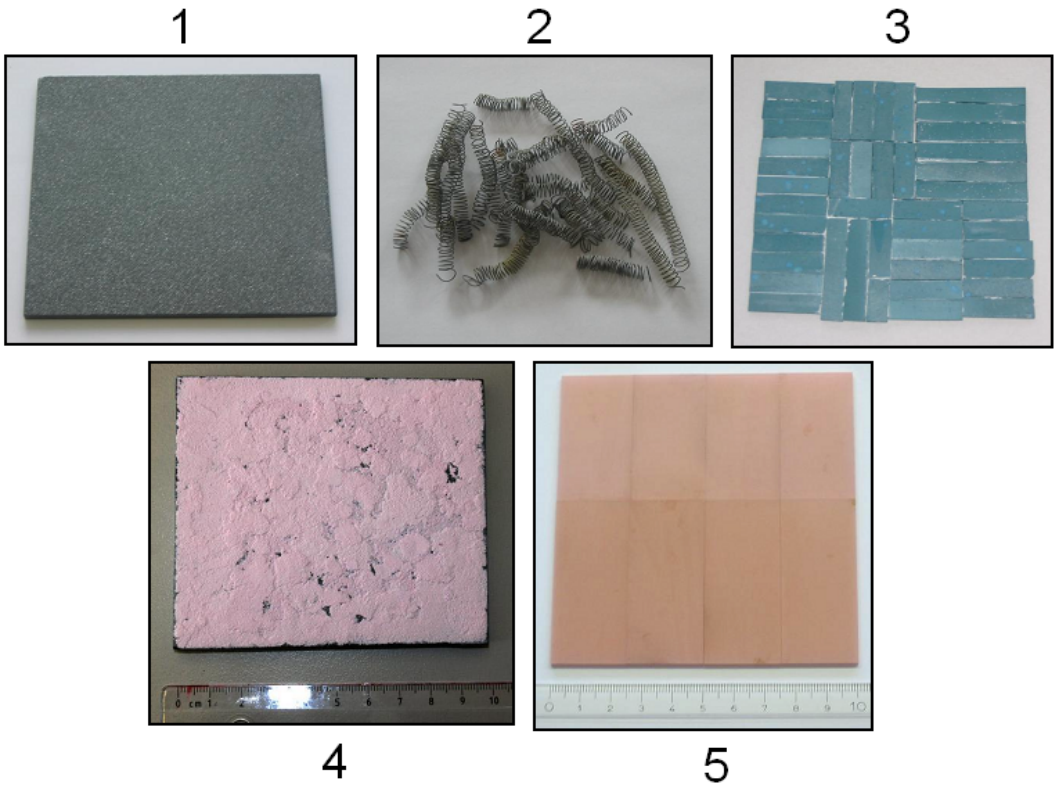

Figure 5.11: Emitter materials used in the TPV device: SiC tile (1), Kanthal wires (2), ceramic $MgAl_2O_4$:Ni (3), SiC tile covered by a porous garnet emitter based on $Er_3Al_5O_{12}$ (4), MGC eutectic ceramic based on $Al_2O_3/Er_3Al_5O_{12}$ (5).

1. SiC: a silicon carbide tile 4 mm thick supplied by Saint-Gobain Ceramics is used as gray not-selective emitter. As already pointed out, silicon carbide has a high emissivity (around 0.9) over the whole wavelength spectrum, approaching the behavior of a black body emitter, and it can withstand very high temperatures.

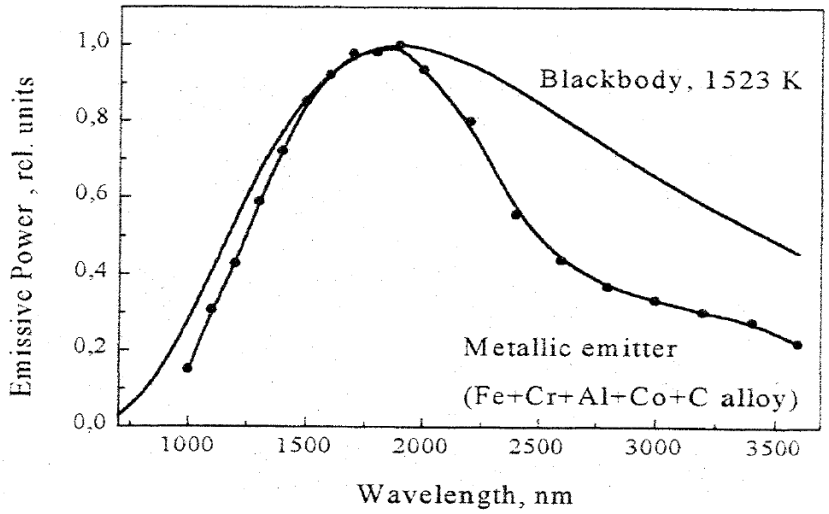

Figure 5.12: Emissive power spectrum of a high temperature alloy based on Fe, Cr and Al compared to the black body one [RKS+99].

2. Kanthal: it is a high temperature alloy based on Fe, Cr and Al able to withstand operating temperature up to 1400 °C. It is a semi-selective emitter: it has a low emissivity in the mid and far IR region, as shown in Figure 5.12. Kanthal wires with a diameter of 0.5 mm [Vol01] are used in the system to optimize the heat transfer with the flame and therefore the generation of thermal radiation.

3. $MgAl_2O_4$:Ni: it is a ceramic material based on a magnesium aluminum spinel doped with nickel. This material has been developed and realized by CEA (Grenoble, FRA), a partner of the Research Training Network, in the framework of a previous project. Unluckily it has not been possible to find reliable data concerning the spectral properties of the material: some information can be found in [FF97], but they refer to spinel not-doped or doped with cobalt. They show good selective properties for this kind of ceramic materials coupled to GaSb cells. However the effect of the nickel doping on the spectral properties is not known and spectral measurements of the same material, but in a crystal form, do not show spectral properties particularly attractive for TPV applications [WA86], [K+96].

4. Garnet emitter based on rare earth oxides: it consists of a SiC tile 4 mm thick over which a thin layer of porous garnet based on $Er_3Al_5O_{12}$ is deposited. The sample has been developed by the University of Lecce [DL+03], [DLT+04] and realized by Salentec (Lecce, Italy). It has very good spectral properties, as shown in Figure 5.13, with an emissivity peak in correspondence of the GaSb bandgap. The porous structure of the emitter layer is useful both to compensate the different thermal expansion of garnet and SiC assuring a good adhesion of the former, and

to shield the radiation coming from the SiC tile, increasing the spectral efficiency.

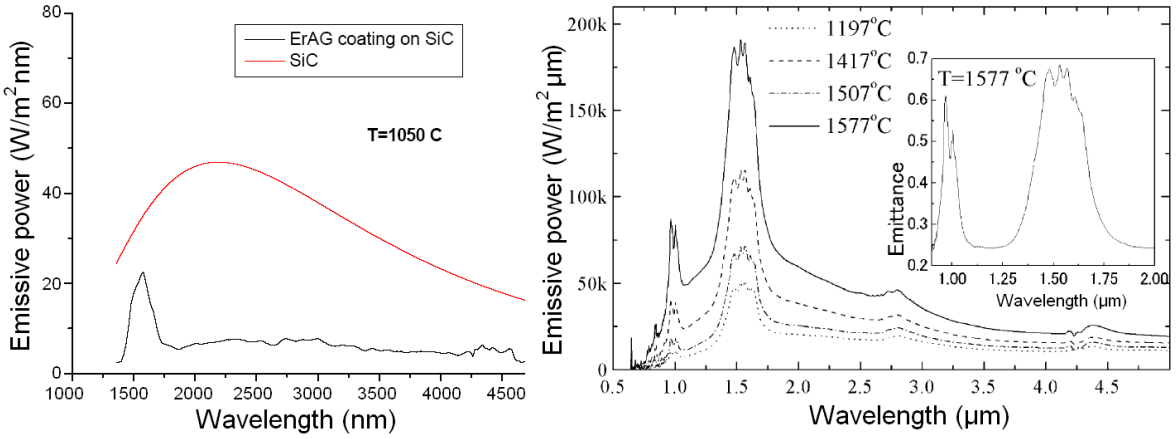

Figure 5.13: Emissive power spectra of erbium garnet emitter on a SiC substrate compared to that of pure SiC [DLT+04] and of the MGC based on $Al_2O_3/Er_3Al_5O_{12}$ eutectic ceramic [NOWY05].

5. MGC based on ErO: Melt Growth Composites are materials used for very high temperature applications: thanks to their structure (see Sec.2.4.3) they have high temperature strength and thermal stability even at 1700 °C. The material used in the TPV system is a tile of MGC eutectic ceramic based on $Al_2O_3/Er_3Al_5O_{12}$ developed and realized by Ube Research Laboratory (Yamaguchi, Japan) [NOM+05], [NOWY05]. Such a material has highly selective spectral properties with an emissivity peak close to the GaSb bandgap due to the presence of erbium oxide (see Figure 5.13).

Filter

The quartz glass used to seal the combustion chamber acts also as an absorptive filter for the incident radiation (see Sec.2.4.4). The glass plate is polished and has a dimension of 200 x 200 x 3 mm. Figure 5.14 shows the transmittance of a fused silica glass 12.7 mm thick [T+70].

Reflecting frame

A reflecting frame is used to minimize the radiation losses due to the gap present between burner and cells. Since the walls of the frame are not active in the generation or in the conversion of the radiation, they must have a reflectivity as high as possible, to minimize the radiation absorption and optimize the optical efficiency $\eta_{optical}$ (Eq.2.2).

The frame used, placed between burner and cells, has a square section with an inner side of 100 mm and it is made of a high-purity porous alumina ceramic, with 99.7% of Al_2O_3 content (Sintox^{TM} AL, from Morgan Advanced Ceramics), which is used normally as laser-reflector material (Figure 5.15). This material has a very high reflectivity (over 0.96) across the wavelength range 500-2500 nm, and very good resistance at high

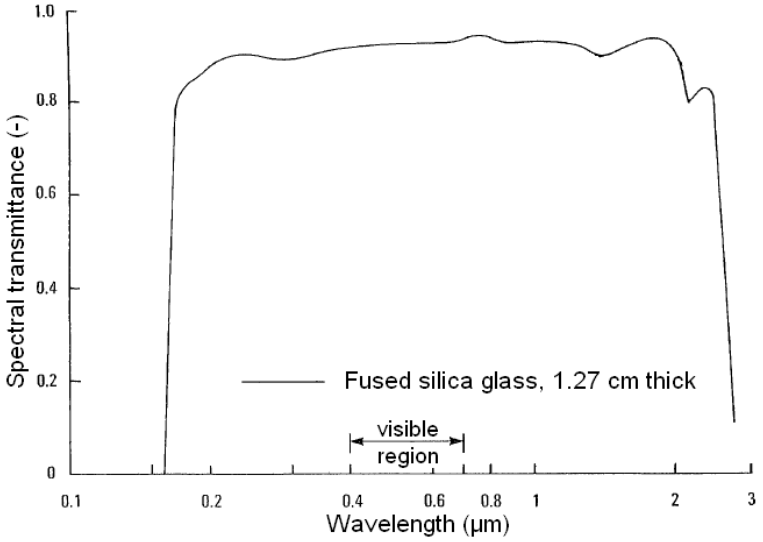

Figure 5.14: Spectral transmittance of a fused silica glass 12.7 mm thick [T$^+$70].

temperatures (over 1300 °C), properties that make it suitable as reflecting material for TPV applications.

5.3.2 Optical system model

In a real TPV system the radiation generated by the emitter is absorbed, transmitted and reflected by surfaces that do not behave as gray bodies: they do not have constant spectral properties over the whole wavelength spectrum and they have also directional properties (i.e. non-diffusive non-gray surfaces). Furthermore, the density of the radiation exchanged depends on the temperature of each surface, which generally is not uniform, and on the geometrical configuration of the cavity. A realistic model of the optical system must take into account all these aspects and implies the implementation of specific and complex methods, like the Ray-tracing method or the Monte Carlo technique [AHL03], which require also a big computational effort.

Such techniques go beyond the purpose of this work. A simpler model is implemented here: it does not aim to simulate and reproduce the behavior of the optical system as realistically as possible, but it has the purpose to evaluate and compare reliably its performance under different system configurations.

The model is based on the following simplifications:

- The surface temperatures of emitter, glass and cells are assumed to be uniform, that means that the spectral properties are constant all over each surface.

- Geometrical factors are not considered: all the view factors are assumed to be equal to one. The radiation losses caused by the reflecting frame are therefore neglected (i.e. $\eta_{optical}$=1). This is reasonable considering the high reflectivity of the reflecting frame and that emitter, glass and cells have the same area A and are placed very close to each other.

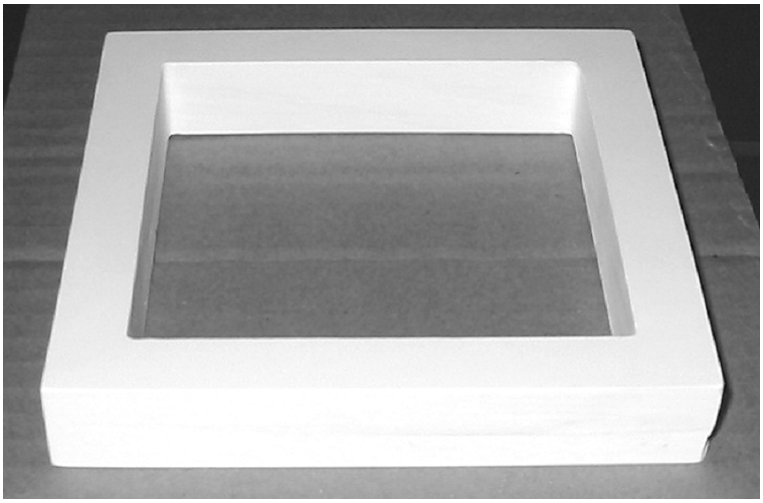

Figure 5.15: The reflecting frame made of high purity porous Al_2O_3.

- The spectral emissivity $\epsilon(\lambda)$ and reflectivity $\rho(\lambda)$ of emitter materials and cells are taken from literature or supplied by the manufacturer. Their dependence on the temperature is not taken into account. Extrapolations are carried out to evaluate such properties in the far IR region, if data are not available. For SiC a constant emissivity of 0.9 is assumed all over the spectrum range.

- The quartz glass is assumed to have a transmissivity τ_g of 0.9 and a reflectivity ρ_g of 0.1 for wavelengths up to $4\,\mu$m and an emissivity ϵ_g of 0.9 and a reflectivity of 0.1 for longer wavelengths.

The approach used to implement the model is based on the two-band model concept [SH75], as represented in Figure 5.16: a model with a partially transparent glass is considered for wavelengths up to $4\,\mu$m while a model with opaque surfaces is assumed for $\lambda > 4\,\mu$m.
Referring to Figure 5.16, for the case of $\lambda < 4\,\mu$m, the monochromatic radiative heat fluxes $q_j(\lambda)$ ($\mathrm{W\,m^{-2}\,m^{-1}}$) received and emitted by each surface result from the following system of equations:

$$\begin{aligned} q_{e,o}(\lambda) &= \epsilon_{e,\lambda} E_{b\lambda}(T_e) + q_{e,i}(\lambda)\rho_{e,\lambda} && (5.31)\\ q_{g1,o}(\lambda) &= q_{g1,i}(\lambda)\rho_g + q_{g2,i}(\lambda)\tau_g && (5.32)\\ q_{g2,o}(\lambda) &= q_{g1,i}(\lambda)\tau_g + q_{g2,i}(\lambda)\rho_g && (5.33)\\ q_{c,o}(\lambda) &= \epsilon_{c,\lambda} E_{b\lambda}(T_c) + q_{c,i}(\lambda)\rho_{c,\lambda} && (5.34) \end{aligned}$$

where the subscripts e, c and g refer respectively to the emitter material, to the cells and to the quartz glass, the subscripts *1* and *2* refer to the first and second glass surfaces, and the subscripts i and o refer to the fluxes incident and emitted. By using the following relations:

$$q_{e,i} = q_{g1,o}, \quad q_{g1,i} = q_{e,o}, \quad q_{g2,i} = q_{c,o}, \quad q_{c,i} = q_{g2,o} \qquad (5.35)$$

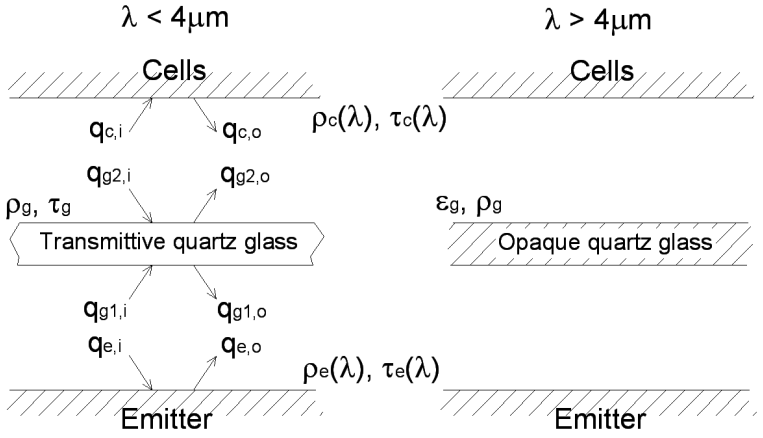

Figure 5.16: Two-band model concept: modelling approach of the optical system. For $\lambda < 4\mu$m the quartz glass is transparent and supports the transmission of the radiation, while for $\lambda > 4\mu$m the quartz glass is opaque and acts as a wall placed between emitter and cells.

the equation system above can be rewritten as:

$$q_{e,o}(\lambda) = \epsilon_{e,\lambda} E_{b\lambda}(T_e) + q_{g1,o}(\lambda)\rho_{e,\lambda} \quad (5.36)$$

$$q_{g1,o}(\lambda) = q_{e,o}(\lambda)\rho_g + q_{c,o}(\lambda)\tau_g \quad (5.37)$$

$$q_{g2,o}(\lambda) = q_{e,o}(\lambda)\tau_g + q_{c,o}(\lambda)\rho_g \quad (5.38)$$

$$q_{c,o}(\lambda) = \epsilon_{c,\lambda} E_{b\lambda}(T_c) + q_{g2,o}(\lambda)\rho_{c,\lambda} \quad (5.39)$$

By setting the emitter and cell temperatures the system can be solved for each value of wavelength in the range from 0 up to 4 μm and the monochromatic radiative heat flux between emitter and cells $q_{e \leftrightarrows c}(\lambda)$ results:

$$\begin{aligned} q_{e \leftrightarrows c}(\lambda) &= q_{e,o}(\lambda) - q_{e,i}(\lambda) \\ &= q_{c,i}(\lambda) - q_{c,o}(\lambda) \end{aligned} \quad (5.40)$$

For wavelengths longer than 4 μm the optical system configuration can be represented as an intermediate opaque wall (the quartz glass) separating the emitter and the cell surfaces. Referring to Eq.2.31 and Eq.2.34, the optical system can be represented as an equivalent electrical circuit in which black body emissive power E_b and radiosity J act as potentials and the radiative heat (A times q) as current. Figure 5.17 shows the equivalent circuits representing the radiative heat powers exchanged between the emitter and the first quartz glass surface ($A\, q_{e \leftrightarrows g1}$), and between the second quartz glass surface and the cells ($A\, q_{g2 \leftrightarrows c}$). For the assumptions made, $q_{e \leftrightarrows g1}$ and $q_{g2 \leftrightarrows c}$ are equal and correspond to the radiative heat flux between emitter and cells $q_{e \leftrightarrows c}$.

Assuming that the two quartz glass surfaces have the same temperature T_g and remembering from the hypothesis made that emitter, cells and glass have the same area A and view factors equal to one, the equivalent electrical circuit of the optical system for $\lambda > 4\mu$m can be represented as in Figure 5.18, in which the monochromatic radiative power is considered. Therefore the monochromatic radiative heat flux between emitter

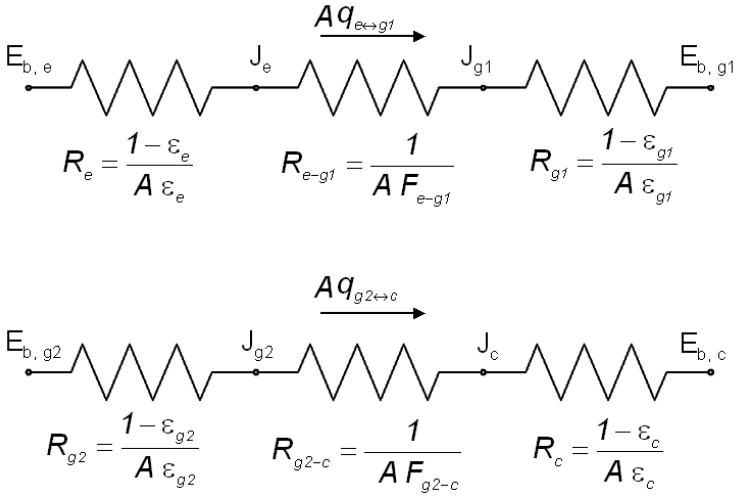

Figure 5.17: Equivalent electrical circuits for the radiative heat transfer for $\lambda > 4\mu$m between emitter and glass (above) and between glass and cells (below).

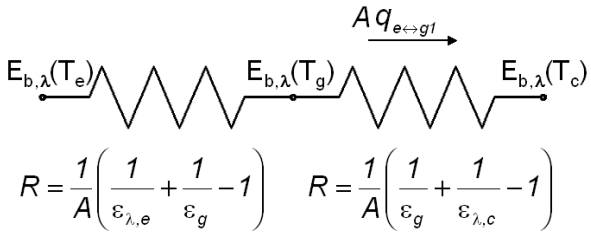

Figure 5.18: Equivalent electrical circuit for the radiative heat transfer between emitter and cells for $\lambda > 4\mu$m.

and cells $q_{e\leftrightarrows c}(\lambda)$ results:

$$q_{e\leftrightarrows c}(\lambda) = \frac{E_{b\lambda}(T_e) - E_{b\lambda}(T_c)}{R_{tot}} = \frac{E_{b\lambda}(T_e) - E_{b\lambda}(T_c)}{\frac{1}{\epsilon_{e,\lambda}} + \frac{1}{\epsilon_{c,\lambda}} + \frac{2}{\epsilon_g} - 2} \tag{5.41}$$

The equation above and Eq.5.40, together, allow to calculate the spectrum of the net radiation generated and absorbed over the whole wavelength range.

The total radiative power density generated by the emitter and absorbed by the cells is calculated by integrating the monochromatic radiative heat flux $q_{e\leftrightarrows c}(\lambda)$:

$$q_{e\leftrightarrows c} = \int_0^\infty q_{e\leftrightarrows c}(\lambda)\mathrm{d}\lambda \tag{5.42}$$

The spectral efficiency of the system, therefore, is:

$$\eta_{spectral} = \frac{q_{rad-matching}}{q_{rad-cells}} = \frac{\int_0^{\lambda_{limit}} q_{e\leftrightarrows c}(\lambda)\mathrm{d}\lambda}{\int_0^\infty q_{e\leftrightarrows c}(\lambda)\mathrm{d}\lambda} \tag{5.43}$$

The simulation approach described above can be used also for optical system configurations in which not only one, but two or more quartz glass plates are placed between

emitter and cells (multiple parallel windows), to improve the spectral efficiency. In the general case of a system of windows composed by two groups of m identical plates (ρ_m, τ_m) and n identical plates (ρ_n, τ_n), the total reflectivity ρ_{tot} and transmissivity τ_{tot} of the glass window system, with a radiation incident on the "m side" and wavelengths smaller than 4 μm, is given by [SH92]:

$$\rho_{tot} = \rho_m + \frac{\rho_n \tau_m^2}{1 - \rho_m \rho_n} \qquad \tau_{tot} = \frac{\tau_m \tau_n}{1 - \rho_m \rho_n} \tag{5.44}$$

For the case of two identical quartz glass plates, therefore, it results:

$$\rho_2 = \rho_{1+1} = \rho_g + \frac{\rho_g \tau_g^2}{1 - \rho_g^2} \qquad \tau_2 = \tau_{1+1} = \frac{\tau_g^2}{1 - \rho_g^2} \tag{5.45}$$

The process can be continued for any value m of plates (e.g. for three plates $\rho_3 = \rho_{1+2}$ and $\tau_3 = \tau_{1+2}$). Similarly Eq. 5.44 can be used for two parallel quartz glasses, one of them having a coating reflecting in the range between 2 and 4 μm. In this case, however, the optical properties must be evaluated as function of the wavelength.

For wavelengths longer than 4 μm, in case of parallel windows, R_{tot} in Eq.5.41 results:

$$R_{tot} = \frac{1}{\epsilon_{e,\lambda}} + \frac{1}{\epsilon_{c,\lambda}} - 1 + m\left(\frac{2}{\epsilon_g} - 1\right) \tag{5.46}$$

in which m is the number of parallel glass windows.

5.4 TPV cells

5.4.1 Cell design

The thermophotovoltaic cells used in the system are based on GaSb and made of MOVPE-grown structures, realized by Fraunhofer Institute for Solar Energy Systems (Freiburg) [SDOB04] in the framework of the research Training Network "Thermophotovoltaic cells based on GaSb". Four arrays of cells have been supplied.

The cell bandgap is equal to 0.68 eV, corresponding to a wavelength limit λ_{limit} of about 1.8 μm. Each array has a dimension of 40.65 x 21.4 mm and it is made of 5 cells, each 20 mm wide, connected in series with the shingling technique by using an electric conductive glue. The top contact grid is designed for current densities of 1 A cm^{-2}.

The cells are glued on an aluminum nitride (AlN) substrate 4 mm thick, which is in contact with the cell cooling frame. AlN is a ceramic material which has an extremely high electric resistivity (over $10^{12}\,\Omega$ cm) to avoid the shorting of the array and at the same time has a very high thermal conductivity (up to 180 W m^{-1}K^{-1}), a fundamental requirement to assure a good thermal transfer between cells and heat sink and therefore to prevent heating and degradation of the cells. The cells, indeed, should not operate over a maximum temperature of 340 K to avoid to be damaged. Figure 5.19 shows one of the four cell arrays used in the system and the EQE measured on one GaSb cell [AD05].

The reference I-V curves of the four modules, supplied by ISE, are shown in Figure 5.20 [AD05]. They have been measured with cells at ambient temperature and using

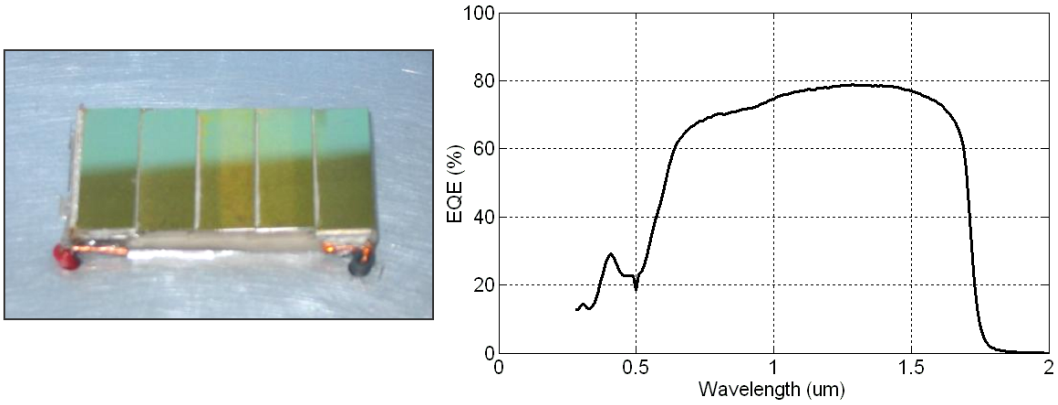

Figure 5.19: Array of cells based on GaSb used in the TPV system and EQE measured on one GaSb cell at 45 °C [AD05].

a flash lamp providing a radiation intensity able to generate a current of 1 A. The fill factor values vary in a range between 0.53 and 0.67.

As written in Sec.2.5, the temperature of the cells affects their efficiency and performance, and its influence is expressed by the temperature coefficients $T_{c-I_{sc}}$, $T_{c-V_{oc}}$ and $T_{c-P_{MPP}}$. Few experimental data are available for the evaluation of the GaSb cell temperature coefficients: in [SAB+05] two different GaSb cells have been tested both at one sun conditions and under light with a higher intensity in order to have a current density of 1.5 A cm^{-2}. The data show a decrease of the absolute value of the temperature coefficients at higher illumination ($T_{c-V_{oc}}$ of -0.349 %/K and $T_{c-P_{MPP}}$ of -0.394 %/K instead of respectively -0.593 %/K and -0.660 %/K for one sun conditions). Nevertheless the tests showed a large difference of the temperature coefficients between the two cells tested: the values reported here are the averaged ones.

More detailed information about the cell design, fabrication and characterization can be found in [SDOB04], [SAB+05] and [SAA+05].

5.4.2 Cell performance simulation

Given the spectrum of the radiation absorbed by the cells (Eq.5.40) and their spectral properties, it is possible to evaluate the amount of radiation converted into electric power and the part lost as thermal heat.

The electrons flux generated per unit of wavelength N_e (electron m^{-2}s^{-1}m^{-1}) is given by the expression:

$$N_e(\lambda) = \frac{q_{e \leftrightarrows c}(\lambda)}{E_{ph}(\lambda)} IQE(\lambda) \tag{5.47}$$

E_{ph} and IQE are respectively the photon energy and the internal quantum efficiency. The former is given by:

$$E_{ph}(\lambda) = \frac{hc}{\lambda} \tag{5.48}$$

with h being the Planck's constant and c the light speed, while IQE corresponds to the product of the measured external quantum efficiency EQE with the cell emissivity ϵ_c, which is plotted in Figure 5.21 [AD05]. Therefore the photovoltaic current density

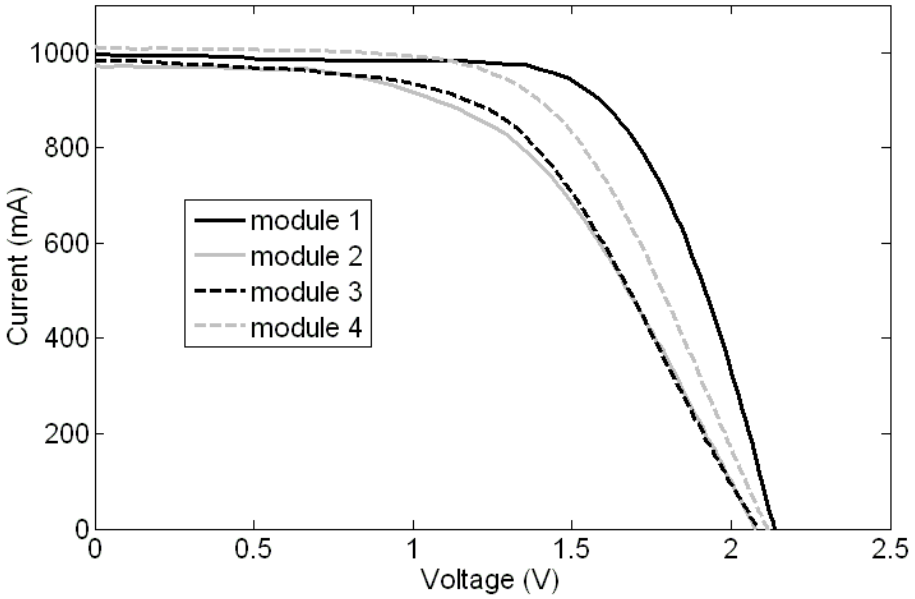

Figure 5.20: I-V curves of the four arrays of cells measured using a flash lamp at ambient temperature [AD05].

($\mathrm{A\,m^{-2}}$) generated by the cells, which corresponds to the short circuit current density J_{sc}, is equal to:

$$J_{ph} = \int_0^\infty N_e e^- \mathrm{d}\lambda \tag{5.49}$$

where e^- is the electron charge, whose absolute value is equal to $1.6\,10^{-19}$ C.

In a real cell the open circuit voltage V_{oc} does not correspond to the band-gap E_g of the cell: even if the generated carriers are separated by a potential corresponding to the band-gap energy, the p-n junction cell gives a voltage output which is only a fraction of this potential.

As pointed out in Sec.2.5 the open circuit voltage and the fill factor do not depend on the spectrum of the incident radiation, but only on the short circuit current density J_{sc} and on the cell temperature. Therefore in order to evaluate theoretically performance and efficiency of a cell, it is necessary to know the dependence of V_{oc} and FF on the short circuit current density and the effect of the temperature on the cell characteristic, i.e. the cell temperature coefficients. These parameters can be measured directly and used, via interpolation or fitting methods, to calculate the cell performance under different operating conditions.

The open circuit voltage can be estimated also theoretically, with a simpler but less accurate method: V_{oc} can be obtained from the diode equation Eq.2.36 by setting I_{cell} equal to zero:

$$V_{oc} = kT \log\left(\frac{I_{ph}}{I_0} + 1\right) \tag{5.50}$$

The saturation current density I_0 depends on the semiconductor material properties (diffusion coefficient, diffusion length, doping level of p- and n-side). An empirical expression proposed in [Gre92] can be used to estimate its minimum value.

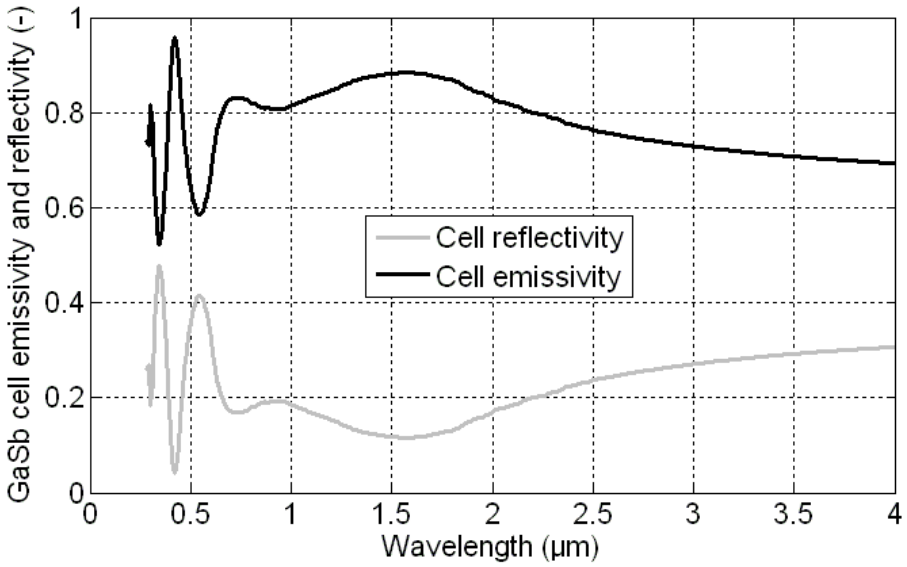

Figure 5.21: Emissivity and reflectivity of the GaSb cells used in the TPV system [AD05].

From the values of V_{oc} and I_{sc} and by knowing the fill factor FF of the cell it is possible to calculate the maximum power density output of the cell (see Eq.2.37) and therefore the cell efficiency related to the spectrum of the radiation absorbed, as defined in Eq.2.4:

$$\eta_{PV} = \frac{P_{el}}{Q_{rad-matching}} = \frac{V_{oc} J_{sc} FF}{\int_0^{\lambda_{limit}} q_{e \leftrightarrows c}(\lambda)\, \mathrm{d}\lambda} \tag{5.51}$$

As pointed out in Sec.2.5.1, there are two main phenomena that limit the cell efficiency and cause heat losses: thermalisation and photon absorption probability, the latter depending on the fact that EQE is less than one. The thermalisation losses ($\mathrm{W\,m^{-2}}$) are expressed by:

$$q_{thermalisation} = \int_0^{\lambda_{limit}} N_e(\lambda)(E_{ph}(\lambda) - V_{oc})\mathrm{d}\lambda \tag{5.52}$$

while the so called parasitic losses ($\mathrm{W\,m^{-2}}$) are given by:

$$q_{parasitic} = \int_0^{\infty} q_{e \leftrightarrows c}(\lambda)(1 - IQE(\lambda))\mathrm{d}\lambda \tag{5.53}$$

By doing an energy balance it must result:

$$q_{e \leftrightarrows c} = V_{oc} J_{sc} + q_{thermalisation} + q_{parasitic} \tag{5.54}$$

5.5 Cell cooling frame

5.5.1 Cooling frame design approach

The cell cooling frame has been designed with the purpose of keeping the cells at a temperature low enough, in safe conditions, without aiming at a compact or highly

efficient design in this first TPV system testing phase. In case of a further prototyping phase, the minimization of the power needed to operate the cooling system (use of air fan or water pump) and the compactness of the unit will become crucial issues.

The approach followed to realize the cooling system is to fix the cells over a metal frame cooled with water flowing through a series of parallel channels drilled in it. The metal frame acts as heat sink for the cells transferring the heat absorbed to the water, which releases it in an air-water heat exchanger coupled to a fan. Figure 5.22 shows a scheme of the cooling frame and of the cooling system concept.

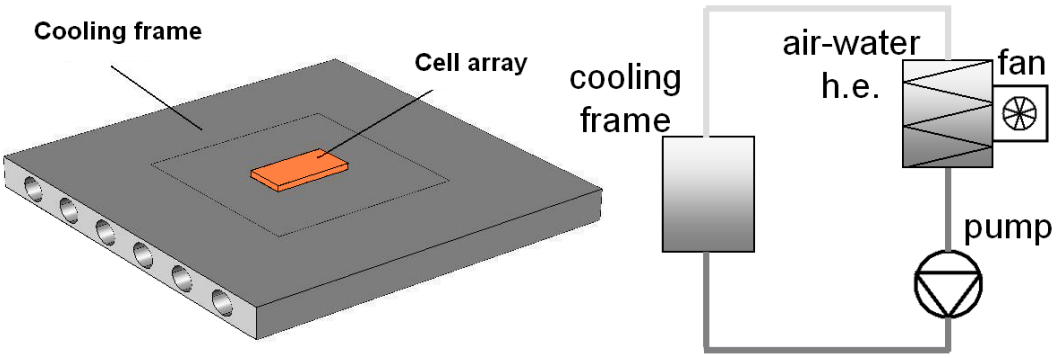

Figure 5.22: Scheme of the cooling frame and of the cooling system design.

Recalling the concept of thermal resistance (Sec.2.3), the total heat transfer resistance between cells and flowing water can be seen as the series of four thermal resistances representing the conduction through cell (R_{cond}^{cell}), cell-metal frame contact ($R_{cond}^{contact}$) and metal frame (R_{cond}^{frame}), and the convection between frame and cooling water (R_{conv}^{water}):

$$R_{tot}^{cell-water} = R_{cond}^{cell} + R_{cond}^{contact} + R_{cond}^{frame} + R_{conv}^{water} \tag{5.55}$$

Conductive and convective thermal resistances are expressed as in Eq.2.11. Optimizing the cooling process means to minimize this overall resistance, i.e. to minimize the last three terms of the equation above since the value of R_{cond}^{cell} is fixed and depends on the cell array design. The following aspects have been considered in the development of the component:

- Cell-frame contact: the cell arrays cannot be fixed mechanically over the metal frame. They are very fragile and they cannot be subjected to almost any load or stress. Furthermore a very good thermal contact between cell array and frame must be assured: the presence of very small air cavities between the two surfaces would increase drastically the contact thermal resistance due to the low air thermal conductivity. For these reasons the arrays are glued to the frame with an adhesive paste which is both thermal conductive and electrical insulating. It is crucial for the thermal management of the cells to use a glue with a thermal conductivity as high as possible. Thermal pastes available on the market have λ varying between 1 and 7 $\mathrm{W\,m^{-1}K^{-1}}$, a value up to 200 times lower than that of metals. Although the very small thickness of the glue layer, therefore, $R_{cond}^{contact}$ can affect significantly $R_{tot}^{cell-water}$.

- Metal frame: the key aspect to minimize R_{cond}^{frame} is to use a metal with a high thermal conductivity. Copper (λ of about 400 $\mathrm{W\,m^{-1}K^{-1}}$) and aluminum (230 $\mathrm{W\,m^{-1}K^{-1}}$) are the two best candidates.

- Water cooling: the heat transfer coefficient α between water and metal frame can be evaluated by using empirical expressions in the form of Eq.2.14. By reducing the channel diameter and increasing the water mass flow, α increases, as well as the pressure drops across the channels. A compromise must be found to assure a good heat transfer and to avoid high pressure drops.

Several possible designs of the component have been evaluated, based on the considerations above. By using the FEM software they have been compared in order to choose the best one, which shows the highest heat transfer between cells and water and in which the pressure drops do not represent a critical issue. The models implemented are based on the Fourier's law of thermal conduction:

$$\frac{\partial(\rho c_p T)}{\partial t} = \nabla(\lambda \nabla T) \tag{5.56}$$

The water flow is not simulated: the heat flux absorbed by the water is calculated by setting the convective heat transfer coefficient α as boundary conditions at the channel walls. α is given by the expression [B$^+$85], [KB01]:

$$\alpha = 0.023 \frac{Nu\lambda}{d} Re^{0.8} Pr^{0.3} \tag{5.57}$$

where d is the channel diameter.

5.5.2 Component realization

The final component realized is shown in Figure 5.23: it consists of a square aluminum frame of dimension 200 x 200 mm with a thickness of 20 mm. Six parallel channels with a diameter of 15 mm are drilled into it and connected in series with a flexible pipe. The conductive adhesive paste used to fix the arrays on the metal has a thermal conductivity of 7.5 $\mathrm{W\,m^{-1}K^{-1}}$ (Arctic Silver Thermal Adhesive®) and it is not removable. To be able to separate the cooling frame from the cells, the cell arrays are glued over an aluminum plate 4 mm thick which is pressed mechanically against the aluminum frame. To optimize the heat transfer between frame and plate a thin thermal conductive graphite film (Keraterm®90) is placed in between.

5.6 Complete TPV system theoretical model

In the previous sections the modelling approaches followed to implement and simulate the theoretical models of the different components have been shown. As already pointed out, in order to understand better the behavior of the system and optimize its operation it is fundamental to take into account all the reciprocal correlations between the different processes involved. Therefore all the theoretical models implemented are coupled as shown schematically in Figure 5.24: the results obtained from the simulation of one

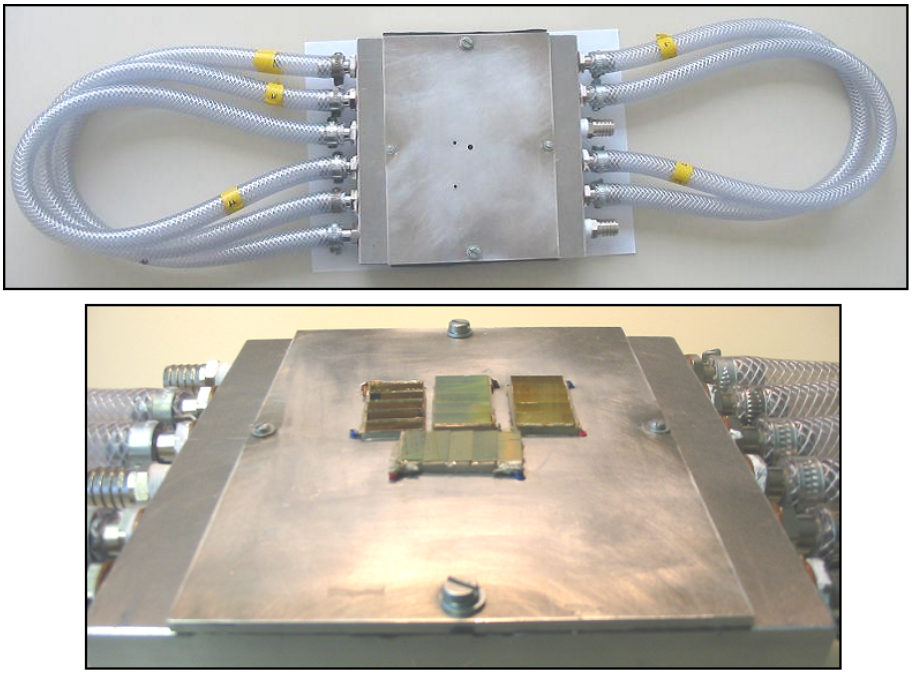

Figure 5.23: Pictures of the aluminum cooling frame after realization and with the cell arrays glued on it.

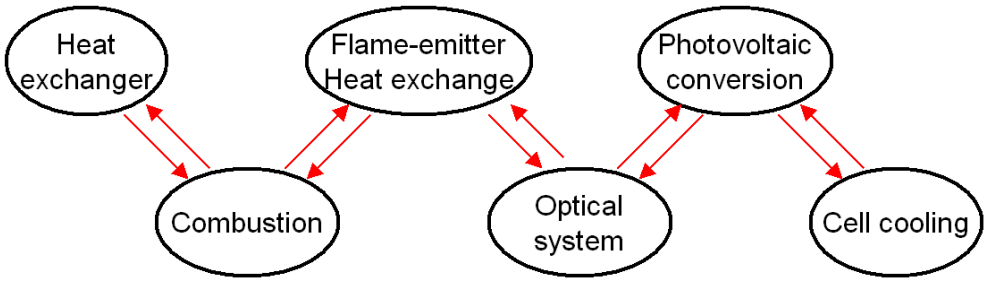

Figure 5.24: Approach followed to implement the theoretical simulation model of the whole TPV system.

component are used as inputs to simulate the other processes. With an iterative process the final results are obtained.

Following this approach the theoretical models of flame-emitter heat exchange, optical system, TPV cells and cooling frame are coupled in a single model, whose geometry is shown in Figure 5.25. The model is solved based on the PDEs and on the expressions reported in the previous sections. To take into account the heat transfer through the air gaps between emitter and glass and between glass and cells, the Fourier's law of thermal conduction (Eq.5.56) is considered, while the convective heat transfer is neglected: during experimental tests, indeed, the generation of convective currents between burner and cells is avoided by placing the cells under the combustion chamber so that the hot air is kept close to the latter.

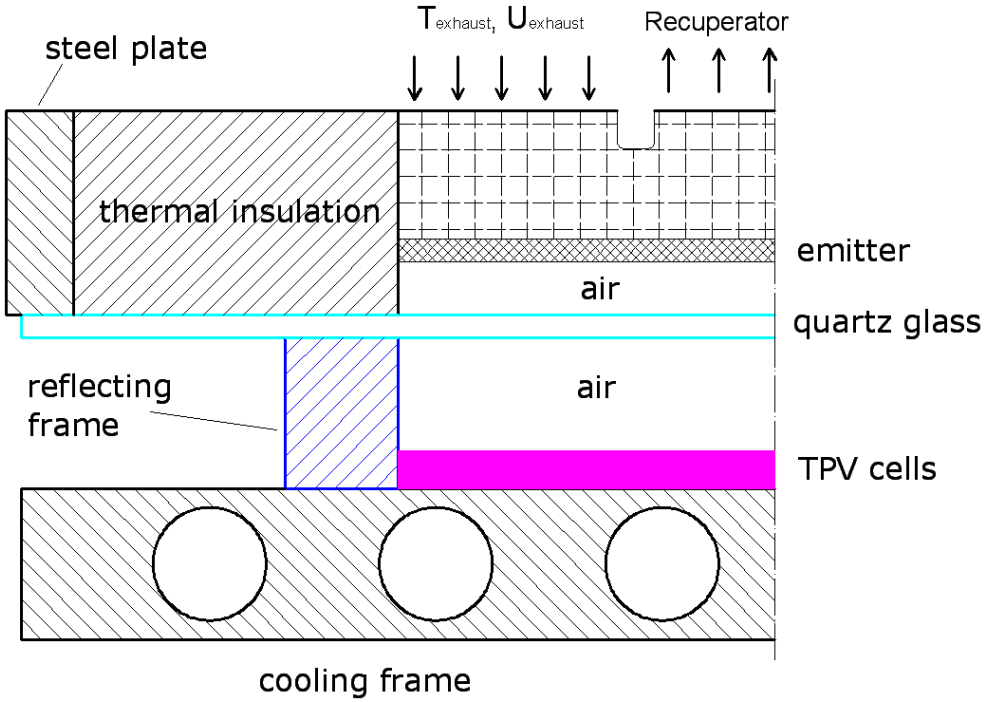

Figure 5.25: Scheme of the model that couples together flame-emitter heat exchange, optical system, photovoltaic conversion and cell cooling.

5.7 Complements to the TPV device

Recuperative burner unit, optical system, cell arrays and cooling frame represent the core of the TPV system. However other components are needed to run the system and operate it under safe conditions.

Air loop

The combustion air is supplied into the recuperative burner unit by means of a fan (RG148 ebm-papst). The air volume flow is constantly monitored via a flowmeter (LB/89, La Tecnica Fluidi). To vary the air flow the fan is coupled to an electronic speed interface based on a PWM control.

Methane loop

In order to evaluate correctly the efficiency of the system it is fundamental to control and monitor accurately the mass flow of fuel, i.e. the chemical power supplied into the system. A massflow controller (Red-y®, Vögtlin Instruments) is used for such a purpose. The controller is connected to a PC with a serial port, which allows to set and monitor directly the methane mass flow. The controller is designed for supplying a maximum mass flow of $0.095\,\mathrm{kg\,h^{-1}}$, which corresponds to a maximum chemical power of about 1320 W, with an accuracy of $\pm 1.5\%$.

Between gas bottle and controller, two pressure reducers are used to scale the pressure from over 150 bar down to 3 bar.

Water loop

Components of the water loop are the pump, the flowmeter, the cooling frame and the air-water heat exchanger coupled to a fan.

To dimension and choose an appropriate pump for this application the water pressure drops Δp must be first evaluated. They correspond to the sum of distributed pressure losses along the pipes and concentrated pressure losses taking place inside cooling frame, heat exchanger and rotameter and where there is a flow cross section change. Generally pressure drops are expressed in the form:

$$\Delta p = \xi \frac{\rho u^2}{2g} \tag{5.58}$$

in which ξ is the so called pressure loss coefficient: it depends mainly on the flow cross section geometry and on the Reynolds number Re. For the heat exchanger (Valeo TA341) and the flowmeter (Profimess SM-15) the value of ξ is supplied by the manufacturer. To evaluate Δp in the pipes and in the cooling frame, empirical values of the pressure loss coefficient can be calculated by referring to [Ide69].

Pressure drops along the water loop have been evaluated depending on the water mass flow, on the pipe diameter and on the cooling frame channel dimension. The final channel and pipe dimensions have been chosen as the best compromise between pressure losses and convective heat transfer coefficient in the cooling frame. Finally, based on the water flow and on the pump head required, the pump has been dimensioned and chosen (Wilo-Stratos 30/1-12 pump).

Logging and monitoring system

Besides the control and the monitoring of the different mass flows supplied into the system, during tests it is necessary to measure the temperatures in the recuperative burner unit and on the cell back surface, and the IV curve of the cell arrays in order to control and evaluate the system performance.

Variable monitored	Sensor/instrument used
Air volume flow	Flowmeter
Water volume flow	Flowmeter
Methane mass flow	Mass flow controller
Pre-heated air temperature	4 thermocouples type R
Exhaust gas temperature, burner outlet	5 thermocouples type R
Exhaust gas temperature, recuperator outlet	1 thermocouple type K
Inlet air temperature	1 thermocouple type K
Back surface cell temperature	1 thermocouple type K
Cell array IV curve	Voltmeter and amperometer coupled to a programmable power supply

Table 5.1: Variables monitored, sensors and instruments used.

In particular, in the recuperative burner unit the temperatures are monitored by means of thermocouples placed at different locations: at the inlet (air and methane

temperature) and outlet (exhaust gas temperature) of the device, and in the combustion chamber, at the preheated air inlet and at the exhaust gas outlet (i.e. respectively outlet and inlet of the heat exchanger on the high temperature side).

To obtain the IV curve of the cells, the cell arrays are connected to a programmable power supply which acts as a variable load: voltage and current are measured while increasing slowly the current through the load. Table 5.1 gives an overview of the different variables measured and of the instruments/measurement sensors used.

All the thermocouple sensors are connected to an Agilent 34410a multiplexer, placed in an Agilent 34970a Data Acquisition Unit. The unit communicates with a PC via a GPIB interface. The temperatures and the methane mass flow are directly monitored on the PC by using a graphical user interface implemented with the software LabVIEW. Such an interface allows also to set the value of the methane mass flow, to log all the data in a Text file and to adjust the measurement sampling time.

Correcting thermocouple measurements

When measuring gas at very high temperatures with thermocouples, attention must be payed to interpret correctly the signal transmitted by the temperature sensor: the temperature displayed by the thermocouple, indeed, is the sensor temperature T_s, and not the gas temperature T_g. To evaluate with a good accuracy the latter, an energy balance on the thermocouple must be made and solved for the gas temperature [Sha98]. Without considering thermal conduction effects on the thermocouple, the heat q_{conv} exchanged via convection between the temperature sensor and the gas must be equal to the heat q_{rad} lost in the ambient through radiation:

$$q_{conv} + q_{rad} = \alpha(T_g - T_s) + \sigma\epsilon_s(T_w^4 - T_s^4) = 0 \tag{5.59}$$

where T_w is the temperature of the wall surrounding the thermocouple. Referring to Eq.2.13 and rewriting the equation above as function of the gas temperature, it follows:

$$T_g = T_s + \sigma\epsilon_s(T_w^4 - T_s^4)\frac{d}{\lambda_g Nu_{d,sph}} \tag{5.60}$$

The Nusselt number $Nu_{d,sph}$ refers in this case to the convective heat transfer over the thermocouple junction, which can be approximated to a sphere of diameter d. The most common empirical expression used for the Nusselt number $Nu_{d,sph}$ at low Reynolds numbers in forced convection is [RM52]:

$$Nu_{d,sph} = 2.0 + 0.6\, Re_d^{0.5} Pr^{1/3} \tag{5.61}$$

in which Re_d and Pr refer to the gas properties evaluated at the free stream.

The emissivity of the thermocouple junction ϵ_s can be evaluated by referring to empirical expressions proposed by [GER80].

Complete final system

Figure 5.26 shows the final TPV device assembled and in operation.

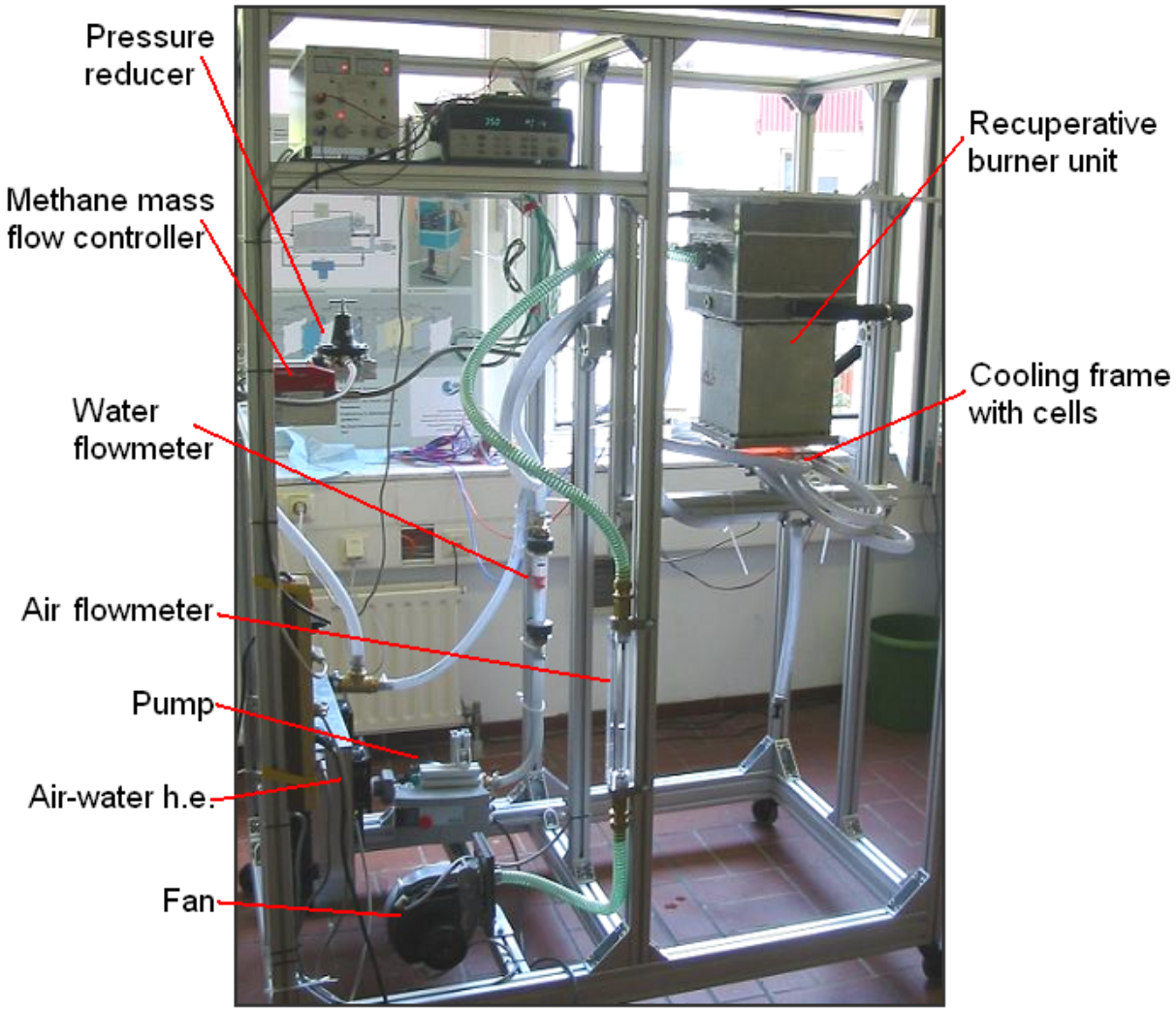

Figure 5.26: Picture of the built TPV system in operation.

6

Experimental and simulation results

6.1 TPV system operating conditions

The driving idea of this work, as already pointed out, is to realize a TPV tester able to operate in different conditions and with different configurations in order to obtain a better knowledge of the technology and understand better in which direction to move for its optimization.

During experimental tests, therefore, the different emitter materials have been tested and chemical power and combustion air number λ (i.e. methane and air mass flow) have been varied in a range between 690 and 1320 W (i.e. from 0.05 to 0.095 $\mathrm{kg}_{fuel}\,\mathrm{h}^{-1}$) and between 2 and 3 respectively.

During operation the device is turned upside-down and the TPV cells are placed under the combustion chamber. In this way the hot air is kept close to the emitter and the convective heat flux between burner and cells is minimized: the heat transfer takes place via radiation and conduction, the latter process being less influent compared to the former due to the low air thermal conductivity.

When the system is started a certain time is required to reach steady state conditions because of the high thermal capacity of the device and the low thermal conductivity of the insulation: Figure 6.1 shows the time-dependent profile of the temperature in the burner and on the back surface of the cells during an experimental test.

6.2 Recuperator effectiveness

The effectiveness ϵ of the recuperator, given its geometry, depends on the mass flow of air and fuel and on the temperatures at the inlet and outlet of the component, and it is defined as described in Sec.2.3.1. The specific heat capacity c_p of air, methane and exhaust gas is not constant, but is a function of the temperature: the equation Eq.2.6, which expresses the amount of heat exchanged by a fluid in the heat exchanger is therefore rewritten more correctly as:

$$Q = \dot{m} \int_{T_{in}}^{T_{out}} c_p \mathrm{d}T \tag{6.1}$$

In the case of experimental tests, temperatures and mass flows are directly measured, while in the theoretical model case the temperature of the pre-heated air entering the

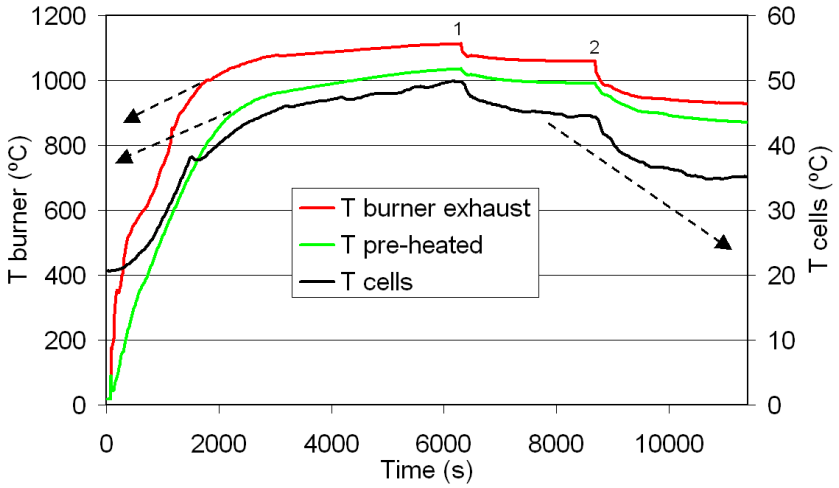

Figure 6.1: Time dependent temperature profiles in the combustion chamber and on the back surface of the cells during an experimental test. The sudden temperature changes at the points 1 and 2 are due to a change of the methane mass flow.

burner and of the cooled exhaust gas exiting the heat exchanger are obtained by solving the theoretical model described in Sec.5.1.2. Figure 6.2 shows an example of the temperature field inside the heat exchanger resulting from simulations.

The values of the heat exchanger effectiveness ϵ obtained from experimental tests and from simulations are plotted in Figure 6.3, as function of the fluid mass flow flowing through the component (i.e. fluid velocity) and of the temperature difference between the two inlets of the recuperator.

The experimental values of ϵ vary between 0.9 and 0.95, showing one of the highest thermal efficiencies so far reported for a recuperator. There is also a good agreement between test and simulation results. The theoretical values obtained show a slightly higher effectiveness (from 0.95 up to 0.96): this is likely due to the simplifications assumed in the geometrical model. However it can be stated from the results obtained that the theoretical model is valid and can be used for further simulations under different operating conditions.

6.3 Performance of the burner unit

6.3.1 Thermal behavior of the emitter materials

The several experimental tests carried out on the TPV device confirmed that almost all the emitter materials used have good thermal properties: the SiC tile, the ErO garnet on the SiC substrate, the Ni doped spinel plate and the Kanthal wires did not show any cracking or degradation even after several hours of operation.

The only emitter material that showed poor thermal resistance properties is the MGC ceramic material. Experimental tests have been realized by an external institute to measure the spectral properties of the emitter at high temperatures [Tob07]: the MGC sample cracked after reaching a certain temperature (around 700 °C) even when heated up very slowly, and even after heating it presented more smaller cracks. Therefore

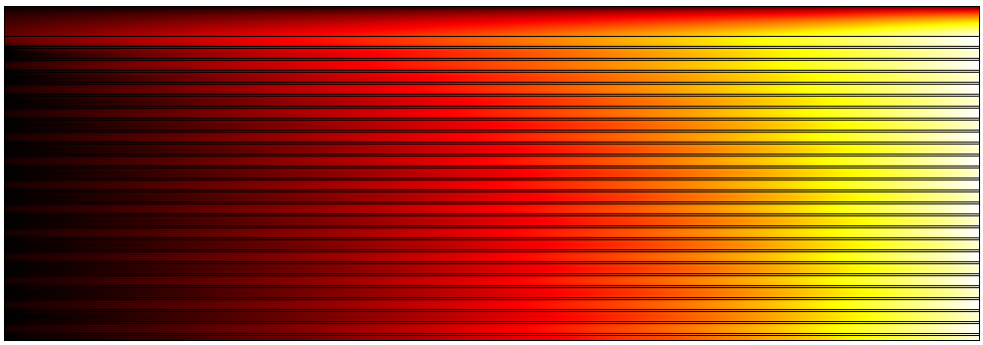

Figure 6.2: Temperature field in the recuperator resulting from the theoretical model simulation. As boundary conditions an air inlet temperature of 300 K, an exhaust gas inlet condition of 1400 K, a fuel mass flow of 0.09 kg h^{-1} and an air number of 2 are assumed.

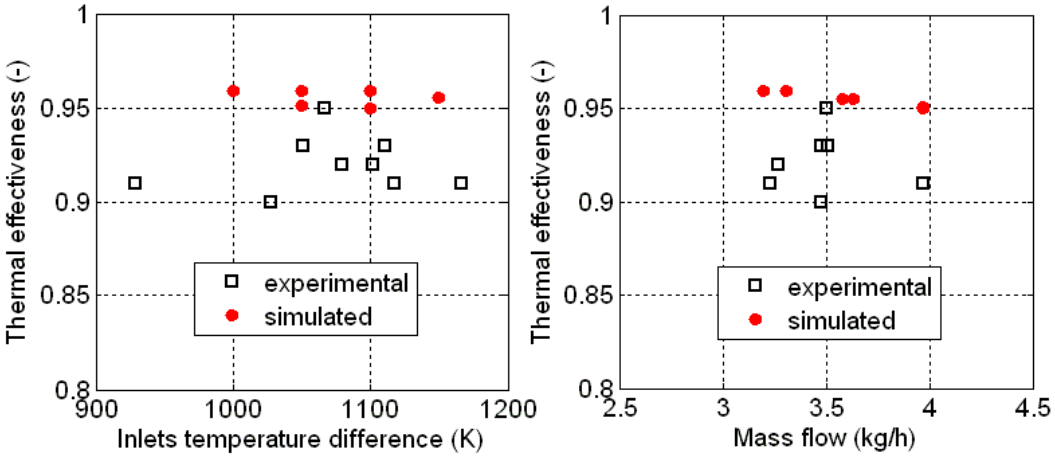

Figure 6.3: Thermal effectiveness of the recuperator obtained from experimental measurements and from theoretical simulations, plotted as function of the temperature difference between the hot and the cold inlets of the component, and of the overall fluid mass flow.

the material is not thermal shock stable and it does not seem to be suitable for TPV applications, even if it has very good spectral selective properties. However, the thermal behavior shown is in contrast with what is reported in literature and by the manufacturer and further investigations are necessary to understand whether such material can be modified and adapted for the use in TPV systems.

6.3.2 Validation of the theoretical model

The thermocouples placed in the combustion chamber allow to evaluate the heat flux entering and exiting the burner, i.e. to evaluate the heat released in it, which includes both emitted power and heat losses. Due to the unavailability of a spectrometer and of a pyrometer it has not been possible, so far, to measure the emitted spectrum of the emitter and its temperature with the system in operation. Therefore the fraction of power converted into radiation and the burner efficiency cannot be measured directly.

However these values can be estimated theoretically, by coupling together and solving the combustion, the flame-emitter heat exchange and the optical system models

as described in Sec.5.6. The temperature of pre-heated reactants and fuel and the air mass flow measured during tests are assumed as inlet boundary conditions, while the temperature of the exhaust gas entering the recuperator is taken as reference temperature to evaluate whether the theoretical model is valid. Figure 6.4 shows an example of the temperature field resulting from simulation in the optical system unit. Figure 6.5

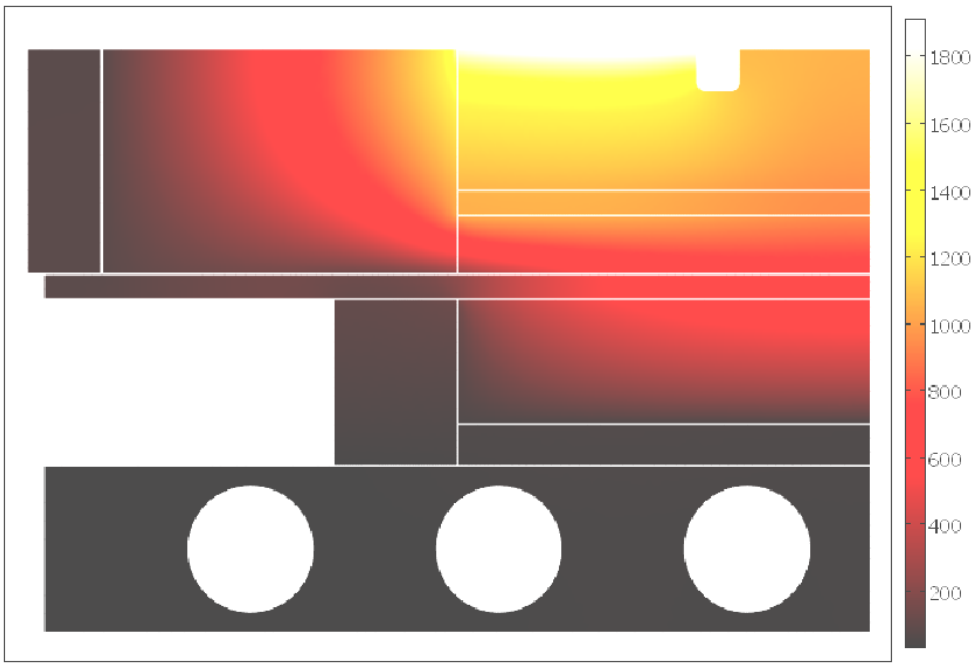

Figure 6.4: Temperature field (in Celsius degree) resulting from simulation in the burner region occupied by SiC emitter and kanthal wires, and in optical system, cells and cooling frame. A chemical power of 1042 W, a pre-heated air temperature of 1281 K (i.e. a flame temperature of 2216 K) and an air number of 2.2 are assumed as boundary conditions.

and Table 6.1 report and compare experimental and simulation results obtained when SiC, Kanthal, ErO garnet and spinel doped with nickel are used as emitters. The three graphs show the temperatures measured at the inlet and at the outlet of the burner, and compare the latter with those resulting from simulations. In the table, together with the burner temperatures, the resulting temperature of the cell back surface is given as further parameter to verify the model validity.

For the SiC and the Kanthal cases the correspondence between experimental and theoretical results is satisfactory: the model seems to reproduce and predict with a good accuracy the operating conditions of the system.

In the Garnet emitter case, instead, the temperatures at the burner outlet resulting from simulations are much higher than those measured. This is not due to a wrong model formulation, but likely to the spectral properties of the emitter, which seems to be less selective than what is reported in literature and assumed in the model. If the garnet emitter had selective spectral properties as in Figure 5.13, in order to emit a same amount of radiative power it should reach much higher temperatures than a less selective emitter like SiC, as confirmed from simulations. Due to its high selectivity, indeed, a smaller part of the heat generated in the combustion would be converted into

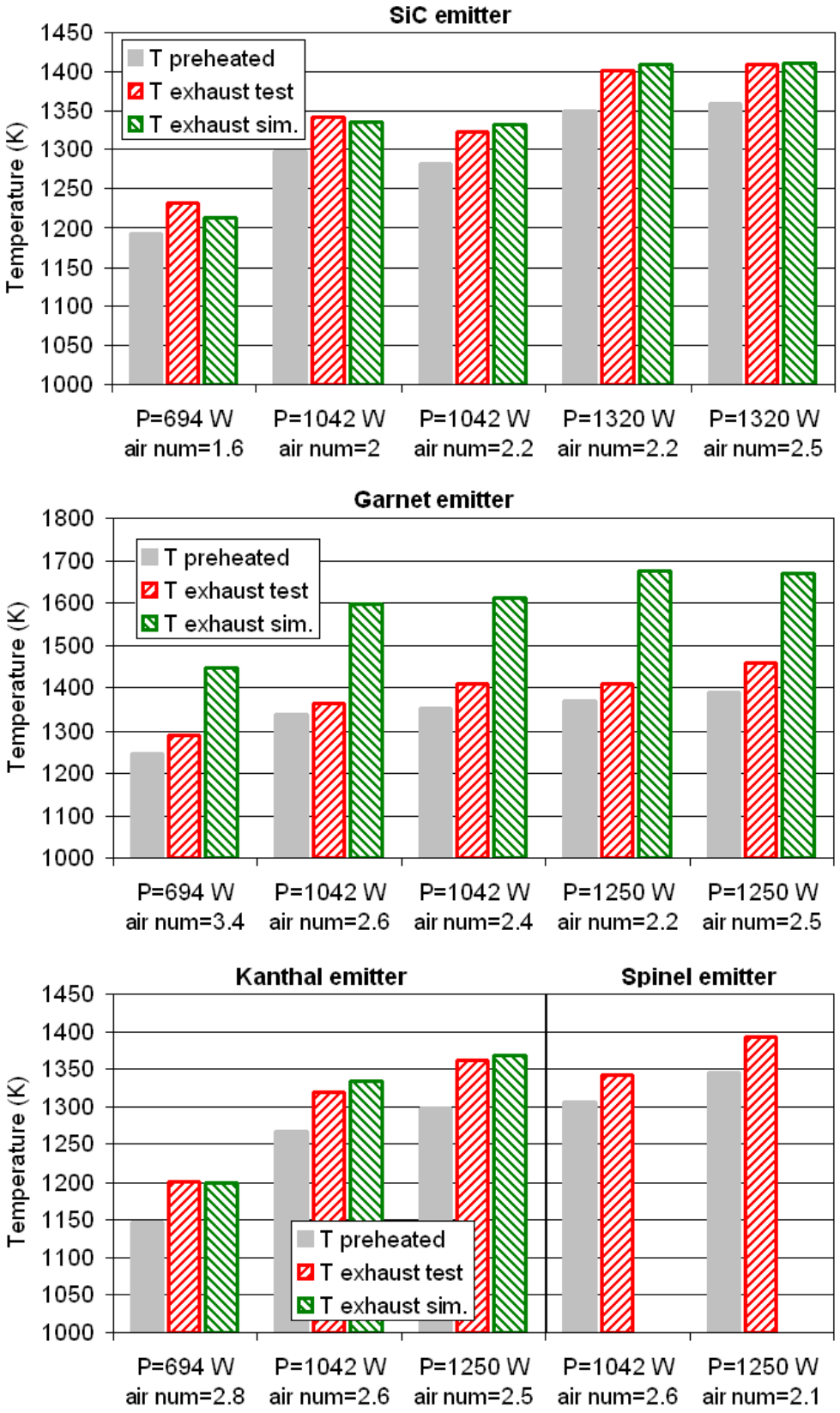

Figure 6.5: Comparison of measured and simulated exhaust gas temperatures obtained when SiC, kanthal, garnet and spinel are used as emitters. Supplied chemical power, air number and preheated air temperature are used as starting conditions for the simulations.

Operating conditions				Experimental results		Simulation results	
Emitter (-)	Power supplied (W)	Air number (-)	T preheated (K)	T exhaust (K)	T cell (K)	T exhaust (K)	T cell (K)
SiC	694	1.6	1193	1231	316	1214	314
SiC	1042	2.0	1298	1341	321	1335	319
SiC	1042	2.2	1281	1323	320	1332	319
SiC	1320	2.5	1349	1401	325	1409	322
SiC	1320	2.2	1359	1409	325	1411	322
Kanthal	694	2.8	1148	1201	308	1200	311
Kanthal	1042	2.6	1267	1319	318	1333	315
Kanthal	1250	2.5	1298	1362	322	1368	317
Garnet	694	3.4	1247	1291	316	1445	312
Garnet	1042	2.7	1267	1340	319	1598	314
Garnet	1042	2.4	1179	1408	320	1611	314
Garnet	1250	2.2	1298	1370	320	1675	316
Garnet	1250	2.5	1392	1457	322	1671	316
Spinel	1042	2.6	1306	1342	320	-	-
Spinel	1250	2.1	1346	1393	324	-	-
Spinel	1250	2.1	1326	1370	323	-	-

Table 6.1: Comparison of experimental and simulation results obtained with SiC, kanthal, garnet and spinel used as emitters. The operating conditions are assumed as starting conditions for the simulations.

radiation and emitted with the consequence that a bigger fraction of the heat generated would be recovered in the heat exchanger, increasing the pre-heated air temperature, i.e. increasing the flame and the emitter temperature, until reaching an equilibrium at a higher temperature. The pre-heated air temperatures measured experimentally, instead, are only slightly higher than those measured in the SiC and Kanthal cases: this can be explained only by a higher spectral emissivity, i.e. by a lower spectral selectivity than expected. This implies therefore a lower equilibrium temperature in the combustion chamber.

The most likely hypothesis to explain such a garnet emitter behavior is that part of the radiation is emitted by the SiC substrate and goes through the very thin porous garnet coating layer, with the consequence of an emission spectrum having less selective properties. However, so far, it has not been possible to measure directly the emission spectrum of the garnet emitter to confirm such hypothesis experimentally and to modify the spectral properties in the theoretical model accordingly.

For the same reason a theoretical model with the spinel emitter could not be implemented: the emissivity spectral data of the material are not available. Experimental tests on the TPV system with this emitter have been carried out, but they cannot be

compared to simulation results in order to estimate the burner and the spectral efficiencies.

From the considerations above it can be stated that the theoretical model proposed to simulate the TPV system operation is valid. However more detailed experimental data (emissivity spectra of garnet and spinel emitter) are needed to confirm directly its validity in specific cases.

In the case of the MGC emitter, it has not been possible to collect experimental data, due to the poor thermal resistance of the material. However its measured spectral properties are used to evaluate their effect on the TPV system performance in the theoretical simulation model.

6.3.3 Burner efficiency calculation

The validated theoretical model is used to evaluate the efficiency and the heat losses of the burner. Table 6.2 shows in detail powers emitted, emitter temperatures and burner efficiencies resulting from the simulation of the system under different configurations and operating conditions.

In the cases of garnet and MGC emitters, the spectral properties assumed in the simulations presented in this chapter are those reported in literature and the temperatures at the inlet of the combustion chamber are obtained with an iterative process by coupling together the recuperator, the combustion and the optical system models and using the chemical power supplied and the combustion air number as boundary conditions.

The results show a very good performance of the recuperative burner unit. Radiation power densities over hundred times higher than the solar radiation are attained (the emitted power refers to the emitter area, equal to $0.01\,\mathrm{m}^2$). Burner efficiencies of over 80% are reached in the simulations: the design of the recuperator-burner-emitter system is one of the most performing so far reported in the TPV system technology (compare with Table 2.1). However, it must be remembered that these results are based on theoretical simulations and must still be confirmed by direct measurements of the emitted radiation spectra.

Other important comments on the results obtained from simulations can be made by looking at the Table 6.2:

- As expected, at a constant air number the burner efficiency decreases slightly by decreasing the chemical power supplied into the device (i.e. decreasing the fuel mass flow). The enthalpy flux entering the device is proportional to the fuel mass flow while the heat losses via conduction through the thermal insulation layer depend basically on the temperature difference between the outer and the inner insulation walls, which does not change significantly. Therefore at a low fuel mass flow the heat losses represent a bigger fraction of the whole thermal power released in the burner.

- At a constant chemical power supplied into the device the burner efficiency increases by reducing the air number: at lower air numbers the temperatures reached in the combustion chamber are higher and the dominating heat transfer process is the radiative conduction in the gas-metal wires structure (see Sec.5.2.2), with the consequence of higher temperatures at the emitter surface and of a larger emitted

Operating conditions				Simulation results			
Emitter (-)	Power supplied (W)	Air number (-)	T preheated (K)	T exhaust (K)	T emitter^{+} (K)	Power emitted (W)	η_{burner} (-)
SiC	694	1.6	1193	1214	1177	582	0.84
	1042	2.0	1298	1335	1289	871	0.84
	1042	2.2	1281	1332	1284	856	0.82
	1320	2.2	1359	1411	1357	1092	0.83
	1320	2.5	1349	1409	1352	1074	0.81
Kanthal	694	2.8	1148	1200	1228	553	0.80
	1042	2.6	1267	1333	1345	848	0.81
	1250	2.5	1298	1368	1395	1005	0.80
Garnet*	417	2.0	1340	1378	1369	295	0.71
	417	2.5	1333	1375	1364	291	0.70
	486	2.0	1396	1436	1426	351	0.72
	486	2.5	1389	1431	1420	345	0.71
	556	1.7	1454	1490	1482	412	0.74
	556	3.0	1439	1483	1473	402	0.72
	694	2.5	1524	1574	1561	512	0.74
	1042	2.5	1705	1758	1736	794	0.76
MGC*	417	2.0	1176	1216	1200	319	0.76
	417	2.5	1175	1216	1198	316	0.76
	486	2.0	1229	1269	1252	378	0.78
	486	2.5	1225	1267	1248	373	0.77
	556	1.7	1280	1316	1301	440	0.79
	556	3.0	1267	1312	1290	426	0.77
	694	2.5	1345	1393	1372	545	0.79
	1042	2.5	1503	1554	1528	841	0.81
	1320	2.5	1603	1657	1627	1078	0.82

+: average values calculated from the total power emitted

*: for simulations with ErO garnet and MGC, the temperature of the pre-heated reactants is calculated from simulation with an iterative process assuming as starting conditions the power supplied and the air number.

Table 6.2: Results from simulations: evaluation of emitter temperature, power emitted and burner efficiency varying emitter materials and operating conditions.

power. In other words, at high mass flows the combustion air acts as a thermal inertia, reducing the temperature of the combustion and therefore that of the emitter. To realize a complete combustion of the fuel, however, an air number higher than one must be always assured.

- At constant inlet conditions (constant fuel mass flow and air number) the burner efficiency is higher when less selective emitters are used. In the case of selective emitters, indeed, higher temperatures, i.e. higher heat losses, are reached in the combustion chamber. This is shown more clearly in Figure 6.6, in which some of the results reported in Table 6.2 are presented: burner efficiency and emitter temperature are plotted for four emitter materials, at two different levels of chemical power supplied. An increase of the emitter temperature corresponds to a decrease of the burner efficiency.

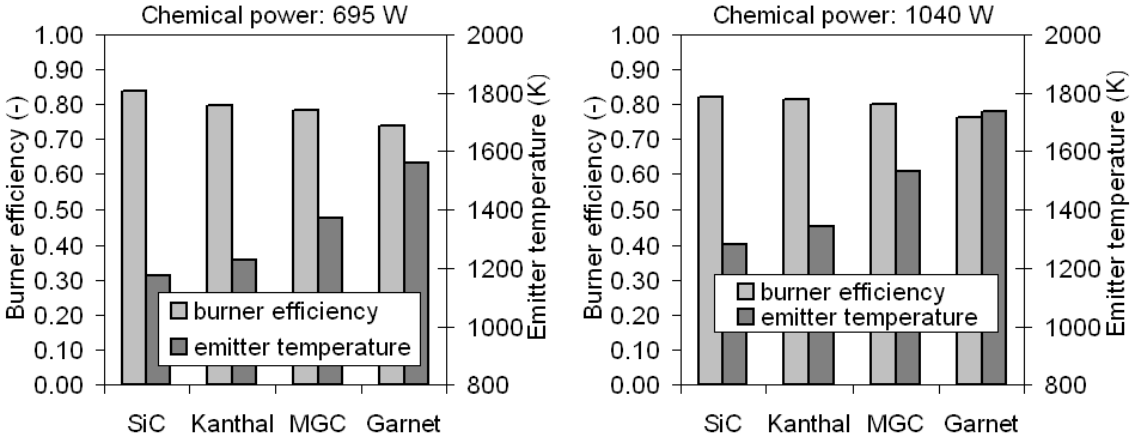

Figure 6.6: Burner efficiency and emitter temperature resulting from simulations (see Table 6.2) are plotted for four different emitter materials. Two different amounts of chemical power supplied (694 W and 1042 W) are considered.

- At constant inlet conditions the emitter temperature increases with the selectivity of the material. The same temperature reached on the SiC surface when supplying a certain amount of chemical power can be reached by using less than half of that amount in the case of garnet or MGC emitter. For the same reason the temperatures reached using garnet or MGC are much higher than in the SiC case, the thermal power released being equal. Such a behavior is shown clearly in Figure 6.7, in which emitter temperature and spectral emission of SiC and ErO garnet are calculated and plotted at a constant value of the total emitted power. The radiative power density corresponds to the integral of the spectral emission over the whole spectrum: due to its higher selectivity the garnet emitter must reach a higher temperature to emit the same amount of radiative power.

6.4 Optical system performance

The spectral efficiency of the optical system $\eta_{spectral}$ is estimated theoretically by using the model described in Sec.5.3.2. Experimental results concerning the radiation spec-

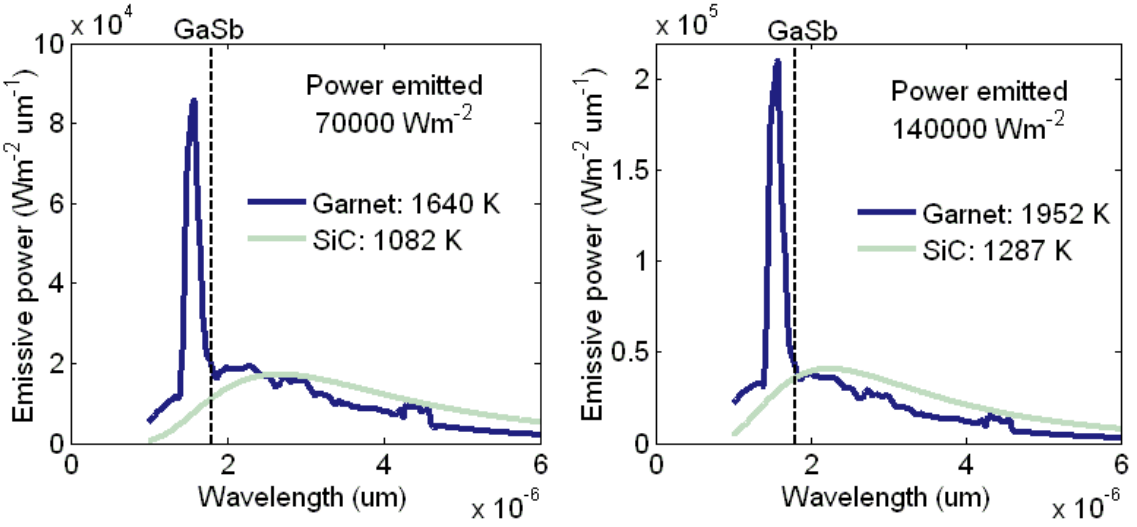

Figure 6.7: Comparison between broad band SiC and selective ErO garnet emitters. Emission spectra and emitter temperatures are given for both of the emitters, assuming a same amount of total radiative power density. Two different power density levels are considered. The spectral properties of garnet are assumed as reported in [DLT+04].

trum emitted by the emitter materials and the radiation spectrum reaching the cells are not available since spectral measurements could not be carried out on the TPV system during experimental tests.

The graphs in Figure 6.8 show the spectral efficiency $\eta_{spectral}$ for each emitter material resulting from simulations and plotted as function of the net radiative power density emitted. The spectral efficiency is calculated with reference to the band gap of the GaSb cell used in the TPV system (0.68 eV). The optical system configuration considered in the simulation consists of the emitter material, a single quartz glass absorptive filter and the cells. It must be kept in mind that in the theoretical model simulation the radiation losses are not taken into account.

Furthermore in real operating conditions the cell arrays do not cover the whole surface facing the emitter area. Part of the radiation emitted, therefore, is absorbed and reflected by the cooling frame aluminum surface, which has a different spectral behavior than the cells. This is not taken into account in the theoretical simulation, which assumes that the cells cover the whole area of 100 cm^2.

As expected, the results plotted in Figure 6.8 show clearly that the spectral efficiency of the system increases with the selectivity of the emitter material. This is due to the more effective selection of the radiation operated by the selective emitter: a bigger fraction of the heat generated is sent back and recovered in the recuperative burner unit, reducing the heat losses in the TPV cells and increasing the emitter temperature, which is, in its turn, another factor that contributes to improve the spectral efficiency of the system. At higher temperatures of the emitter, indeed, the resulting emitted spectrum is shifted towards shorter wavelengths and therefore a larger fraction of photons emitted has energy higher than the cell bandgap and is convertible into electric power.

In terms of overall efficiency the use of selective emitters is more advantageous: the lower burner efficiency is largely compensated by the much higher spectral performance.

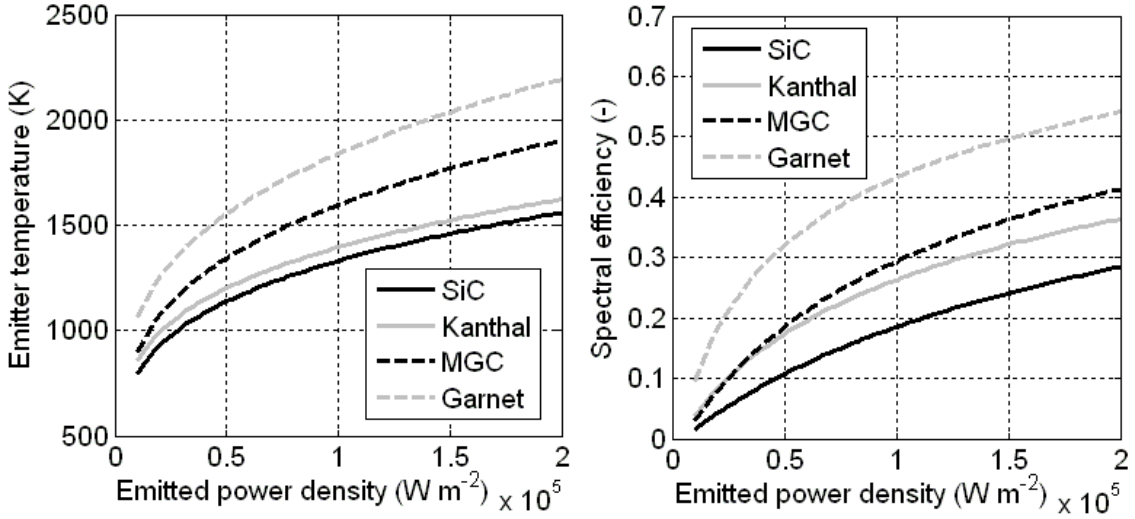

Figure 6.8: Results of the optical system simulation. The emitter temperature and the spectral efficiency are plotted as function of the net emitted power and varying the emitter materials.

This is pointed out in Figure 6.9. The spectral efficiency resulting from simulations is plotted in the left graph, assuming same chemical power supplied and emitter temperatures as in the right graph of Figure 6.6: the value of the efficiency $\eta_{spectral}$ varies from 0.16 for the SiC case up to 0.4 for the garnet emitter case. The right graph couples together the performance of the burner unit and of the optical system: the product of burner and spectral efficiency is plotted, assuming the same operating conditions as in the left graph. It is evident the higher performance of the burner-optical system section when selective emitters are used.

In terms of power, instead, the use of gray or less selective emitters allows to reach, at a fixed temperature, a higher radiative power density, as it can be seen from Figure 6.8.

The high temperatures reached in the burner when using a selective emitter represents so far one of the biggest technological limits for TPV systems: the spectral efficiency and the power emitted are limited by the thermal resistance of emitter and recuperative burner unit. In the case of the present TPV device and assuming to use an ErO garnet emitter with the spectral properties as reported in Figure 5.13, the radiative power density could not exceed values of about 50000 $\mathrm{Wm^{-2}}$, corresponding to a maximum spectral efficiency of about 0.33, in order to limit the temperature of the emitter and of the exhaust gas to values not higher than 1300 °C, which is the maximum operating temperature withstood by the recuperator.

This maximum potential spectral efficiency reachable by the present system is not very high if compared to other existing TPV systems (see Table 2.1). In the experimental tests carried out this value is even lower because of the lower selectivity of the emitters used.

The low efficiency of the optical system is due to the poor selection of the emitted radiation realized by the absorptive filter: the effect of the quartz glass, indeed, is limited basically to an absorption of the wavelengths longer than 4 μm, which are partially re-radiated back to the emitter. Compared to other filter types (e.g. dielectric, plasma

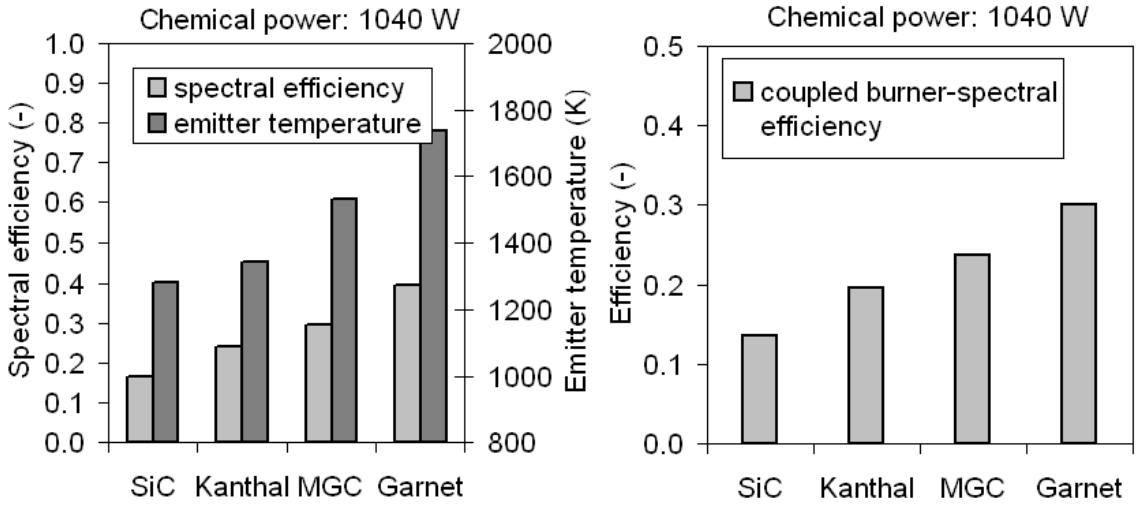

Figure 6.9: Results of the optical system simulation assuming the same operating conditions as in the right graph of Figure 6.6: a chemical power of 1040 W is supplied and four emitter materials are considered. Spectral efficiency and emitter temperature are plotted on the left, while on the right the burner and spectral efficiencies are coupled together.

or frequency selective surface filters: see Sec.2.4.4) the quartz glass has a lower spectral performance and limits the whole spectral control of the system, which does not reach satisfactory spectral efficiency values, especially when gray or broad band radiators are used as emitters.

6.5 Cell performance

During experimental tests the cell arrays are not connected and their characteristic curves are measured separately, for each single module. Figure 6.10 shows, as an example, the IV curves obtained from three different modules using Kanthal as emitter and varying the chemical power supplied into the device.

An overview of the experimental results concerning the performance of the cell arrays is presented in Figure 6.11, which shows for each array the open circuit voltage V_{oc} and the fill factor FF measured in the experimental tests plotted against the short circuit current density J_{sc}. V_{oc} and FF do not depend directly on the radiation spectrum but only on the short circuit current and on the cell temperature.

Referring to the diode equation (Eq.2.35) the open circuit voltage of a cell should increase with the logarithm of the short circuit current density. However this is valid for cells at a constant temperature. In the experimental tests the array temperature increases with the density of the incident radiation, i.e. with the short circuit current (see Figure 6.12): the higher cell temperature causes a reduction of the open circuit voltage, which balances the V_{oc} increase due to the higher radiation density. This behavior can be noticed also in [SAA+05], in which GaSb cell arrays of the same type used in the present work have been used in a TPV system. Nevertheless in the present tests the V_{oc} voltage drop is much higher than expected: only a very high temperature coefficient $T_{C-V_{oc}}$, in the range of 0.8-0.9 %/K, could explain such a big drop: such a value of $T_{C-V_{oc}}$

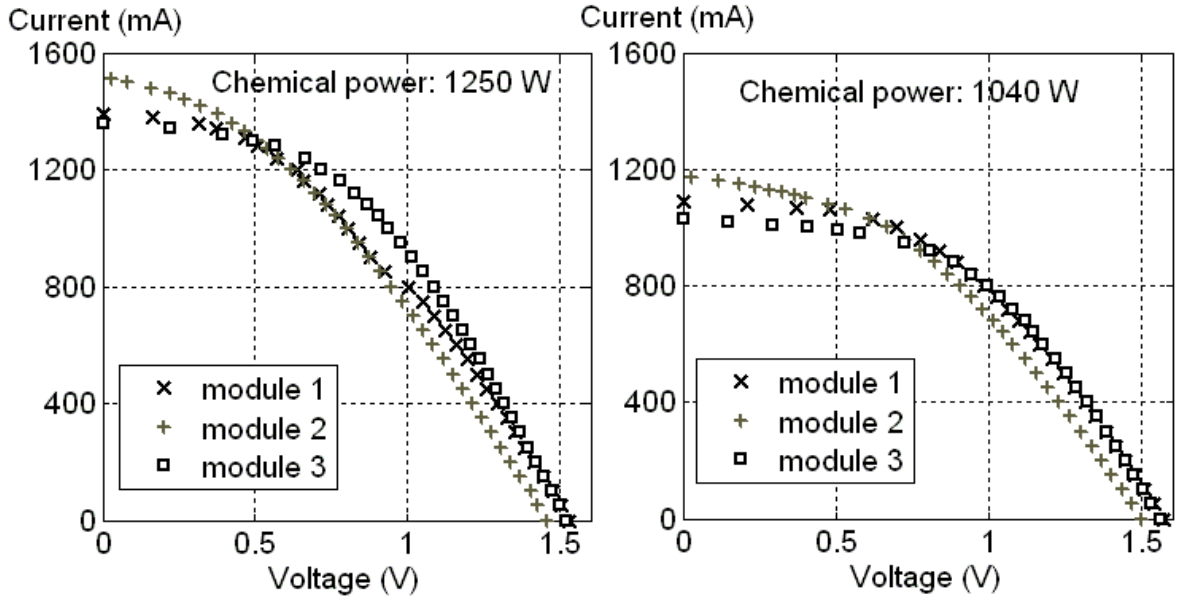

Figure 6.10: Characteristic curves of three TPV cell arrays measured during experimental tests using Kanthal as emitter material.

is over twice the values reported in literature for GaSb cells under high radiation density operating conditions.

The fill factor values are lower than those reported in literature: the modules used in the present device have fill factors varying from 0.53 up to 0.67 for a corresponding short circuit density of 0.625 $\mathrm{Acm^{-2}}$, in front of a FF value reported in [SDOB04] of over 0.70 at similar operating conditions. At higher current densities and higher cell temperatures it can be noticed that the FF values decrease even more, reducing furthermore the cell performance. A similar behavior for this kind of cell array in similar operating conditions is also reported in [SAA+05].

From the graphs in Figure 6.11 it can be noticed also a low result reproducibility, with a significant data dispersion. The variation of the cell temperature is not sufficient to explain such a system behavior. However, also in [SAA+05] the difficulty in reproducing results within the system is pointed out.

The calculation of the experimental cell efficiency η_{PV} can be carried out only if the spectrum of the incident radiation is known. In the present work a direct measurement of the cell efficiency could not be realized. When using SiC and Kanthal emitters, an evaluation of η_{PV} can be made referring to the maximum electric power measured on one cell module and using the theoretical model described in Sec.5.3.2 to calculate the monochromatic radiation heat flux $q_{e \leftrightarrows c}(\lambda)$.

The efficiency is calculated referring to the net convertible power flux incident on the cells (see Eq.2.40) in the case that the TPV cells cover completely the area delimited by the reflecting frame (100 $\mathrm{cm^2}$).

The highest cell efficiencies η_{PV} obtained are equal to 6.48% in the case of SiC emitter at a temperature of 1289 K, and to 4.36% for the Kanthal material at 1354 K. These efficiency values are much lower than those calculated theoretically (see Sec.5.4.2), referring to the cell array properties reported in literature [SDOB04], [SAA+05], [SAB+05]:

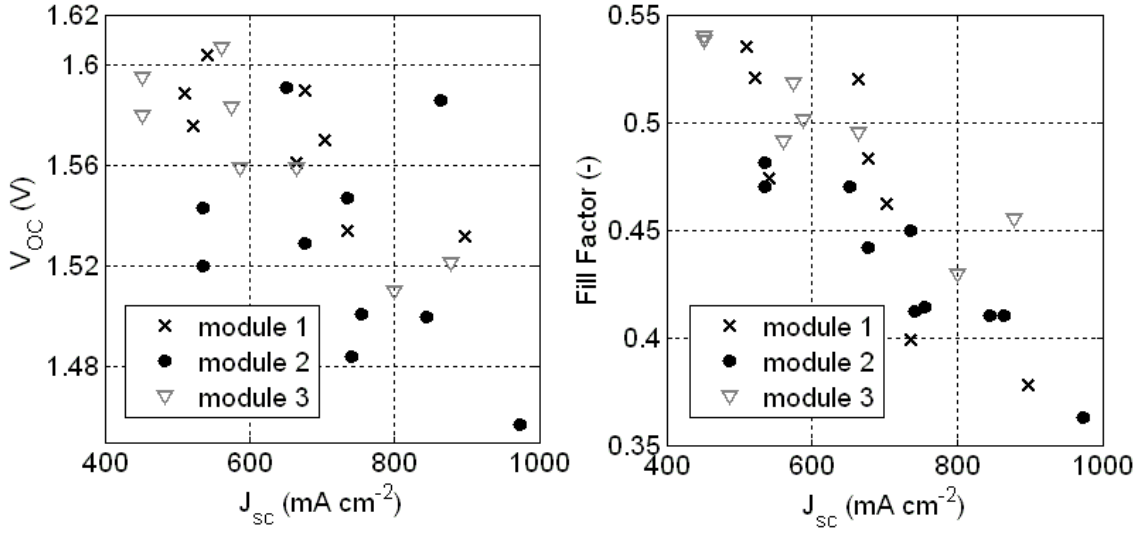

Figure 6.11: Open circuit voltages and fill factors plotted as function of the short circuit current density: results from the experimental tests.

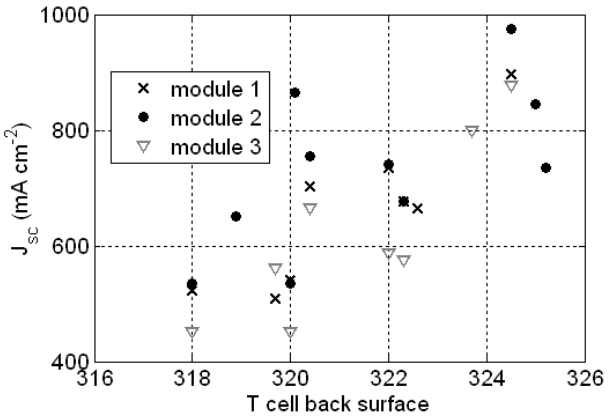

Figure 6.12: Short circuit current density plotted against the temperature of the cell back surface: results from the experimental tests.

with the same emitter temperatures as in the two cases above and with cells at 332 K, indeed, the cell efficiency would be equal to 22% and 21% respectively. Also the short circuit current density J_{sc} measured experimentally is lower than expected, being up to three times smaller than what results from simulations.

From the results and the comments above it can be stated that the performance of the TPV cells is worse than expected, compromising the efficiency of the whole TPV system.

It must be pointed out that the practical realization of the TPV modules is very difficult and material consuming. Many cells are damaged both in the production and in the assembling phase. Completed modules are very fragile and tend to change characteristics and deteriorate due to thermal cycles and mechanical stress resulting from the tests. In particular it has been noticed that the electric connectors cause contact problems frequently and the grid fingers connected to the busbars tend to get detached from the cell surface reducing partially the cell array performance and inducing also

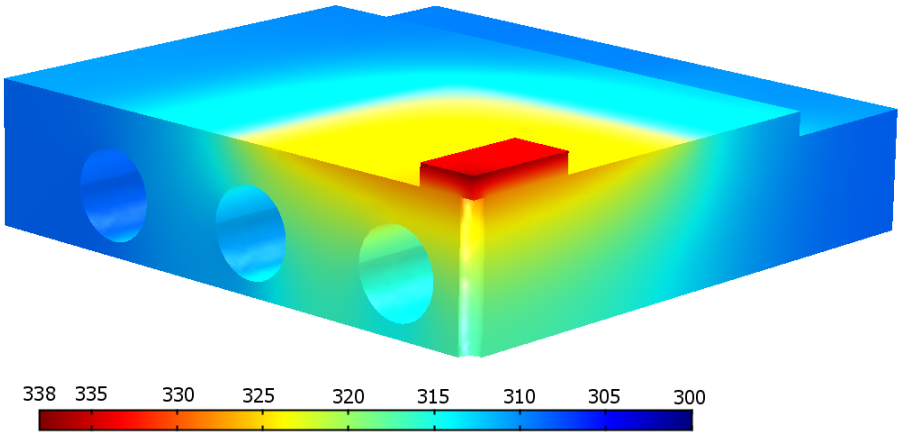

Figure 6.13: Temperature field (in Kelvin degrees) on the aluminum cooling frame resulting from simulation. A radiative power flux of 145000 Wm^{-2} is assumed over the area delimited by the reflecting frame (100 cm^2).

a partial shorting of the cell with the aluminum cooling frame. Due to these contact problems it has not been possible to obtain experimental data for the fourth cell array.

6.6 Cooling frame design validation

As pointed out in Sec.5.5.1, the design of the aluminum cooling frame has been chosen after comparing and simulating different possible designs. In order to assure a safe cell cooling even at extreme operating conditions, simulations have been carried out, in which a radiation heat flux up to 145000 Wm^{-2} has been assumed. Figure 6.13 shows the temperature field in the final aluminum frame design resulting from the model simulation.

The experimental tests confirmed the effectiveness of the component: the highest temperature measured on the back surface of the cell arrays during operation is of 325 K, corresponding to a front surface cell temperature of 333 K: the threshold of 343 K, over which the cells are exposed to the risk of damage, is not overcome.

6.7 TPV system efficiency

Table 6.3 gives an overview of the performance of the TPV system showing the highest power outputs and efficiencies obtained during experimental tests. The value of the electric power output refers to a single cell array, while the system efficiency is calculated extrapolating the power density output to the whole area which is supposed to be covered by the cells (100 cm^2 instead of 34.1 cm^2, which is the area covered by four modules). The experimental efficiency so defined is compared in the table to the system efficiency resulting from simulations. The results reported in the table are presented graphically in Figure 6.14: the graphs point out the power fractions both converted and lost for each process and for the whole device when SiC, Kanthal and ErO garnet are used as emitter.

Operating conditions			Experimental results			Simulation results			
Emitter	P chemical	Air number	P output 1 module	P output density	η_{TPV}	η_{burner}	$\eta_{spectral}$	η^{+}_{PV}	η_{TPV}
(-)	(W)	(-)	(W)	(Wm^{-2})	(%)	(%)	(%)	(%)	(%)
SiC	1042	2.0	0.81	945	0.91	84	17	22	3.1
SiC	1042	2.2	0.78	915	0.88	82	16	24	3.2
Kanthal	1042	2.6	0.79	932	0.89	81	24	22	4.3
Kanthal	1250	2.5	0.94	1104	0.88	80	26	21	4.6
Spinel	1042	2.6	0.69	805	0.77	-	-	-	-
Spinel	1250	2.0	0.83	971	0.78	-	-	-	-
Garnet*	1042	2.7	0.76	886	0.85	76	39	22	6.7
Garnet*	1250	2.2	0.87	1022	0.82	78	43	20	6.9

+: the cell array properties used in the simulation are those reported in [SAA+05] and [SAB+05].
*: for simulations with ErO garnet the emission spectrum of Figure 5.13 is considered.

Table 6.3: Electric power output and overall efficiency of the TPV device from experimental tests and comparison with theoretical simulation results.

To evaluate theoretically the cell efficiency the cell array properties reported in [SAA+05] and [SAB+05] are considered. The simulation results concerning the ErO garnet emitter are obtained assuming an emission spectrum as given in [DLT+04]. The theoretical system efficiency does not take into account the radiation losses, i.e. $\eta_{optical}$ is assumed equal to 1.

The experimental results show an overall system performance much worse than expected: the highest efficiencies obtained are equal to 0.9%.

Such a bad system performance is strongly limited by the cell efficiency and degradation, with the consequence of a test result flattening and the impossibility to notice the different spectral behavior of the emitter materials.

Another limit of the system is represented by the low efficiency of the spectral control. SiC and Kanthal are respectively a gray and a semi-selective emitter and do not realize a narrow selection of the spectrum, causing high thermal losses. The garnet and MGC emitters based on the rare earth oxides, instead, are supposed to have higher selective spectral properties. Nevertheless the former did not confirm such a high selectivity during experimental tests, while the latter could not be used in the device because it showed a poor thermal shock resistance. In the case of the spinel $MgAl_2O_4$:Ni emitter, spectral emission data are not available, but looking at the temperatures measured in the combustion chamber during experimental tests, it has not been noticed any highly selective spectral property.

The difference between the experimental and the theoretical results reported in Table 6.3 is very large and can be explained by the performance of cells and emitters worse than expected: referring to the cell and emitter properties reported in literature, indeed, system efficiencies higher than 4.5% could be attained.

Another factor limiting the system efficiency is the low performance of the quartz glass absorptive filter (see Sec.6.4): even assuming the emission spectra reported in literature of the ErO garnet or of the MGC ceramic material, the resulting spectral

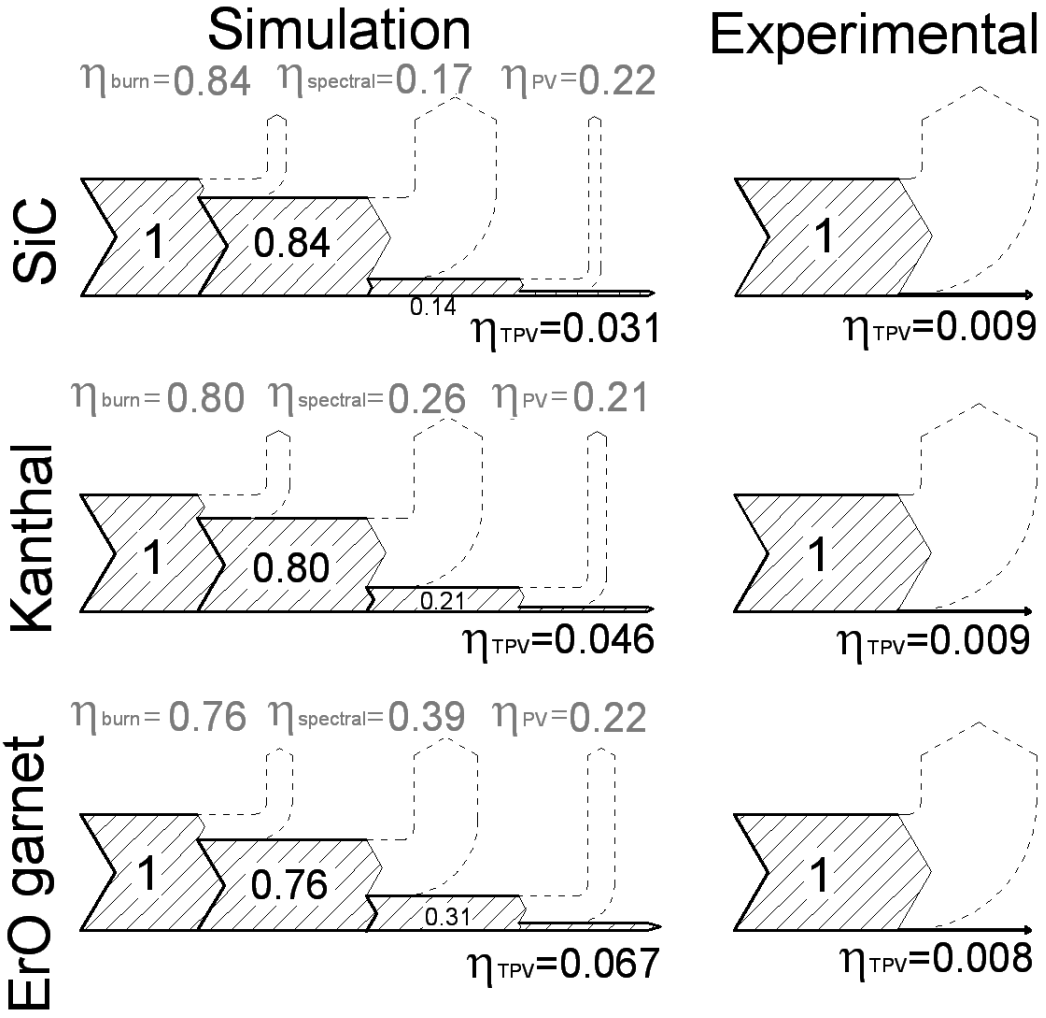

Figure 6.14: TPV system efficiencies resulting from simulations and experimental tests. The data refer to Table 6.3. The simulation results show the efficiency, the power converted (filled area) and lost (dashed arrows) for each process involved in the TPV system. The power fluxes are expressed as the fraction of the input chemical power.

efficiency of the present optical system could not reach values higher than 0.5 unless realizing temperatures higher than 2000 K in the combustion chamber. The use of a different and more performing filter could improve drastically the spectral efficiency and therefore the performance of the TPV device.

Although the system performance is lower than expected, the design approach used to develop and build the TPV device is considered valid and reliable. The system, indeed, has a solid and compact design and offers the possibility to be used as a TPV tester: its configuration can be changed easily by varying and replacing the single optical system components (filter and emitter materials) and the cell arrays (different cell arrays can be glued over different cooling aluminum frames with the same design).

6.8 Further system improvements

The low system efficiency so far obtained does not depend so much on the TPV system design as rather on single component performances. For this reason improvements to the system can be realized in a relative simple and straightforward way without modifying completely or re-designing the device structure. The modular design of the device, indeed, allows to modify independently components and materials involved in the TPV process.

This section describes a series of small modifications and improvements which can be carried out on the existing system to increase its efficiency and performance.

Recuperative burner unit

The recuperative burner unit has very high thermal effectiveness and burner efficiency, nevertheless its design presents still some limits due to the maximum temperature that the component can withstand. As shown in Figure 6.8, the spectral efficiency of the system increases with the selectivity of the optical system and with the emitter temperature. In the case of a very narrow selection of the radiation there is the risk that emitter and exhaust gas reach temperatures higher than 1300 °C, which is the maximum temperature withstood by cordierite, with the consequence of degradation and damage for the recuperative heat exchanger.

For this reason it would be reasonable to use a different material to build the recuperative burner unit, with a higher resistance to thermal shock and to high temperatures. One of the best candidates is the silicon carbide, able to withstand temperatures up to 1600 °C. Compact heat exchanger based on SiC microchannels with a high effectiveness are already available on the market [Cer07] and could be modified and used for TPV applications.

Another approach to follow for the development of the recuperative burner unit is based on the regenerative heat exchanger concept. Several regenerator cartridges made of SiC foam or honeycomb structure, disposed parallely, could be used to realize a regenerative burner unit, following the scheme proposed in [Wün03]. Such fix bed regenerator heat exchangers reach effectiveness values over 90% and have a compact design and a relatively simple geometry. On the other hand they are more complex than the traditional recuperators since they need valves and switches for the control of the component.

Optical system

The spectral efficiency of the system is limited by the bad selection of the emitted spectrum in the mid and far IR regions, due to the low reflectivity of the quartz glass used as filter. A first improvement of the spectral control could be realized in two different simple and relatively straightforward ways.

One possibility is to use several parallel quartz glass windows instead of a single one: Figure 6.15 shows the spectral efficiency and the emitter temperature resulting from simulations varying the number of parallel quartz windows placed between emitter and cells (see Sec.5.3.2). The emitter materials assumed in the simulations are the gray emitter SiC and the selective emitter based on ErO garnet.

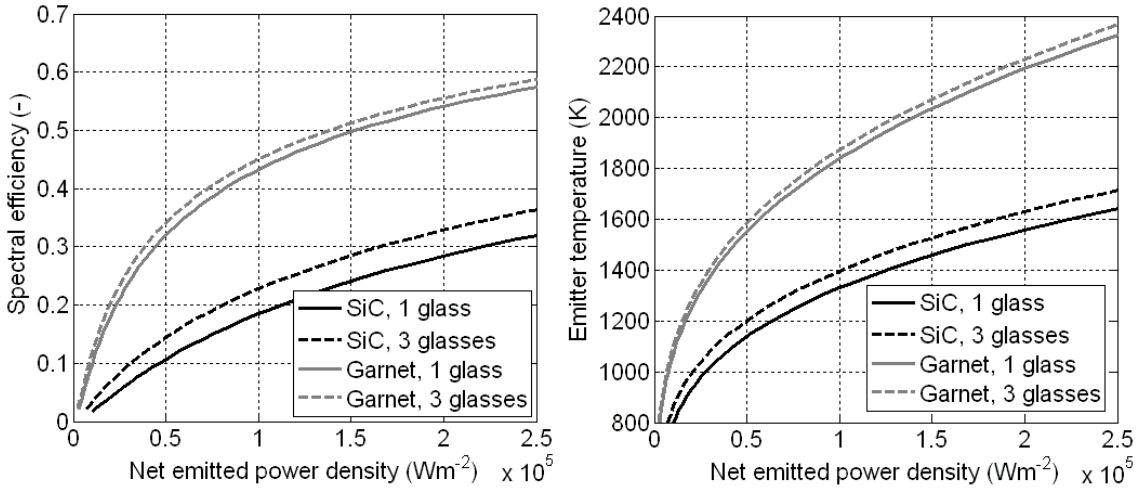

Figure 6.15: Spectral efficiency and emitter temperature plotted as function of the net emitted power. The results are obtained from simulations, varying the number of quartz glasses placed between emitter and cells and assuming either SiC or ErO garnet as emitter material.

With such an optical system configuration a higher fraction of the radiation emitted having $\lambda \geq 4\,\mu$m is absorbed and emitted back to the emitter by the multiple glass window, reducing the amount of not-convertible radiation reaching the cells and increasing the emitter temperature. As shown by the graphs, this approach is more effective and there is a larger spectral efficiency increase when a less selective material is used as emitter, due to the higher amount of long wavelengths present in its spectrum.

The second possibility is to use two parallel quartz glasses, the second of them coated with a filter aiming at increasing the reflectivity of the glass in the region between λ_{limit} and $4\,\mu$m. Figure 6.16 shows the spectral transmissivity of the simulated filter coating the glass [AD05] and the spectral efficiency resulting from simulations.

Compared to the case of multiple parallel windows, the use of such a configuration would allow to reach even higher spectral efficiencies (an increase of over 10% in the case of SiC). The filter, indeed, reflects back to the emitter a big part of the radiation in the range between λ_{limit} and $4\,\mu$m, which would be absorbed by the cell in case of using a normal quartz glass.

Spectral efficiencies even higher could be reached if referring to the characteristics of state of the art TPV filters reported in literature. Nevertheless a filter for TPV applications should be designed taking into account the experimental operating conditions of the specific TPV device (e.g. temperature, thermal stresses, emitter material): referring to spectral properties of TPV filters present in literature and adapting them to the own TPV system theoretical simulations is a wrong procedure, which can bring to unreliable results.

In the present work the cell arrays do not cover the whole area irradiated by the emitter: part of the radiation is absorbed and reflected by the aluminum cooling frame and therefore the operating conditions are different from those realized if the whole aluminum frame area delimited by the reflecting frame were covered by cells. To improve

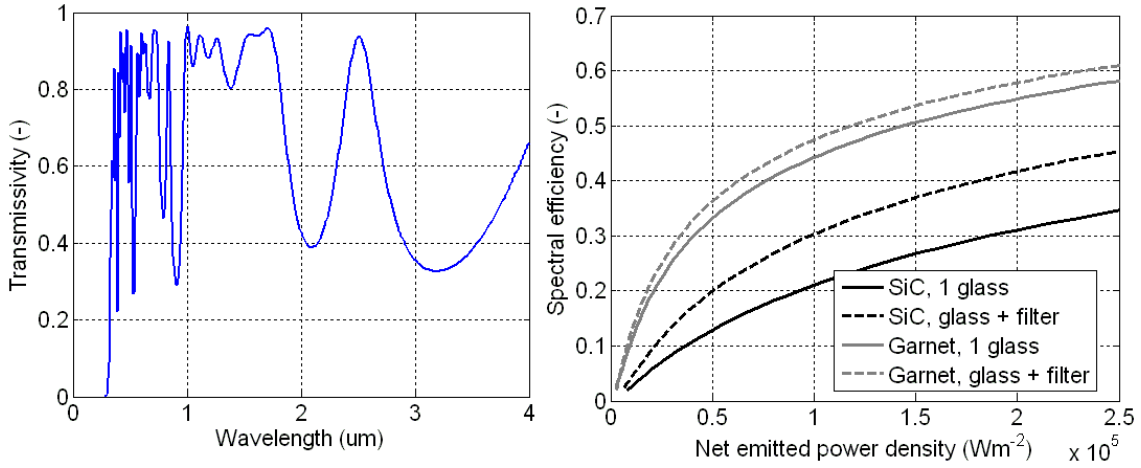

Figure 6.16: The graph on the left shows the spectral transmissivity calculated via simulation of a quartz glass coated by a dielectric filter [AD05]. The spectral performance of the optical system assuming such filter properties is compared to that obtained in the case of a simple quartz glass absorptive filter: the graph on the right plots the spectral efficiency resulting from simulations for both of the cases. The efficiency is plotted as function of the net emitted power and SiC and ErO garnet are assumed as emitter materials.

the performance of the system a solution would be to cover or coat the part of the aluminum surface directly exposed to the radiation with a reflecting material or a golden film. Instead if the purpose is to test the system reproducing as close as possible the operating optical conditions reached in the "final" system (whole cooling frame covered by working cells), a possible and not expensive solution is to cover the remaining part of the frame with broken or not working cells.

TPV cells

From the results of the experimental tests carried out with the present cell arrays it can be stated that the first fundamental requirement for TPV cells is a good resistance to degradation at the extreme operating conditions present in the device. As already written, if the cells used had properties as reported in literature, the measured system efficiency could improve up to 5 times without any further system modification. Testing the cells and measuring their properties under conditions similar to those present in the device is a crucial and fundamental step to avoid unexpected low cell efficiencies.

A further system improvement could be obtained by using cells designed for a higher current density: simulations showed that values higher than $3\,\mathrm{A\,cm^{-2}}$ can be easily reached in the present system, if referring to the bandgap and the EQE of the cells currently used. Use of higher current density cells would allow to limit the series resistive losses, i.e. to reduce the FF drops even at high radiation densities. TPV cells based on GaSb designed to generate current densities up to $5\,\mathrm{A\,cm^{-2}}$ have been already realized and tested [AK+05].

Experimental tests

Besides improving the system design, it is fundamental to be able to measure directly the operating conditions and the performance of each single component, in order to understand better the behavior of the system and analyze accurately each process involved. For this reason a pyrometer and a spectrometer are instruments absolutely necessary in order to know the performance of recuperative burner and optical system and therefore the cell efficiency, by measuring the temperature and the emitted spectrum of the emitter.

More detailed measurements on the TPV system would allow also to validate more correctly the theoretical models used and, in case, to modify and correct them accordingly.

7

Conclusions

A small methane-fuelled TPV system has been developed and brought successfully into operation. It is the first TPV device ever reported that can be used as TPV tester: its design allows to change easily the system configuration, varying the combination of emitter materials and cells.

The system showed a performance lower than expected: the maximum measured efficiency is equal to 0.9%, in front of a minimum target of 2%. However the design of the system can be considered valid and reliable: such a low performance of the device is mainly due to an unexpected bad operation of single components (cells and selective emitters) and to a not sufficient selective filtering of the radiation emitted, those aspects being adjustable and improvable without re-designing the entire system. Another limit of the system is represented by the unavailability of instruments to measure the emitter temperature and the spectrum of the radiation emitted, not allowing to measure directly the burner efficiency and the performance of the optical system.

Parallely to the device realization, a theoretical simulation model of the whole system has been developed and implemented with a commercial FEM based software. For the first time a detailed simulation of the recuperative heat exchanger and of the combustion chamber has been included in the simulation of a TPV system.

The results of the simulations are in good agreement with the experimental measurements obtained, confirming the validity of the model. More detailed measurements, however, are necessary to evaluate whether the model is valid also in different operating conditions.

The TPV system, able to generate a thermal power up to 1300 W, can be divided basically in three parts: the recuperative burner unit, the optical system and the TPV cells.

The recuperative burner unit includes a recuperative heat exchanger and the combustion chamber. Its design is taken from a previous PhD thesis and a few modifications have been carried out to improve its reliability. It is based on a ceramic matrix of microchannels in which combustion air and exhaust gas flow and it acts as a counter-current heat exchanger: its design allows to reach an heat exchanger effectiveness of over 0.9. Such a value, resulting from theoretical simulations and confirmed by experimental tests, represents one of the highest effectivenesses ever reported for TPV system recuperators.

The burner is realized as a cavity in the upper part of the recuperator and it is sealed

on the top by a quartz glass which acts as an absorptive filter. Five emitter materials, placed inside or over the combustion chamber and with different spectral properties have been used during experimental tests: a silicon carbide plate, which is a broad band radiator, thin wires of Kanthal which is an high temperature alloy, a ceramic tile made of magnesium aluminum spinel doped with nickel, and two selective emitter materials based on rare earth oxides: a Melt Growth Composite eutectic ceramic and a SiC tile coated with a porous garnet erbium oxide.

The heat transfer between flame and emitter material is a crucial process for the TPV system performance. Good results have been obtained by filling the volume of the burner cavity between combusted gas and emitter tiles with the Kanthal wires, which support the flame-to-emitter heat transfer process via flow-mixing and radiative transfer. Heat-to-radiation conversion ratios of over 80% have been obtained from simulations, whose validity has been confirmed by a close correspondence between the temperatures measured and those resulting from the model.

The experimental tests pointed out also a performance of garnet and MGC emitter worse than expected: unlike what is reported in literature, the former did not show very highly selective properties while the latter revealed a poor thermal shock resistance.

The use of a quartz glass as absorptive filter, furthermore, did not support a narrow selection of the radiation, with the consequence of high thermal losses in the cells and a lower efficiency of the spectral control. However the TPV device is realized so that the optical system configuration can be easily modified to house further quartz glasses or an optical filter between the burner unit and the cells. Both of these two modifications would increase the spectral efficiency, as it results from simulations.

Four arrays of GaSb TPV cells (bandgap of 0.68 eV) have been used during tests. They are placed over an aluminum frame cooled with water and designed for this specific application. The frame design allows to substitute simply the cells used to modify the system configuration. The TPV cells tested in the present work exhibited performance and efficiency worse than expected and did not confirm properties and characteristics reported in literature, showing also signs of degradation. Referring to the nominal properties of the cells, simulations showed that a system efficiency of over 5% could be reached, without modifying the device configuration.

For what concerns the theoretical model implementation, the complexity of the device and of the different processes involved obliged to assume simplifying, but realistic, hypothesis.

A single-step reaction mechanism has been used to represent the laminar diffusion flame in the burner, avoiding to simulate hundreds of elementary chemical reactions. Before being used in the TPV simulation, this simplified model has been validated referring to a well-known combustion case reported in literature.

In the modelling of the flame-to-emitter heat transfer process the volume occupied by the exhaust gas and the Kanthal wires has been considered as a single heterogeneous structure consisting of an open-cell highly porous material filled with gas. This allowed to simplify the geometry and the mathematical formulation of the model: referring to cases reported in literature an overall thermal conductivity of the structure has been defined and calculated, which includes heat transfer by radiation, conduction and convection and

mixing of fluids. Even if this specific model could not be validated directly, the good correspondence between the temperatures measured experimentally and those obtained from simulations proved its reliability.

The simulation of the optical system has been implemented following the method based on the two-band model concept, without considering the geometric factors and assuming a mono-dimensional model: the geometry of the optical system components and the high reflectivity of the reflecting frame justified this approach.

The performance of the system reported in the present work and the current state of the art of the technology show clearly that TPV is not yet a mature technology and needs further improvements to reduce the costs and increase the system efficiency.

TPV, however, has the potential to become already in the close future a competitive energy conversion technology for some specific applications: used as small power supplies for off-grid applications, as off-grid heating appliances and for waste heat recovering, TPV systems could play very soon an important role in these niche markets. A simulation done to evaluate the effect of a small TPV device as back-up generator for a standalone PV system showed that TPV can be advantageous economically reducing the overall system costs.

As final conclusion it should be again pointed out that TPV is a complex and highly interdisciplinary technology which involves several and different research fields. The optimization of the device does not depend only on the optimization of single components, but also on the whole system design and on the interactions between the different processes.

For these reasons projects based on cooperations and partnerships between universities and research institutes having experience in different research fields are fundamental to increase the knowledge on the technology and improve significantly the performance of TPV systems.

Bibliography

[ABG+00] M. J. Assael, E. Bekou, D. Giakoumakis, D. G. Friend, M. A. Killeen, J. Millat, and A. Nagashima. Experimental data for the viscosity and thermal conductivity of water and steam. *Journal of Physical and Chemical Reference Data*, 29(2):141–166, 2000.

[AD05] P. Abbott and F. Dimroth. Private communications, 2005. Fraunhofer Institute for Solar Energy Systems.

[AHL03] J. Aschaber, C. Hebling, and J. Luther. Realistic modelling of TPV systems. *Semiconductor Science and Technology*, 18:158–164, 2003.

[AK+05] V. M. Andreev, V. P. Khvostikov, et al. Thermophotovoltaic converters with solar powered high temperature emitters. In *Proc. 20th European PV Solar Energy Conference*, 2005.

[AKG+04] T. Aicher, P. Kästner, A. Gopinath, A. Gombert, A. W. Bett, T. Schlegl, C. Hebling, and J. Luther. Development of a novel TPV power generator. In *Sixth Conference on Thermophotovoltaic Generation of Electricity*, AIP Conference Proceedings 738, pages 71–78, 2004.

[And02] V. M. Andreev. An overview of TPV cell technologies. In *Fifth Conference on Thermophotovoltaic Generation of Electricity*, AIP Conference Proceedings, 653, pages 289–304, 2002.

[B+85] C. Bonacina et al. *Trasmissione del calore*. Cleup Editore, 1985.

[B+02] B. Bitnar et al. Characterisation of rare earth selective emitters for thermophotovoltaic applications. *Solar Energy Materials and Solar Cells*, 73:221–234, 2002.

[Bar] J. Bard. Applications and markets for TPV systems. Clean Energy Power 2006, Berlin. Presentation at the 2^{nd} Conference for Thermophotovoltaic: Science to Business, 19 Jan 2006.

[Bar05] J. Bard. Hausenergieversorgung mit Brennstoffzellen. In *OTTI Profiforum: Stationäre und portabel Brennstoffzellensysteme*, Regensburg, Februar 2005.

[BBKM87] A. Boushehri, J. Bzowski, J. Kestin, and E. A. Mason. Equilibrium and transport properties of eleven polyatomic gases at low density. *Journal of Physical and Chemical Reference Data*, 16(3):445–466, 1987.

[BDP+04] B. Bitnar, W. Durisch, G. Palfinger, et al. Practical thermophotovoltaic generators. *Semiconductors*, 38(8):941–945, 2004.

[BFP04] T. Bauer, I. Forbes, and N. Pearsall. The potential of thermophotovoltaic heat recovery for the UK industry. *International Journal of Ambient Energy*, 25(1):19–25, 2004.

[BFPP05] T. Bauer, I. Forbes, R. Penlington, and N. Pearsall. Heat transfer modelling in thermophotovoltaic cavities using glass media. *Solar Energy Materials and Solar Cells*, 88(3):257–268, 2005.

[Bit03] B. Bitnar. Silicon, germanium and silicon/germanium photocells for thermophotovoltaics applications. *Semiconductor Science and Technology*, 18:221–227, 2003.

[BM94] L. Broman and J. Marks. Co-generation of electricity and heat from combustion of wood powder utilizing thermophotovoltaic conversion. In *The First NREL Conference on the Thermophotovoltaic Generation of Electricity*, AIP Conference Proceedings 321, pages 133–138, 1994.

[BMD+02] B. Bitnar, J. C. Mayor, W. Durisch, A. Meyer, G. Palfinger, F. von Roth, and H. Sigg. Record electricity-to-gas power efficiency of a silicon solar cell based TPV system. In *Fifth Conference on Thermophotovoltaic Generation of Electricity*, AIP Conference Proceedings, 653, pages 18–28, 2002.

[Bos05] R. Bosch. Perspective on fuel cells vs. incumbent technologies. In *2005 Fuel Cell Seminar*, 2005.

[Bro95] L. Broman. Thermophotovoltaic bibliography. *Progress in Photovoltaics: Research and Applications*, 3:65–74, 1995.

[BS78] R. Bauer and E. U. Schlünder. Effective radial thermal conductivity of packings in gas flow. *International Chemical Engineering*, 18(2):181–204, 1978.

[BS06] H. D. Baehr and K. Stephan. *Heat and Mass Transfer*, chapter 5, pages 594–611. Springer, 2006.

[CdRL03] G. Colangelo, A. de Risi, and D. Laforgia. New approaches to the design of the combustion system for thermophotovoltaic applications. *Semiconductor Science and Technology*, 18:262–269, 2003.

[CdRL06] G. Colangelo, A. de Risi, and D. Laforgia. Experimental study of a burner with high temperature heat recovery system for TPV applications. *Energy Conversion and Management*, 47:1192–1206, 2006.

[Cer07] `http://www.ceramatec.com`, 07-2007.

[Cha98] M. W. Chase. NIST-JANAF Themochemical Tables, Fourth Edition. *Journal of Physical and Chemical Reference Data*, Monograph 9, 1998.

[CLTC05] J. K. Carson, S. J. Lovatt, D. J. Tanner, and A. C. Cleland. Thermal conductivity bounds for isotropic, porous materials. *International Journal of Heat and Mass Transfer*, 48:2150–2158, 2005.

[CM00] V. V. Calmidi and R. L. Mahajan. Forced convection in high porosity metal foams. *ASME Journal of Heat Transfer*, 122:557–565, 2000.

[Cou99] T. J. Coutts. A review of progress in thermophotovoltaic generation of electricity. *Renewable and Sustainable Energy Reviews*, 3:77–184, 1999.

[D+99] C. L. DeBellis et al. Component development for 500 watt diesel fueled portable thermophotovoltaic (TPV) power supply. In *Fourth NREL Conference on Thermophotovoltaic Generation of Electricity*, AIP Conference Proceedings, 460, 1999.

[DBvRP03] W. Durisch, B. Bitnar, F. von Roth, and G. Palfinger. Small thermophotovoltaic prototype systems. *Solar Energy*, 75:11–15, 2003.

[DL+03] D. Diso, A. Licciulli, et al. Erbium containing ceramic emitters for thermophotovoltaic energy conversion. *Materials Science and Engineering: B*, 98:144–149, 2003.

[DLR] DLR. Institute of Combustion Technology. Private communications.

[DLT+04] D. Diso, A. Licciulli, G. Torsello, S. Tundo, M. Mazzer, and M. Lomascolo. Study and optimization of ceramic coatings for thermophotovoltaic applications. In *Sixth Conference on Thermophotovoltaic Generation of Electricity*, AIP Conference Proceedings 738, pages 237–243, 2004.

[DM79] F. Demichelis and E. Minetti. A solar thermophotovoltaic converter. *Solar cells*, 1:395–403, 1979.

[DMCL94] P. Du Plessis, A. Montillet, J. Comiti, and J. Legrand. Pressure drop prediction for flow through high porosity metallic foams. *Chemical Engineering Science*, 49:3545–3553, 1994.

[Du 92] P. Du Plessis. Pore scale modeling for flow through different types of porous environments. In M. Quintard and M. Todorovic, editors, *Heat and Mass Transfer in Porous Media*, pages 249–262. Elsevier, 1992.

[Duf05] T. Duffar. Thermo-Photo-Voltaic cells based on GaSb - Final report. Research Training Network FP5, 2005. Contract number HPRN-CT-2001-00199.

[Efo07] `http://www.efoy.eu`, 04-2007.

[F+89] L. M. Fraas et al. GaSb booster cells for over 30% efficient solar-cell stacks. *Journal of Applied Physics*, 66(8):3866–3870, 1989.

[F+02a] FaberMaunsell Ltd et al. Micro and mini CHP markets, assessment and development plan - EU SAVE report. Technical report, European Commission, Directorate-General Energy and Transport, April 2002.

[F+02b] L. Fraas et al. TPV tube generators for apartment building and industrial furnace applications. In *Fifth Conference on Thermophotovoltaic Generation of Electricity*, AIP Conference Proceedings, 653, pages 38–48, 2002.

[F+02c] L. Fraas et al. Thermophotovoltaics for combined heat and power using low NOx gas fired radiant tube burners. In *Fifth Conference on Thermophotovoltaic Generation of Electricity*, AIP Conference Proceedings, 653, pages 61–70, 2002.

[FAH03] L. M. Fraas, J. E. Avery, and H. X. Huang. Thermophotovoltaic furnace-generator for the home using low bandgap GaSb cells. *Semiconductor Science and Technology*, 18:247–253, 2003.

[FBH+99] L. Fraas, R. Ballantyne, S. Hui, S. Ye, S. Gregory, J. Keyes, J. Avery, D. Lamson, and B. Daniels. Commercial GaSb cell and circuit development for the Midnight Sun TPV stove. In *Fourth NREL Conference on Thermophotovoltaic Generation of Electricity*, AIP Conference Proceedings, 460, 1999.

[FBS64] A. Fortini, P. Bauduin, and P. Sibillot. Realisation d'un convertisseur thermophotovoltaique. In *Sixth AGARD Combustion and Propulsion Colloquium*, Cannes, 1964.

[FDO+06] J. Fernandez, F. Dimroth, E. Oliva, M. Hermle, and A. W. Bett. Characterisation and simulation of germanium TPV cells. In *Seventh Conference on Thermophotovoltaic Generation of Electricity*, AIP Conference Proceedings 890, 2006.

[FF97] L. Ferguson and L. Fraas. Matched infrared emitters for use with GaSb TPV cells. In *Third NREL Conference on Thermophotovoltaic Generation of Electricity*, AIP Conference Proceedings, 401, pages 169–179, 1997.

[Fla01] M. Flamme. Low NOx combustion technologies for high temperatures applications. *Energy Conversion and Management*, 42:1919–1935, 2001.

[FLEK+02] J. G. Fleming, S. Y. Lin, I. El-Kady, R. Biswas, and K. M. Ho. All-metallic three-dimensional photonic crystals with a large infrared bandgap. *Nature*, 417:52–55, 2002.

[FS+01] L. Fraas, J. E. Samaras, et al. TPV generators using the radiant tube burner configuration. In *Proc. 17th European PV Solar Energy Conference*, Munich, Germany, October 2001.

[FSAM00] L. Fraas, J. Samaras, J. Avery, and L. Minkin. Antireflection coated refractory metal matched emitters for use with GaSb thermophotovoltaic generators. In *28th IEEE Photovoltaic Specialist Conference*, page 1020, Anchorage, AK, 2000.

[G+68] P. Gray et al. Investigation of a PIN-structure germanium photovoltaic cell. Report Da-28-043-AMC-01978(E), Cambridge, MA: MIT Press, 1968.

[GAG+06] V. A. Gevorkyan, V. M. Aroutiounian, K. M. Gambaryan, A. H. Arakelyan, I. A. Andreev, L. V. Golubev, and Y. P. Yakovlev. The growth of low band gap InAsPSb based diode heterostructures for thermo-photovoltaic application. In *Seventh Conference on Thermophotovoltaic Generation of Electricity*, AIP Conference Proceedings 890, 2006.

[GC02] B. S. Good and D. L. Chubb. Theoretical comparison of erbium, holmium and thulium aluminum garnet selective emitters. In *Fifth Conference on Thermophotovoltaic Generation of Electricity*, AIP Conference Proceedings, 653, pages 142–151, 2002.

[GER80] W. L. Grosshandler, M. Engel, and A. Russell. Emissivity of thermocouples for combustion measurements. In *Western States Section of the Combustion Institute, Spring Meeting*, 1980.

[Glo07] `http://www.globalte.com`, 04-2007.

[GM04] G. Guazzoni and S. Matthews. A Retrospective of Four Decade of Military Interest in Thermophotovoltaics. In *Sixth Conference on Thermophotovoltaic Generation of Electricity*, AIP Conference Proceedings 738, 2004.

[Gom02] A. Gombert. An overview of TPV emitter technologies. In *Fifth Conference on Thermophotovoltaic Generation of Electricity*, AIP Conference Proceedings, 653, pages 123–131, 2002.

[Gre92] M. A. Green. *Solar cells: Operating principles, technology and system applications.* University of New South Wales, 1992.

[Gua72] G. Guazzoni. High temperature spectral emittance of oxides of erbium, samarium, neodymium and ytterbium. *Applied Spectroscopy*, 26(1):60–65, 1972.

[Hau63] R. W. Haushalter. Engineering investigation of a thermophotovoltaic energy converter. Final Report Contract No. DA-44-009-AMC-622(T), General Motors Defense research Laboratories, Santa Barbara, CA, 1963.

[HBGW99] A. Heinzel, V. Boerner, A. Gombert, and V. Wittwer. Microstructured tungsten surfaces as selective emitters. In *Fourth NREL Conference on Thermophotovoltaic Generation of Electricity*, AIP Conference Proceedings, 460, pages 191–196, 1999.

[HEE99] C. L. Hackert, J. L. Ellzey, and O. A. Ezekoye. Combustion and heat transfer in model two-dimensional porous burners. *Combustion and Flame*, 116:177–191, 1999.

[HMHS04] W. E. Horne, M. D. Morgan, W. P. Horne, and S. Sundaram. Frequency selective surface bandpass filters applied to thermophotovoltaic generators. In *Sixth Conference on Thermophotovoltaic Generation of Electricity*, AIP Conference Proceedings 738, pages 189–197, 2004.

[HMS02] W. E. Horne, M. D. Morgan, and V. S. Sundaram. 500 watt diesel fuel TPV portable power supply. In *Fifth Conference on Thermophotovoltaic Generation of Electricity*, AIP Conference Proceedings, 653, pages 91–100, 2002.

[Hor77] W. E. Horne. Conversion of solar to electrical energy, 1977. US Patent 4,313,024.

[Ide69] I. E. Idel'Cik. *Memento des pertes de charge*. Eyrolles Editeur, 1969.

[Jx001] Glass project fact sheet: Thermophotovoltaic electric power generation using exhaust heat, September 2001. Office of Industrial Technologies Energy Efficiency and Renewable Energies - U.S. Department of Energy.

[K+96] N. V. Kuleshov et al. Spectroscopy of excited states of a magnesium aluminum spinel crystal doped with nickel. *Optics and Spectroscopy*, 81(5):760–763, 1996.

[KB01] F. Kreith and M. S. Bohn. *Principles of Heat Transfer*. Brooks-Cole, 2001.

[KG72] E. Kittl and G. Guazzoni. Design analysis of TPV-generator system. In *Proc. 25th Power Sources Symposium*, pages 106–109, 1972.

[KG99] J. Knobloch and A. Goetzberger. Physicalische grundlagen von solarzellen. In *Photovoltaik - Strom aus der Sonne: Technologie, Wirtschaftlichkeit und Marktentwicklung*, pages 1–14. Verlag Müller, 1999. Fourth edition.

[Kol56] H. H. Kolm. Solar-battery power source, quarterly progress report. Technical report, Solid State Research, Group 35, MIT Lincoln Laboratory, 1956.

[L+04] A. Luque et al. FULLSPECTRUM: a new PV wave making more efficient use of the solar spectrum. In *Proc. 19th European Photovoltaic Solar Energy Conference and Exhibiton*, Paris, 2004.

[L+05] A. Luque et al. FULLSPECTRUM: a new PV wave making more efficient use of the solar spectrum. *Solar Energy Materials and Solar Cells*, 87:467–479, May 2005.

[Laq97] E. Laqua. *Untersuchungen zur Integration eines thermophotovoltaischen Wandlers in ein Gasheizgerät*. Phd thesis, Kassel University, 1997.

[Mai95] C. Maier. *Untersuchungen der thermophotovoltaischen Energiekonversion mit gasheritzten Strahlern*. Msc thesis, Karlsruhe University, 1995.

[Mic07] `http://www.microchap.info`, 05-2007.

[MSC80] R. E. Mitchell, A. F. Sarofim, and L. A. Clomburg. Experimental and numerical investigation of confined laminar diffusion flames. *Combustion and Flame*, 37:227–244, 1980.

[MSWC99] O. Morrison, M. Seal, E. West, and W. Connelly. Use of a thermophotovoltaic generator in a hybrid electric vehicle. In *Fourth NREL Conference on Thermophotovoltaic Generation of Electricity*, AIP Conference Proceedings, 460, 1999.

[Nel02] R. E. Nelson. TPV Systems and State-of-Art Development. In *Fifth Conference on Thermophotovoltaic Generation of Electricity*, AIP Conference Proceedings, 653, 2002.

[Nel03] R. E. Nelson. A brief history of thermophotovoltaic development. *Semiconductor Science and Technology*, 18:141–143, 2003.

[NOM+05] N. Nakagawa, H. Ohtsubo, A. Mitani, K. Shimizu, and Y. Waku. High temperature strength and thermal stability for melt growth composite. *Journal of the European Ceramic Society*, 25:1215–1257, 2005.

[NOWY05] N. Nakagawa, H. Ohtsubo, Y. Waku, and H. Yugami. Thermal emission properties of $Al_2O_3/Er_3Al_5O_{12}$ eutectic ceramics. *Journal of the European Ceramic Society*, 25:1285–1291, 2005.

[Ota07] `http://www.otag.de`, 05-2007.

[PBD+03] G. Palfinger, B. Bitnar, W. Durisch, J. C. Mayor, D. Grützmacher, and J. Gobrecht. Cost estimate of electricity produced by TPV. *Semiconductor Science and Technology*, 18:254–261, 2003.

[QH02] K. Qiu and A. C. S. Hayden. Electric power generation using low bandgap TPV cells in a gas-fired heating furnace. In *Fifth Conference on Thermophotovoltaic Generation of Electricity*, AIP Conference Proceedings, 653, pages 49–58, 2002.

[QH03] K. Qiu and A. C. S. Hayden. Thermophotovoltaic generation of electricity in a gas fired heater: influence of radiant burner configurations and combustion process. *Energy Conversion and Management*, 44:2779–2789, 2003.

[QH06] K Qiu and A. C. S. Hayden. TPV power generation system using a high temperature metal radiant burner. In *Seventh Conference on Thermophotovoltaic Generation of Electricity*, AIP Conference Proceedings 890, 2006.

[R+04] T. D. Rahmlow et al. Thermophotovoltaic spectral control. In *Sixth Conference on Thermophotovoltaic Generation of Electricity*, AIP Conference Proceedings 738, pages 180–188, 2004.

[RKS+99] V. D. Rumyantsev, V. P. Khvostikov, S. V. Sorokina, V. I. Vasil'ev, and V. M. Andreev. Portable TPV generator based on metallic emitter and 1.5-Amp GaSb cells. In *Fourth NREL Conference on Thermophotovoltaic Generation of Electricity*, AIP Conference Proceedings, 460, pages 384–393, 1999.

[RM52] W. E. Ranz and W. R. Marshall. Evaporation from drops. *Chemical Engineering Progress*, 48:141–146 and 173–180, 1952.

[RS01] W. Roth and A. Steinhüser. Photovoltaik in der Telekommunikation, Telematik und Telemetrie. In *16 Symposium Photovoltaische Solarenergie*. Otti, 2001.

[RVA+04] C. M. Ruiz, O. Vigil, C. Algora, D. Martin, V. Bermudez, and E. Dieguez. Transparent conducting oxides as antireflection coatings for GaSb TPV cells. In *Sixth Conference on Thermophotovoltaic Generation of Electricity*, AIP Conference Proceedings 738, pages 221–229, 2004.

[SAA+05] T. Schlegl, P. Abbott, T. Aicher, F. Dimroth, G. Siefer, R. Szolak, and A. W. Bett. GaSb based PV modules for a TPV generator system. In *Proc. 20th European PV Solar Energy Conference*, June 2005.

[SAB+05] G. Siefer, P. Abbott, C. Baur, T. Schlegl, and A. W. Bett. Determination of the temperature coefficients of various III-V solar cells. In *Proc. 20th European PV Solar Energy Conference*, June 2005.

[Sch71] R. J. Schwartz. A theoretical and experimental investigation of planar PIN thermophotovoltaic cells. Technical report, Purdue University, 1971. Contract No. DAAB07-70-C-0129.

[SDOB04] T. Schlegl, F. Dimroth, A. Ohm, and A. W. Bett. TPV modules based on GaSb structures. In *Sixth Conference on Thermophotovoltaic Generation of Electricity*, AIP Conference Proceedings 738, pages 285–293, 2004.

[SH75] R. Siegel and N. A. Hussain. Combined radiation, convection, and conduction for a system with a partially transmitting wall. Nasa Technical Note D-7985, Lewis Research Center, 1975.

[SH92] R. Siegel and J. R. Howell. *Thermal radiation heat transfer*. Taylor & Francis, third edition, 1992.

[Sha98] C. R. Shaddix. Practical aspects of correcting thermocouple measurements for radiation loss. In *Western States Section of the Combustion Institute, Fall Meeting*, 1998.

[SKY02] H. Sai, Y. Kanamori, and H. Yugami. Spectrally selective emitters with deep rectangular cavities fabricated with fast atom beam etching. In *Fifth Conference on Thermophotovoltaic Generation of Electricity*, AIP Conference Proceedings, 653, pages 155–163, 2002.

[SMH00] V. Sundaram, M. D. Morgan, and W. E. Horne. Bandgap-engineered thermophotovoltaic devices for high efficiency radioisotope power. Report, EDTEK, Kent, WA (US), 2000. DOE Contract Number: FG03-95ER81957.

[SMK89] M. D. Smooke, R. E. Mitchell, and D. E. Keyes. Numerical solution of two-dimensional axisymmetric laminar diffusion flames. *Combustion Science and Technology*, 67:85–122, 1989.

[SOK97] A. Schock, C. Or, and V. Kumar. Small radioisotope thermophotovoltaic (RTPV) generators. In *The Second NREL Conference on the Thermophotovoltaic Generation of Electricity*, AIP Conference Proceedings 358, pages 81–97, 1997.

[Sus07] `http://www.sustainablevillage.com`, 04-2007.

[Swa80] R. M. Swanson. Recent developments in thermophotovoltaic conversion. In *Proc. International Electron Devices Meeting*, pages 186–189, Washington DC, 1980.

[T+70] Y. S. Touloukian et al. *Thermal Radiative Properties, Nonmetallic Solids*, volume 8 of *Data Series*. Plenum Publishing Corporation, 1970.

[TD06] W. Tobler and W. Durisch. Slurry- and plasma-spray coating of selective emitting rare-earth oxides on high temperature substrates. In *Seventh Conference on Thermophotovoltaic Generation of Electricity*, AIP Conference Proceedings 890, 2006.

[The07] `http://www.thermalforce.de`, 06-2007.

[Tob07] W. Tobler. Private communications, 2007. Paul Scherrer Institut.

[Udo07] `http://www.udomi.de`, 06-2007.

[Ult07] `http://www.ultracellpower.com`, 06-2007.

[V+06] A. S. Vlasov et al. TPV systems with solar powered tungsten emitters. In *Seventh Conference on Thermophotovoltaic Generation of Electricity*, AIP Conference Proceedings 890, 2006.

[Vol01] W. Volz. *Entwicklung und Aufbau eines thermophotovoltaischen Energiewandlers*. Phd thesis, Kassel University, 2001.

[W+01] J. Warnatz et al. *Combustion: Physical and Chemical Fundamentals, Modeling and Simulation, Experiments, Pollutant Formation*. Springer, third edition, 2001.

[WA86] C. Wyon and J.J. Aubert. Czochralski growth and optical properties of magnesium-aluminium spinel doped with nickel. *Journal of Crystal Growth*, 79:710–713, 1986.

[WAA+04] M. W. Wanlass, S. P. Ahrenkiel, R. K. Ahrenkiel, J. J. Carapella, R. J. Wehrer, , and B. Wernsman. Recent advances in low-bandgap, InP-based GaInAs/InAsP materials and devices for thermophotovoltaic (TPV) energy conversion. In *Sixth Conference on Thermophotovoltaic Generation of Electricity*, AIP Conference Proceedings 738, pages 427–435, 2004.

[Wan04] C. A. Wang. Antimony-based III-V thermophotovoltaic materials and devices. In *Sixth Conference on Thermophotovoltaic Generation of Electricity*, AIP Conference Proceedings 738, pages 255–266, 2004.

[WC99] E. M. West and W. R. Connelly. Integrated development and testing of multi-kilowatt TPV generator systems. In *Fourth NREL Conference on Thermophotovoltaic Generation of Electricity*, AIP Conference Proceedings, 460, pages 446–456, 1999.

[WD81] C. K. Westbrook and F. L. Dryer. Simplified reaction mechanism for the oxidation of hydrocarbon fuels in flames. *Combustion Science and Technology*, 27:31–43, 1981.

[Wed63] B. D. Wedlock. Thermo-photo-voltaic conversion. *Proceedings of IEEE*, 51:694–698, 1963.

[Wer63] J. J. Werth. Thermo-photovoltaic converter with radiant energy reflective means, 1963. US Patent 3,331,707.

[Whi07] `http://www.whispergen.com`, 05-2007.

[Wil50] C. R. Wilke. A viscosity equation for gas mixtures. *Journal of Chemical Physics*, 18(4):517–519, 1950.

[Wil04] C. Wilcox. Micro-CHP: The technology finally takes off. 2004. Second CHAPNET Network Conference.

[Wil06] D. Wilt. Thermophotovoltaics for space power applications. In *Seventh Conference on Thermophotovoltaic Generation of Electricity*, AIP Conference Proceedings 890, 2006.

[WR79] P. Würfel and W. Ruppel. Upper limit of thermophotovoltaic solar energy conversion. *IEEE Transactions on Electron Devices*, 27(4):745–750, 1979.

[WS67] D. C. White and R. J. Schwartz. P-I-N structures for controlled spectrum photovoltaic converters. In *Proc. of NATO AGARD Conference (Cannes, France, March 1964)*, pages 897–922. Gordon and Breach, 1967.

[Wün03] J. G. Wünning. FLOX® - Flameless combustion. In *Thermprocess Symposium*, 2003.

[WW92] J. A. Wünning and J. G. Wünning. Brenner für die flammlose oxidation mit geringer NO-bildung auch bei höchster luftvorwärmung. *Gas Wärme International*, 41(10):438–444, 1992.

[WWB61] D. C. White, B. D. Wedlock, and J. Blair. Recent advance in thermal energy conversion. In *Proc. 15th Power Sources Conference*, pages 125–132, 1961.

[XSLL93] Y. Xu, M. D. Smooke, P. Lin, and M. B. Long. Primitive variable modeling of multidimensional laminar flames. *Combustion Science and Technology*, 90:289–313, 1993.

[YSY03] H. Yugami, H. Sasa, and M. Yamaguchi. Thermophotovoltaic systems for civilian and industrial applications in Japan. *Semiconductor Science and Technology*, 18:239–246, 2003.

[ZHS+01] M. Zenker, A. Heinzel, G. Stollwerck, J. Ferber, and J. Luther. Efficiency and power density potential of combustion-driven thermophotovoltaic systems using GaSb photovoltaic cells. *IEEE Transactions on Electron Devices*, 48(2):367–376, 2001.

[ZLH04] C.Y. Zhao, T.J. Lu, and H.P. Hodson. Thermal radiation in ultralight metal foams with open cells. *International Journal of Heat and Mass transfer*, 47:2927–2939, 2004.

Acknowledgments

This dissertation resumes the major part of the work that I carried out at ISET since November 2003. During these four years I learned many things and made many new experiences which made me grow not only professionally but most of all humanly. Like in every research work, there have been moments of enthusiasm and satisfaction as well as moments of frustration and discouragement. This PhD thesis and more generally this period of my life would have not been possible without the constant help and support of many people which stood always by me, both at work and in the everyday life, giving me the energy and the motivation to go on in the difficult moments and making me enjoy these years in Kassel.

First of all I would like to thank sincerely Jochen Bard: he has been following me in every step of my work, helping me and giving me the opportunity to grow professionally, always ready to discuss, suggest, motivate and encourage me, but also letting me time and space to undertake my own decisions and responsibilities. Many many thanks for all the nice discussions and moments shared together, both professional and extra-professional.

An "enthusiastic" thank to my supervisor Professor Jürgen Schmid, for giving me the possibility to do the PhD and for the contagious enthusiasm and optimism he always showed every time we discussed about it. More than once he gave me simple but very sensible advices helping me to face problems encountered during my work.

Thanks also to Professor Peter Zacharias for accepting gladly and without hesitation to be my second supervisor.

I would like to thank Peter Caselitz, for supporting constantly my work during these four years: he showed always confidence in me, both encouraging me when I was stuck with my thesis and giving me the possibility to work on new and interesting topics while continuing my PhD.

A big thank to all my colleagues Bahram, Christian, Dirk, Jochen, Markus, Martin, Melanie, Nandi and Sasa for making the work at ISET nice and pleasant and for supporting me constantly, helping me in the everyday practical problems.

Many thanks also to Nanda and Farooq, who helped me to set up the logging system and the monitoring graphical user interface during my experimental work.

I would like to thank Herbert Lindenborn for allowing me to use the facilities of the Communications Laboratory at the Department of Electrical Engineering and Computer Science at the University of Kassel.

The realization of my PhD would have not been possible without the help and the collaboration of other research institutes. With DLR Institute of Combustion Technology and in particular Massimiliano Di Domenico I had very fruitful discussions on combustion modelling and simulation. Frank Dimroth and Paul Abbott from Fraun-

hofer Institute for Solar Energy Systems supplied and repaired the GaSb cell arrays and have been always at disposition when documentation, info and technical support were needed. Narihito Nakagawa from Ube Industries realized a sample of MGC material for our device and Walter Tobler from Paul Scherrer Institut took detailed pictures and carried out spectral measurements on emitter samples. Many many thanks to all of them!

A very special thank to Doris, whose energy, determination and care always helped me, especially during the first months in Kassel.

Thanks also to all the friends I met in Kassel, who shared with me many happy moments.

E adesso vorrei continuare in italiano... Il mio primo pensiero va a mamma e papà. Li voglio ringraziare per il loro enorme affetto, perchè mi hanno sostenuto ed incoraggiato in ogni momento, perchè mi hanno accompagnato restando sempre al mio fianco, ma lasciando che fossi io a trovare la mia strada.

Grazie a Lorenzo, anche lui sempre presente e sempre pronto ad incoraggiarmi: per la fiducia che ha in me e per le fraterne chiacchierate avute con lui, in cui poche parole chiare e dirette fanno molto di più di mille discorsi.

Un grazie a tutti i miei amici di Verona, in particolare a Mario, Matteo, Francesco e Silvia, perchè nonostante i 900 chilometri che da più di quattro anni ci separano, sono sempre presenti, pronti ad ascoltare e ad essere ascoltati. Ed un grazie anche agli altri coraggiosi che sono venuti in terra teutonica a trovarmi: Gino, Lollo, Francesca, Mary P. e Sabina.

Ma se sono riuscito a scrivere il mio dottorato è anche e soprattutto merito tuo, Céline. Grazie per tutto quello che mi hai dato e continui a darmi: per il tuo amore e il tuo sostegno sempre presenti, per la tua pazienza, la tua forza, la tua allegria, la tua tenerezza e la tua fiducia. Sei il mio sole.